Viviane Silva Teixeira

Development of a System for Fast Identifiation and Characterization of Biological Cells

Wissenschaftliche Beiträge zur Medizinelektronik

Band 11

Herausgegeben von

Prof. Dr. Wolfgang Krautschneider

Viviane Silva Teixeira

Development of a System for Fast Identification and Characterization of Biological Cells

Wissenschaftliche Beiträge zur Medizinelektronik

Bibliografische Information der Deutschen Nationalbibliothek

Die Deutsche Nationalbibliothek verzeichnet diese Publikation in der
Deutschen Nationalbibliografie; detaillierte bibliografische Daten sind
im Internet über http://dnb.d-nb.de abrufbar.

Abstract

Electrical Impedance Spectroscopy (EIS) consists in the application of a small voltage or current to a material, varying its frequency in a wide range and measuring its response to the estimulation. In this sense, the spectral behavior of the observed substance is obtained, as for each discrete frequency point one value of impedance is measured. Specifically when applied to biological systems it is called Bio-Impedance Spectroscopy (BIS).

This research is about applying EIS to biological systems in order to characterize them. Specifically, the fundamental research question was to identify whether different cell types and tissues could be distinguished by means of EIS. The research was further narrowed by applying BIS to distinguish cancer cells and tumors from their healthy counterparts. The knowledge gap in this field is immense; the applications to medicine unforeseen. For as simple as the technique is, it is amazing how powerful it is. Applications of the technique researched during the five-year period of this PhD are:

- Distinction between metastatic and non-metastatic cancer cells

- Distinction between healthy tissues and cancer tumors based on their spectral response

During this research one physical characteristic was encountered which allows the distinction between metastatic and non-metastatic cancers: the cell surface charge. For all researched cancer groups (prostate, colorectal, breast and leukemia) the cell surface charge per cm^2 was found to be smaller for more metastatic cancers than for less metastatic ones. At the moment of the publishing of this Thesis, no other work in Literature is known to have identified so clearly such a physical parameter that distinguishes metastatic cancers from non-metastatic ones.

To be able to measure the impedance of biological cell suspensions and tissues up to very low frequencies (f < 1 kHz) a four-electrode-terminal measurement setup was used.

Therefore a new chamber which allowed for the measurements of the cells suspensions was developed. To measure the tissues an array of four-electrodes in a special configuration was used. The advantages of measuring cells and tissues at low frequencies is that in such frequencies a different physics is occurring therefore the amount of charge "perceived" is much larger than in higher frequencies. Nevertheless, due to strong artifacts caused by electrode polarization only with a four-electrode-terminal setup the experiments can be performed. Developing such geometry and system which allowed to eliminate all the artifacts in low frequencies was a quite challenging task. Not only to the geometry, but significant attention was also given to the materials of the chamber and the metals used to contact the biological tissues as the majority of materials are poisonous to the cells and kill them.

Throughout this research it was observed that healthy and cancerous cells and tissues have a different spectral behavior. This difference in the frequency behavior is closely correlated to the effects of the cancer in the cells and tissues. Through the signal processing of the experimental results considerable interesting information from the status of the cancers could be extracted. For physicians at the hospital, the technique may open a better understanding of cancers and may help in the gain of useful information in a clinical context to support the decision of the best therapies for patients.

Another topic discussed includes the proposal of the architecture of an implant to be placed inside solid tumors in vivo and monitor tumor response to treatment through BIS. Additionally, two different architectures of a sensor to measure the cancer metabolites or biomarkers concentration in vitro or in vivo were proposed.

Acknowledgements

Contents

List of Figures

List of Tables

Glossary

AC Alternate current

AML Acute myeloid leukemia

AR Androgen receptor

ATP Adenosine Tri-Phosphate

BIS Bio-Impedance Spectroscopy

BSUT Biological system under test

CAF Cancer associated fibroblasts

CT Computed Tomography

CE Counter electrode

CPE Constant Phase Element

DL Double Layer

ECM Equivalent Circuit Model

EEI Electrode-electrolyte interface

EIS Electrical Impedance Spectroscopy

FCS Fetal Calf Serum

IDE Interdigitated Electrodes

IFP Intratumoral fluid pressure

IHP Inner Helmholtz Plane

MDS myelodysplatic syndrome

MRI Magnetic Resonance Imaging

OCP Open Circuit Potential

OHP Outer Helmholtz Plane

PBS Phosphate Buffer Saline

PC Prostate cancer

PET Positron Emission Tomography

PSA Prostate specific antigen

RE Reference electrode

SOA State of the Art

TME Tumor micro-environment

WE Working electrode

WS Working sense electrode

2T Two-electrode-terminal setup

3T Three-electrode-terminal setup

4T Four-electrode-terminal setup

List of Symbols

Symbol	Description	Units
C_{diff}	Diffuse layer capacitance	F/m^2
C_{DL}	Double layer capacitance	F/m^2
CG	Geometric capacitance	pF
C_H	Helmholtz capacitance	F/m^2
C_{mem}	Cell membrane capacitance	$\mu F/cm^2$
D	Particle's diffusion coefficient	cm^2/s
d_{OHP}	Length of Outer Helmholtz plane	nm
E_A	Activation energy	$kcal/mol$
e_0	Elementary charge	C
K_B	Boltzmann constant	J/K
L_D	The same as λ_{Debye}	nm
J_0	Electrode exchange current density	A/cm^2
n_0	Bulk number of ions in electrolyte	$ions/liter$
N	Counterion density on a typical cell	cm^{-2}
R_{col}	Radius of the large colloidal particle	m
R_{CT}	Charge transfer resistance	Ωcm^2
r_{ion}	Ion radius	nm
R_s	Medium or solution resistance	Ω
u	Mobility of the ion in free solution	m^2/sV
u_{ic}	Lateral mobility of ions in the ionic cloud	m^2/sV
V_{mem}	Resting potential from cell membrane	mV

Symbol	Description	Units
V_T	Thermal voltage	mV
W_0	Warburg element constant	Ω
Y_0	Capacitance of constant phase element	F
z	Valence of the ion	$-$
δ	Distance between ion and its counter charge	nm
$\Delta\varepsilon_\alpha$	Amplitude of the alpha dispersion	$-$
$\hat{\varepsilon}$	Complex dielectric permittivity	F/m
ε_0	Vacuum permittivity	F/m
ε_r	Dielectric constant or relative permittivity	$-$
ε_{low}	Relative permittivity limit at zero frequency	$-$
$\varepsilon_{intcells}$	Relative permittivity limit between α and β relaxations	$-$
η	Viscosity of the suspending medium	Ns/m^2
σ	Conductivity	S/m
Φ	Volume fraction of suspended alive cells	$-$
τ_α	Relaxation time of alpha dispersion	s
ω	Angular frequency	rad/s
λ_{Debye}	Debye length	nm

Chapter 1

Introduction

Electrical Impedance Spectroscopy (EIS) also known as Bio-Impedance Spectroscopy (BIS) when applied to biological contexts is a simple and powerful technique to characterize systems. It consists in the application of a small amplitude voltage signal to a system and measuring its current response (potentiostatic EIS). If a current is applied and the voltage is measured it is called galvanostatic EIS. Current established applications of the technique are the characterization of battery systems, evaluation of painting quality in painting industry, estimation of body and fat composition in athletes, evaluation of food quality control and currently under development to distinguish healthy from diseased cells and tissues [1–5].

The fascinating about applying BIS to biological material is that biological systems present a special signature in frequency, similar to a fingerprint, which relates closely to their internal structure and status. Therefore interesting insights can be derived from the experimental results to characterize such systems. When comparing the impedance spectrum of cancer cells and tissues with healthy ones even more striking conclusions can be drawn. The spectrum of such tissues and cells is quite different from their healthy counterparts which is directly related to the effects of the cancer in the healthy systems. In the next chapter a short revision about the topic of BIS is presented and the following chapters will show more details on how the impedance spectrum of healthy and cancer cells and tissues can be analysed and correlated to their status. In this sense, BIS used in

clinical context has the promise of being an excellent tool to aid physicians in evaluating cancer status and the effectiveness of different therapies.

1.1 Purpose of the Work

The purpose of this research is to develop methods and tools to distinguish different cell types and tissues, with a special focus on distinguishing cancer cells and tissues from healthy ones. This project was financed by ProExzellenzia Program 4.0 and by the Research Center of Medical Technology Hamburg (FMTHH).

Applications of the results include the distinction of cancer and healthy tissues in a clinical context (Chapter 7), for instance, by defining tumor boundaries during surgery for tumor removal. Identification of the mechanisms which lead to metastasis, providing input to develop a new wave of less aggressive medicaments for cancer treatment based on the blocking of specific ionic channels present at the cell membrane (Chapter 5). Evaluation of cells response to chemotheraphy by identifying the most effective chemotheraphy agent for each cell type and the best concentration to give to patients (Chapter 6).

1.2 Thesis Outline

The structure of this doctoral thesis is organized as follows:

Chapter 2 presents a literature review of several topics important for the thesis, for instance, the structure of biological cells and their composition, Electrical Impedance Spectroscopy, graphical representation and mathematical formulation of impedance data, among others.

In chapter 3 a detailed description of the four-electrodes-terminal (4T) system developed is given. The development of such a system was essential to perform the electrochemical experiments in cells suspensions up to frequencies below 1 kHz.

In chapter 4 a large set of experimental results from the impedance measurements of several cancer cell lines using the 4T chamber described in Chapter 3 is presented and compared. Also the interpretation and correlation with physical parameters of the system is mentioned. To complete the chapter useful recommendations to perform future experiments are given.

In chapter 5 the experimetal results of cells suspensions are processed to extract the cell's external surface charge and this charge is correlated with the metastatic potential of the cancer cells.

In chapter 6 adherent cell cultures are measured using an interdigited electrode system (IDE) to evaluate their growth and response to two different types of chemotheraphy medication.

In chapter 7 the impedance spectrum of several healthy organs and tumors from mice is measured and compared. Interesting insights could be obtained from this chapter to distinguish cancer from healthy tissues. Chapter **??** concludes the thesis and gives recommendations for future research.

The topic of cancer is huge and very complex, as cancer is a single name for a large set of diseases with some common characteristics (uncontrolled cell proliferation, ability to form distant metastasis) nevertheless with lots of differences among the different types of cancers. Therefore finding characteristics which are common to the majority of cancer types is essential and this doctoral thesis has made an important step towards this direction. As cancer is already of major medical concern and with population aging it will evolve into a leading cause of death worldwide[1], any new research which supports physicians in understanding cancer mechanisms and providing better treatments to patients is a valuable contribution to humanity.

---

[1]It is estimated that with population aging, during the next 20 years up to 25% of European and North American populations will die of cancer [6].

1.3 Contributions

The first contribution to the state of the art of this doctoral thesis was the development of a cheap, easy to produce and scalable four-eletrode-terminal chamber system (4T) using 3D printing techniques. Since the concept up to the first prototype two years were necessary and throughout the last five years several improved versions were produced. The last and smallest version is presented in chapter 3. It belonged to this task finding the best geometry, the size, how to produce it efficiently in a cheap way, the chamber material and specially important was the identification of a proper metal (Pt) to interface directly with the cancer cells inside the electrochemical chamber without killing them and providing an stable open circuit potential for the experiments in low frequencies. The challenge on performing impedance experiments in liquids for frequencies below 1 kHz lies on the double layer effects which hide the real response from the biological systems. Therefore, finding a geometry which does not distort the electric field, which eliminates or reduces the double layer effects to a minimum and producing it in a cheap and fast way was a great contribution.

A second and important contribution to the state of the art was to find one characteristic specific from the cells, the external cell surface charge, and correlate it with their metastatic potential. The ability to separate charge between the extracellular and intracellular medium is affected by the cancer, i.e., metastatic cancer cells in general show a lower capacity to separate charge between the two media. In other words, in general, the cell membrane of more metastatic cancers will be leakier than less metastatic cancers. This will translate into a higher (towards positive values) resting membrane potential, namely, a depolarized cell membrane potential. As the depolarization of cell membrane potential functions as a signaling for the cells to start their cycle of division [7], this result is of extreme importance for Medicine. Translating into other words, possibly the development of new drugs which block specific ionic channels in specific types of cancers can reduce the aggressivenes of the cancer by causing the shifting of the resting potential of the cancer cells towards more negative values (hyperpolarization) and reducing the speed of cancer proliferation. Important to highlight is that given the complexity of the metastatic process this is certainly not the only mechanism leading to it. Additionally, for each

type of cancer it has to be researched which specific channels should be blocked in order not to affect the surrounding healthy cells blocking their channels too.

A third contribution to the state of the art was to perform a large number of experiments with a broad set of cancer cell types and repeating the experiments with different cell seeds to give more confidence to the results. Additionally the identification of some of the mechanisms that affect cancer cells impedance spectral behavior (conductivity of the supernatant, temperature, volume fraction of suspendend cells, frequency) and the suggestion of new experimental practices to reduce the experimental spread. The majority of the results published in literature refer to experiments which were not repeated with different cell seeds, therefore being hard to generalize such results.

A fourth contribution was to find two common characteristics that distinguish most types of cancers from healthy tissues and proving them by the repetition of the experiments, namely, the higher tumor conductivity and lower impedance magnitude when compared to healthy tissues. There are a few studies in literature [3, 8] which also reported the observation of a higher conductivity in tumors, nevertheless here the study was extended through a large set of experiments, a large set of repetitions, a large number of healthy tissues compared to the tumor ones and the measurement of two different types of tumors.

The last contribution to science was the extension of the experimental results of epsilon and sigma for a large number of tissues up to very low frequencies. Literature is scarce or inexistent for several organs in frequencies below 1 kHz and this study makes a significant contribution in this direction by using a four electrode terminal setup. The values of dieletric constant and sigma for the tissues are used in dosimetry studies, namely, to evaluate the effects of electromagnetic fields in human tissues interacting with such fields and to stablish safe limits for such interaction.

Minor contributions include:

- Proposal of the architecture of the implant (appendix A).

- Proposal of an improved version of interdigitated electrodes system to measure adherent cells and observe their growth and response to chemotheraphy (chapter 6).

- Proposal of a method to measure the cell to cell junctions resistance strength and correlate it with the metastatic potential of cancer cells (chapter 6).

The architecture of the implant was developed in LTSpice with discrete macro components and is described in figure A.1. Of course when developing the miniaturized version of such circuit instead of using discrete components, a couple of transistors should replace the function of those macro components, for instance one can think of replacing the operational amplifiers in figure A.2 to a simplified version of a differential amplifier with five transistors. The architecture of a four electrode terminal potentiostat is proposed in figure A.2 and is a combination of three differential amplifiers with five buffers. Observe that for measuring the impedance of cancer tumors up to frequencies below 1 kHz necessarily a four-electrode-terminal (4T) architecture must be used. The lock-in detection described in Appendix A is used to separate the real and imaginary parts of the signal. Alternative archiectures are proposed in literature, for instance using an integrator instead of a frequency mixer, nevertheless such archicture requires a long integration time in order to have a reasonable signal to noise ratio. Given the low frequencies used in such 4T experiments, the lock-in detection using frequency mixing was preferred for being faster.

1.4   List of Publications

Here there is a list of international and national conference publications and presentations, both as a first author or co-author, produced during the PhD (1-8) and the master thesis (9-10) which preceeded the PhD as a preparation for it. The publications are listed in chronological order.

1. V. S. Teixeira, V. Labitzky, U. Schumacher, W. Krautschneider. Use of Electrical Impedance Spectroscopy to Distinguish Cancer from Normal Tissues with a Four Electrode Terminal Setup. In: 54th DGBMT Annual Conference, 29 Sept – 1st October, 2020, Leipizig, Germany.

2. V.S. Teixeira, T. Barth, V. Labitkzy, U. Schumacher, W. Krautschneider. Electrical Impedance Spectroscopy for Characterization of Prostate PC-3 and DU 145 Cancer

Cells. 41st Annual International Conference of IEEE Engineering in Medicine and Biology Society (EMBC), 23-27 July 2019, Berlin, Germany.

3. T. Barth, V. S. Teixeira, W. Krautschneider. Designing electrodes for electrical impedance spectroscopy in a four terminal setup. Additive Manufacturing Meets Medicine 2019, Lübeck, Germany.

4. T. Barth, V. S. Teixeira, W. Krautschneider. Chamber miniaturization for four terminal electrical impedance spectroscopy. Additive Manufacturing Meets Medicine 2019, Lübeck, Germany.

5. V. S. Teixeira, J. J. Montero-Rodríguez, W. Krautschneider. Bioimpedance Spectroscopy for Characterization of Healthy and Cancerous Tissues. IEEE International Conference on Electrical Engineering and Photonics EExPolytech-2018, 22-23 October 2018, Saint Petersburg, Russia.

6. V. S. Teixeira, J-P Kalckhoff, W. Krautschneider, D. Schröder. Bioimpedance Analysis of L929 and HaCaT Cells in Low Frequency Range. Current Directions in Biomedical Engineering 2018; 4(1):1-4. In: 52nd DGBMT Annual Conference, 26-28 September, 2018, Aachen, Germany.

7. V. S. Teixeira, J-P Kalckhoff, W. Krautschneider, D. Schröder. Electrical Impedance Spectroscopy Measurement of in Vitro Cells Solutions in order to Distinguish Different Cells Types. SAFE Workshop – annual conference on Microsystems, Materials, Technology and RF Devices, Twente University, Enschede, The Netherlands, June, 2018 (Poster and Presentation)

8. V.S. Teixeira, J-P Kalckhoff, W. Krautschneider. Impedance Spectroscopy Measurement of Ionic Solutions in Order to Distinguish between the Different Ions. In: ICT Open 2017 Conference Proceedings der NWO, 2017, p. 14-17 Amersfoort, The Netherlands, March 21-22, 2017.

9. V. S. Teixeira, D. L. Villarreal, D. Schöder, W. Krautschneider. Circuit Modelling of Action Potential Generation and Propagation in Damaged Nerve Cells. ICT Open Conference, March 2015, Amersfoort, The Netherlands. (Poster & Presentation)

10. V. S. Teixeira, D. L. Villarreal, D. Schöder, W. Krautschneider. Concise simulator for neuromuscular stimulation. 11. Hamburger Studententagung für Innovative Medizin und Biotechnologie, May 14, 2014, Hamburg, Germany.

Chapter 2

Theoretical Background

All existing matter is formed of atoms. And the atoms themselves are formed of electrons (negatively charged), protons (positively charged) and neutrons (no charge). The atoms that form the matter stay together by means of atomic (intramolecular) and intermolecular forces. When an external electric field is applied to such charged matter it provokes the rearrangement of the charges. Free charges physically move (drift) and cause conduction currents. Bound charges which are attached to their molecules are displaced and orient themselves in the direction of the electric field causing a displacement current. If the impedance of such matter is measured, the effects of the conduction currents will be observed externally in the real part of the impedance, while the effect of the displacement current will be measured in the imaginary part of the impedance.

Non-metallic materials show the ability to be polarized, namely to show an increase in its dielectric constant value when submitted to the influence of an external electric field. The external electric field causes the redistribution of charges present on the material and its dielectric response is a measure of how strong this charge redistribution occurs. In this sense, dielectric spectroscopy, or more precisely when applied to biological materials biopimpedance spectroscopy, is the science that correlates the dielectric properties of biological materials with its microscopic polarization and conduction behavior [9]. Considering that each biological material has its own characteristic dielectric behavior, this behavior can be correlated to its internal structure. That is a powerful concept and it
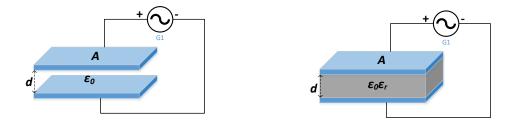
FIGURE 2.1: Illustration of dielectric constant concept using a parallel plate capacitor example

will be extremely useful especially when dealing with cancer tissues as will be shown in future chapters.

Figure 2.1 illustrates the concept of dielectric constant using a parallel plate capacitor example. In a perfect empty parallel plate capacitor (left figure) its capacitance C_0 is given by equation 2.1, where ε_0 is the vacuum permittivity, A is the area of the electrodes, which are separated by a distance d. If a dielectric material is inserted between the two metal plates (right figure), an increase in the capacitance is observed due to the additional charge density induced by the electric field and this capacitance is given by equation 2.2. The additional increase in the capacitance is a measure of the ability of the material to polarize and it is called its dielectric constant or ε_r. For most materials, including biological cells and tissues, ε_r varies with frequency.

$$C_0 = \frac{\varepsilon_0 A}{d} \tag{2.1}$$

$$C = \varepsilon_r C_0 = \frac{\varepsilon_r \varepsilon_0 A}{d} \tag{2.2}$$

2.1 Biological Cells

Any organism which is alive is formed of cells. Cells are membrane enclosed living units able to duplicate themselves and form new cells. A new cell only is formed by a pre-existing one. Cells are basically divided in two types: prokaryotics and eukaryotics. Prokaryotics are simple single celled organisms, which do not have a membrane enclosing their nucleus and organelles. For all prokaryotes the DNA floats in the cytosol together with the other cell organelles.

2.1.1 The Eukaryotic Cell

In contrast to prokaryotic, eukaryotic cells have their genetic material, i.e. the DNA, separated from the other cell components by a membrane forming the nucleus. Additionally, eukaryotes have membrane enclosed organelles. In general, they are larger and more complex than prokaryotes. They can live as single celled organisms (e.g. yeast, amoebae) or as multicellular organisms (e.g., plants, funghi and animals). All multicellular organisms are formed from cells. The most common organelles found in animal cells will be described in the next subsections.

2.1.1.1 Nucleus

The nucleus is a double membrane enclosed organelle which contains the genetic material of the cell, the DNA. In eurkaryotic cells it is normally the largest organelle. The DNA is responsible for keeping and carrying the genetic information from the cell and transmitting this information to its progeniture. The double membrane which encloses the nucleus is called nuclear envelope.

2.1.1.2 Cytosol

The cytosol is the liquid material which fills the cell in between the cellular membrane and the nuclear envelope. The cytosol is crowded of large and small molecules, nutrients and

organelles. In the cytosol proteins are fabricated by ribosomes and also the digestion of nutrients occurs. In the cytosol the three different types of cytoskeleton filaments moves proteins and organelles inside the cell. Also there, molecules are in constant random and thermal motion and in collision.

2.1.1.3 Mitochondria

Mitochondria are responsible for the cellular respiration. They are found in all eukaryotic cells and harvest energy from the oxidation of sugars. During this process they produce Adenosine Tri-Phosphate (ATP) which is the main energy source of the cells. By this way they consume oxygen and release carbon dioxide, therefore the name cellular respiration. Similar to the nucleus, they also contain DNA and are enclosed within two membranes where the inner is highly convoluted and the outer membrane is smooth. Mithocondria also reproduce by dividing in two.
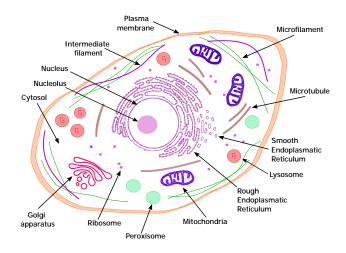
FIGURE 2.2: Diagram of an eukaryotic cell showing its main internal organelles. Observe that differently from the prokaryotic cells, the eukaryotic cells have all their organelles enclosed between membranes, especially the nucleus.

2.1.1.4 Endoplasmic reticulum

The endoplasmic reticulum is responsible for fabricating most of the cell membrane components and the materials to be exported out of the cell. Its membrane is contiguous to the nuclear membrane. Researchers observed that cells specialized in protein secretion have a very large endoplasmic reticulum [6].

2.1.1.5 Golgi Apparatus

The Golgi apparatus is a stack of flat sacs that modifies molecules fabricated in the endoplasmic reticulum and pack them to be transported to another cell organelle or to be expelled from the cell.

2.1.1.6 Lysossomes

Lysossomes are small, irregularly shaped organelles responsible for the intracellular digestion. They digest and release nutrients for the cell and also break unwanted molecules for recycling or excretion.

2.1.1.7 Cytoskeleton

The cytoskeleton in resemblance to human skelet can be considered the cell skelet. It is responsible for cell's movements and also for the movement of large molecules, organelles and chromossomes inside the cells during cell division. It is composed of three types of filaments: actin, microtubules and intermediate filaments. Actin are the thinnest filaments, followed by intermediate and the thickest are the microtubules. The three types of filaments organized together give the cell its strength, control its shape and drives and guides its movements. Therefore, cytoskeleton filaments are responsible for governing the internal cell organization and its external characteristics.

2.1.1.8 Peroxisomes

Peroxisomes are small membrane enclosed sacs. They are the place where hydrogen peroxide is used to inactivate toxic molecules for the cell. They also form membrane enclosed vesicles to carry components from one organelle to the other.

2.1.2 Cellular Membrane

Cellular membranes are the enclosing protection layer of eukaryotic cells; they separate the extracellular fluid from the intracellular. Among its important functions are the active and passive transport of ions (e.g. Na^+, K^+, Cl^-) from the inside to the outside and from the outside to the inside of the cell through specific protein ionic channels. They are also responsible for keeping the resting potential between the inside of the cell and the outside in a stable value that varies according to the cell type[1]. Cell membranes give the cells their shape and allow the connection to neighbooring cells or extracellular matrix through attachment proteins (cadherins and integrins) to form the tissues. They are also populated by sensor proteins that allow them to communicate and exchange signals with each other and receive signals from the environment.

Cellular membranes are mainly composed of a phospholipid bilayer transpassed by different types of proteins. The type of proteins present differs from one membrane to each other, what gives its proper characteristics. Each phospholid molecule is formed from a hydrophilic ("water loving") head facing the water environment and a hydrophobic ("water fearing") tail, facing the interior of the membrane. Prokaryotic cells, e.g. bacteria and archea, have only the extracellular membrane while eukaryotic cells have the external and also internal membrane compartiments for the organelles. Although the membranes arrangement is similar, the proteins present in the cellular membrane and in the membranes of the internal organelles differ significantly [6]. Cellular membranes have a thickness that varies from 3 nm up to 10 nm depending on how the proteins are considered.

---

[1]For example: giant squid axon -70 mV; human sensory nerves from peripheral nervous system -90 mV. For a more complete list of cell membrane potential variation according to different cell types please see reference [7].

TABLE 2.1: Electrical parameters for the Giant Squid Axon (neuronal cell type).
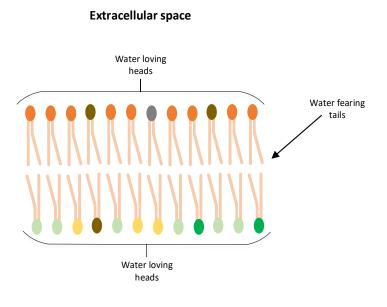
Param	Description	Value	Reference
G_{mem}	Conductance of membrane for live cell	$2mS/cm^2$	[10, 11]
C_{mem}	Cell membrane capacitance	$1\,\mu F/cm^2$	[11]
V_{mem}	Resting cell membrane potential	-70 mV	[11]

The cell membrane is elastic and allows the cell to change its shape and move. This is important for several cell types, e.g. human keratynocytes or skin cells, that need to move fast and connect to each other when skin is wounded to prevent excessive bleeding and the invasion of external microorganisms. The membrane is also not static, but behaves like a two dimensional fluid where molecules that form it can move in the plane and also change position. That allows molecules and proteins to diffuse easily through the membrane layer. The fatty acids that compose membrane cells are mainly formed in the endoplasmic reticulum and special enzymes called flippases position the phospholipids in the right place, even changing from one monolayer to the other. It means that the composition of the membranes facing the cytosol of the cell is different from the composition facing the extracellular medium. That also applies to organelles's membrane. This characteristic is very important for proper function of the proteins that transpasses the cell membranes.

The lipid bilayer of cell membranes works mainly as a barrier for diffusion. Nevertheless, most of membrane functions are performed by their attached proteins. In animal cells proteins constitute approximately 50% of the membrane mass [6], the rest being the phospholipids and carbohydrates. Given the difference in size and weight, i.e. phospholipids are much smaller, proteins are less abundant than phospholipids.

2.2 Electrical Properties of Biological Systems

Live biological cells solutions and tissues show dispersions when submitted to frequency variable electric fields. The mechanisms behind the dispersions are, nevertheless, diverse. In low frequency ranges, ionic clouds are formed around suspended charged colloidal particles, e.g. biological cells and tissues. The deformation of the clouds caused by

FIGURE 2.3: Schematic structure of phospholipid bilayer that composes cell membranes. Observe that the hydrophilic heads face always the aquous environment and the tails the middle of the membrane, far from the water. Observe also that composition of the lipid bilayer facing the cytosol is different from the one facing the extracecllular medium (illustrated by different colors).
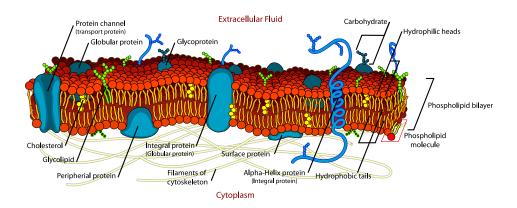
FIGURE 2.4: Detailed schematic of a cell membrane, showing its different components including several types of proteins, carbohydrates, phospholipid molecules, cholesterol and the filaments that gives its strength and allows the cell to change its shape and move. Extracted from [12].

frequency variable electric fields gives rise to α-dispersion. The enourmous values of dielectric constants observed in biological materials in low frequencies are due to α-dispersion [13–16].

From approximately 100 kHz to some tenths of MHz Maxwell-Wagner effects lead to β-dispersion. The relaxation is caused by charge separation and accumulation at the interfaces between the extra- and intra-cellular fluids due to the cellular membranes. Charge needs time to accumulate in one side (intra-) and the other (extra-) cellular medium. Therefore when the frequency of the electric field increases and the charges are not able to follow its speed β-relaxation is observed. The time constant of the relaxation mechanism will depend on the cell membrane capacitance and resistance, intra- and extra-cellular fluids resistivities and also from the cell radius [14, 17, 18].

The γ-dispersion is observed above 1 GHz and is due to the high water content existent inside cells and tissues. Considering that water relaxes close to 20 GHz, γ-effect is attributed to the dipolar relaxation of water dipoles inside biological matter. Another small dispersion (δ) extending from approximately 100 MHz until some GHz due to protein bound water can also be observed [14, 17].

The discussed so far brings the important question: What is a dispersion? Dispersion is defined as the variation of the dielectric properties of biological material, e.g. biological cells suspensions and tissues, observed when those materials are submitted to frequency variable electric fields. It is in normally expressed as a decrease in the dielectric constant or permittivity $\varepsilon(f)$ and an increase in the conductivity $\sigma(f)$ of the biological material as the frequency of the applied electric signal increases. Schwan in 1994 in his famous paper [14] illustrates the expected dispersions of biological cells suspensions and tissues (see fig. 2.5). Alternative representations like Bode plots, Nyquist plots and conductivity are also extensively used and will be presented in future sections. Only polarizable materials will exhibit dispersions; non-polarizable dielectric or metals will not present any [10].

Similar to a signature or fingerprint the dispersion curve or the characteristic spectral behavior of biological cells suspensions can possibly be used to differentiate cell types and status. In [19] authors measured the electric properties of two lines of breast cancer cells, compared with normal healthy breast cell tissue and showed in their results that the
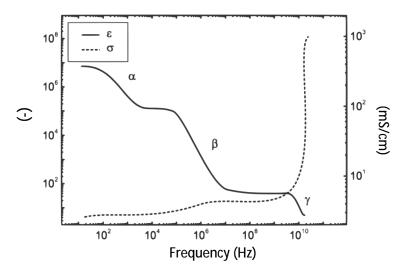
FIGURE 2.5: Illustration of the expected relaxations or dispersions in biological cells suspensions. The continuous line represents the permittivity or dielectric constant and the dashed line the conductivity of the biological material. Adapted from [14].

three types of cells have a characteristic electrical signature variable with frequency that can be used to differentiate among the cell types. In another study, O' Rourke *et al.* in [20] measured the dielectric properties in-vivo and ex-vivo of human normal, malignant and cirrhotic liver tissues and they found significant differences in their wideband values.

The frequency dependency of the dielectric properties of biologic materials when submitted to an electric field is attributed to the membrane polarization phenomena. Even when membrane polarization is well defined on a wide frequency range, the exact interaction mechanisms inside the cellular environment are not completely understood. Therefore, dielectric spectroscopy performed at the cellular and molecular level is progressively emerging as a diagnostic technique as it permits the non-invasive, label-free and real-time probing of cells in their culture biological medium [21]. One of the major challenges on using this technique for diseases diagnosis is the miniaturization of the analyzing tools. Most of the existing ones are bulky and the cells have to be removed from their medium in order to have their electrical characteristics measured. The actual and major cellular analysis tools are optical detection based and also require bulky equipment as long as fluorescent tags that can interfere with cell activity and vitality and also have a time-consuming preparation phase.

2.3 Electrical Impedance Spectroscopy

Electrical Impedance Spectroscopy (EIS) or Bio Impedance Spectroscopy (BIS) when applied to biological matter is a simple and powerful technique to characterize systems. It consists in the application of a small amplitude frequency variable voltage signal to a material or sample and measuring its current response (potentiostatic EIS). For biological systems as very low AC voltages are used, e.g. 14 mV, no stress is exerted to the substance. Compared to conventional procedures for characterization BIS offers great advantage, as often staining has to be used in those procedures to identify the cells which degrades their vitality. If a current is applied and the voltage is measured it is named galvanostatic EIS. Current established applications of the technique are the characterization of battery systems, evaluation of painting quality in painting industry, estimation of body composition, evaluation of food quality control and currently under development to distinguish healthy from diseased cells and tissues [1, 3–5, 19–24].

The interesting about applying BIS to cancer tissues is that they have a spectral behavior quite different from their healthy counterparts and this has all to do with the effects of the cancer in the tissues themselves. Also, interesting information and conclusions can be drawn from the analysis and comparison of the spectral response of healthy and cancer tissues. Values such as cell membrane capacitance, cytoplasmatic resistance, tissue conductivity, among others are examples of parameters that can be derived. In this chapter a short revision about the topic is presented and the following chapters will show more details on how the impedance spectrum of healthy and cancer cells and tissues can be analysed and correlated to their status. In reality it means that BIS has the promise of being an excellent tool to aid hospital doctors in evaluating cancer status and the effectiveness of theraphies.

2.3.1 Mathematical Concept of Impedance

Impedance is defined as the ratio of the voltage applied per current measured of a system or sample. Mathematically:

$$Z(\omega) = \frac{V(\omega)}{I(\omega)} \tag{2.3}$$

Alternatively, it can also be expressed as the ratio of the sinusoidal signals applied and measured:

$$Z(\omega) = \frac{V_0 sin(\omega t)}{I_0 sin(\omega t + \theta)} \tag{2.4}$$

The same equation can also be expressed in polar coordinates as:

$$Z(\omega) = \frac{V_0}{I_0} \frac{e^{j\omega t}}{e^{j\omega t + \theta}} \tag{2.5}$$

The variable ω is the angular frequency of the signals, V_0 is the amplitude of the applied voltage and I_0 the amplitude of the measured current. Z represents the magnitude of the impedance and the angle θ is the phase angle between voltage and current. Observe that the three equations show the same information in different ways. The amplitude of the applied signal V_0 should be small enough in order to keep the linearity of the system and avoid harmonics. The frequency response of the substance can be identified and it is specific for the substance under investigation. As impedance varies with frequency, it has a defined value for each discrete frequency point.

Impedance can also be expressed as a function of permittivity or dielectric constant (ε) and conductivity (σ) of the sample as:

$$Z(\omega) = K * \left(\frac{1}{\sigma(\omega)} + \frac{1}{j\omega\varepsilon_0\varepsilon_r(\omega)} \right) \tag{2.6}$$

Where ε_0 is the permittivity of vacuum and ε_r is the relative permittivity of the medium. The constant K or cell constant defines the geometry of the measurement setup and is calculated as the ratio of the distance of the electrodes per area (see fig. 2.1). For a parallel plate geometry, where electrodes are of rectangular shape with area A and separated by a distance d the cell constant is calculated as:

$$K = \frac{d}{A} \tag{2.7}$$

In a situation where it is not possible to determine K analytically it can be determined experimentally by measuring a standard solution, e.g. *KCl*, with known conductivity.

The relative permittivity $\varepsilon_r(\omega)$ expresses the ability of the system to store electrical energy and it is related to the capacitance of the system or equivalently the imaginary part of the impedance [10]. While the conductivity $\sigma(\omega)$ represents the ability of the system to conduct electrical energy with its free charges. Inside cells and tissues the conductivity is caused by the movement of free charges, e.g. free ions abundant in biological media, and the permittivity is caused by charge separation and accumulation at the interfaces of cell membranes. Observe that both σ and ε for biological tissues and cells are frequency dependent.

While $\varepsilon(\omega)$ and $\sigma(\omega)$ represents the stored and transmitted energy respectively, the impedance $Z(\omega)$ in its general terms expresses the ability of a system to resist the passage of electric current. The impedance is defined as an extension to Ohm's law of electric current where not only the resistance to the passage of current expressed in the real part of the impedance is considered, but also the stored energy in the system represented in the imaginary part. The phase angle θ in equation 2.5 shows how much the electric current generated in the biological system will lag the voltage applied to it. A summary of the mathematical representation of impedance data is given in table 2.2.

2.3.2 Graphical Representation of Impedance Data

Impedance data can be represented in several forms, by means of polar Bode plots where impedance magnitude and phase are plotted against frequency or alternatively as rectangular Bode plots as real and imaginary parts against the frequency. Other useful representations include Nyquist plots, modulus plot and permittivity and conductivity plots. Different representations of the experimental data allow to visualize distinct details of

TABLE 2.2: Mathematical representation of impedance data.

	Equation	Description
(a)	$Z(\omega) = \dfrac{V(\omega)}{I(\omega)} = \dfrac{|V|}{|I|} \angle\phi = |Z|\angle\phi$	Magnitude $|Z|$ and phase ϕ
(b)	$Z(\omega) = K\left(\dfrac{1}{\sigma(\omega)} + \dfrac{1}{j\omega\varepsilon_0\varepsilon_r(\omega)}\right)$	Conductivity σ and permittivity ε
(c)	$Z(\omega) = R + j\omega X$	Real R and imaginary X part of impedance
(d)	$|Z| = \sqrt{R^2 + X^2}$	Magnitude of impedance
(e)	$\phi = 57.3\tan^{-1}\dfrac{X}{R}$	Phase of impedance
(f)	$K = \dfrac{d}{A}$	Cell constant. The letter A indicates electrode's area and d their separation distance
(g)	$\sigma(\omega) = \dfrac{K}{R(\omega)}$	Sample conductivity
(h)	$\varepsilon(\omega) = \varepsilon_r\varepsilon_0 = \left|\dfrac{K}{j\omega X}\right|$	Sample permittivity
(i)	$C = \dfrac{1}{j\omega X}$	Sample capacitance
(j)	$\omega = 2\pi f$	Angular frequency

dispersions that often are not easily visible in other types, therefore in the data interpretation more than one representation type is normally used. Figure 2.6 shows a summary of the most common representations.

2.3.3   Electrical and Electrochemical Circuit Elements

While in normal electric circuits there exists real resistors, capacitors, inductors, among others, in biological systems such elements do not exist, but are used as an abstraction to interpret the ability of such biological systems to conduct currents and separate charges.
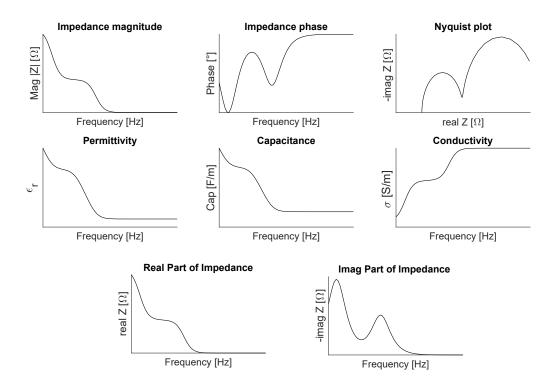
FIGURE 2.6: Graphical representation of impedance data. Observe the similarity between the different representation types; this is not by case as several representations are derived one from each other. The distinct visualizations of impedance data facilitate the analysis and interpretation of the experimental data and allows to search for "hidden" effects or dispersions. Directly from the graphs, several values can be read like the value of the medium resistance R_s from the Nyquist plot and the values of the relaxation frequencies f_c from the Bode plots.

When fitting experimental impedance data of biological cells and tissues the following elements are normally used: resistors "R", capacitors "C", Constant Phase Elements "CPE's", inductors "L" and Warburg Elements "W".

The resistor *R* is a linear element, which follows Ohm's law in all currents and voltages. The value of its impedance is constant and independent of the frequency and the currents flowing through a resistor are always in phase with the voltages. In biological systems resistors represent the current measured by external devices as an effect of the movement of free charges, specifically ions abundant in biological media, e.g. Na^+, K^+, Cl^-. Alternatively resistors will also represent the charge exchange between the interfaces of

electrodes and biological media, also called charge transfer resistance R_{CT}. Important to highlight is that, depending on the application, a very large R_{CT} is desirable, i.e. that very few or zero current is injected in the biological system.

The second most commonly used element, the capacitor has only an imaginary impedance component which value decreases as the frequency of the sinusoidal signal applied increases. The currents flowing through a capacitor are phase shifted 90° in relation to the voltages. In biological systems capacitors represent the cell membranes and their ability to separate charges, accumulate charge at the interfaces of different materials and polarize, i.e., change orientation within the electric field.

The third most common element used to fit impedance data of biological systems is the Constant Phase Element or CPE, which is a variation from the traditional capacitor. While in normal electrical circuits a CPE is inexistent, in electrochemical systems they are very common. A CPE behaves like a "capacitor", nevertheless it has an impedance dependence in relation to frequency as a function of an exponent α that varies from $0 < \alpha < 1$. In real electrochemical systems capacitors are never "perfect capacitors" and imperfections in the surface of cells and electrodes are compensated by the exponent in the CPE element. The value of the real capacitance can be calculated directly from the CPE's value [25].

Inductors L like capacitors have only an imaginary part of impedance, which value increases with the frequency. All the currents flowing through inductors are -90° phase shifted in relation to the voltages. For the normal electrochemical systems analyzed in this thesis, namely cells suspensions and solid tissues, inductive behavior will appear only as a parasitic effect due to cables or experimental errors due to potentiostat non-idealities [26].

The last element that may appear when fitting impedance data of tissues and cells suspension is the Warburg element. It is used to model the diffusion of reactant species in the electrolyte specially visible in low frequencies. In high frequencies, reactants do not have enough time to move and the Warburg element value decreases. It is easy to see it from the Nyquist plots where it appears as a straight line with an angle of 45°. Borkholder in his thesis [27] gives an excellent visualization of the process generated by a Warburg element. Basically it is well represented by a resistance R_W in parallel with a capacitance

TABLE 2.3: Common circuit elements used to fit impedance data of biological cells suspensions and tissues.

Element	Current vs. Voltage	Equation
R	$v(t) = R * i(t)$	$Z_R = R$
C	$i(t) = C * dv(t)/dt$	$Z_C = 1/j\omega C$
L	$v(t) = L * di(t)/dt$	$Z_L = j\omega L$
CPE	$i(t) = Y_0 * \partial^\alpha v(t)/\partial t^\alpha$	$Z_{CPE} = 1/Y_0(j\omega)^\alpha$
W	$i(t) = W_0 * \partial^\beta v(t)/\partial t^\beta$	$Z_W = 1/W_0(j\omega)^\beta$

C_W, with the magnitudes of both the real and imaginary part of such impedance equal, what justifies the 45° in the Nyquist plot.

Table 2.3 shows a summary of each element, its explanation and its mathematical behavior with the frequency. The variables R stands for resistance, C for capacitance, L for inductance, Y_0 for capacitance of the constant phase element and W_0 Warburg element constant. The parameter α in table 2.3 will have a value between $0 < \alpha < 1$ and $\beta = 0.5$. The study and definition of fractional derivatives is out of scope of this thesis; detailed discussions can be found in [28–30].

2.3.4 Conditions for Valid EIS Data

In order for EIS experimental results to be valid, the system should be linear, casual and stable [10, 31, 32]. A linear system, will obey Ohm's law in all its frequencies, namely $V = ZI$, i.e., the of value of the impedance Z is independent of the magnitude of the applied potential. A linear system means also that no harmonics are generated. In order for EIS systems to be linear a perturbation small enough, namely $\leq 50mV$ should be used [10, 27, 31, 32]. Specially in electrochemical cells as in these systems the electrodes are in direct contact with the electrolyte and large signals not only generate harmonics, but also increase the speed of electrode's corrosion rate. In that case, the difference in electrode corrosion state generates strong artifacts in low frequencies during the experiments what invalidates the measured data.

The second condition for valid EIS data is stability. A stable system does not change during the measurement. EIS experiments only work if the system is stable during the whole measurement. Therefore, open circuit potential (OCP) should be checked always before and possibly after each experiment.

The last condition for valid EIS data is casuality, that is the system responds only to the applied perturbation. So all the responses measured in the system, come from the applied potentials.

Chapter 3

Development of a Four Electrode Terminal Chamber System

In this chapter the detailed steps in the development of a four-electrodes-terminal (4T) chamber system to measure the impedance of suspended cells is described. The objective of such system is to allow the measurement of the impedance of suspended biological cells in low frequency ranges, i.e. $f < 1\ kHz$, with a minimum error. At those frequency ranges, electrode polarization or double layer (DL) effects create a large parasitic impedance on the system which prevents the observation of the real impedance of the cells. Nevertheless DL effects are not the only artifacts that appear in those frequencies; others may also show up and are discussed in a dedicated section. One section is also dedicated to explain how to be sure before performing any suspended cells experiment that the measurement has no artifact and that the observed response comes really from the biological cells.

3.1 Electrode Polarization in Low Frequencies

3.1.1 Interfacial Capacitance

Strong salts, e.g. $NaCl$, KCl and $CaCl_2$ when added to water dissociate into ions to form electrolytes. When metals are immersed in electrolytes, chemical reactions occur exchanging electrons between the solution and the electrode causing the accumulation of charge close to electrode surface. This space charge region close to electrode is called in literature as double layer DL [10, 27]. The DL is formed between the metal surface and the electrolyte with exact structure difficult to estimate, and several authors worked on modelling it throughout the years: Helmholtz (1879), Gouy (1910) and Chapman (1913). A more complete and well-accepted model turned to be a combination of the works of the three of them summarized by Stern (1924) and is called Helmholtz-Gouy-Chapman-Stern model, where the charge accumulation in this layer is modelled by the so-called interfacial or double layer capacitance C_{DL} [10, 27, 33].

This interfacial capacitance is simply a circuit element which is used to model the complex electrochemical phenomena occurring due to electrode-electrolyte contact. The C_{DL} is divided in three parts: the Inner Helmholtz Plane (IHP), Outer Helmholtz Plane (OHP) and the diffuse space charge (see figure 3.1). The IHP is composed of adsorbed ions and oriented water dipoles direct in contact with the electrode surface. The OHP is formed of immobile hydrated ions tightly packed above IHP and attached to it. The last layer, the diffuse space charge, contains mainly partially mobile oriented water dipoles and hydrated ions. The three layers of space charge are modelled by two capacitances in series, namely C_H where IHP and OHP effects are combined in one capacitance representing the immobile charges and $C_{diffuse}$ that represents the capacitance generated by the partially mobile charges of the diffuse layer.

In the Helmholtz space, potential is maximum at the electrode interface and decays linearly until the boundary between OHP and diffuse layer; this boundary also separates immobile from mobile charges. In the diffuse space charge the potential drop is approximately exponential and the charges although being able to move partially do not have the same mobility as the charges in the bulk electrolyte. Figure 3.2 shows the potential
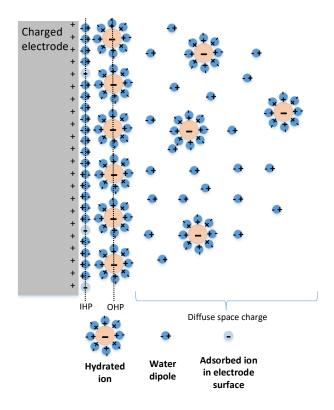
FIGURE 3.1: Illustration of the DL space charge showing its composing parts: Inner Helmholtz Plane (IHP), Outer Helmholtz Plane (OHP) and diffuse space charge.

profile drop from the double layer and equations 3.1, 3.2 and 3.3 how C_{DL} is calculated. The variables from equations 3.1 to 3.3 are detailed described in table 3.1. In the table, "Exp" indicates the data that comes from experiments.

$$C_H = \frac{\varepsilon_0 \varepsilon_{OHP}}{d_H} \tag{3.1}$$

$$C_{diff} = \frac{\varepsilon_0 \varepsilon_{diff}}{L_D} \cosh\left(\frac{zV_0}{2V_T}\right) \tag{3.2}$$

$$L_D = \sqrt{\frac{\varepsilon_0 \varepsilon_{diff} V_T}{2n_0 z^2 q}} \tag{3.3}$$

In equation 3.1 C_H is the Helmholtz capacitance per electrode area, formed by adsorbed
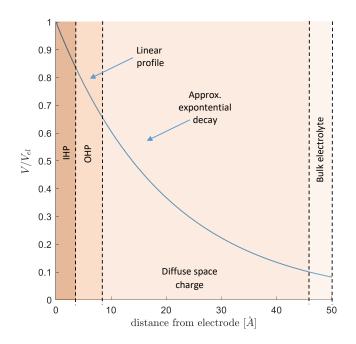
FIGURE 3.2: Potential profile distribution close to electrode surface. The closest layer to electrode is IHP, the second layer is OHP and the third layer the diffuse space charge. Observe that the potential drop is nearly linear in the IHP and OHP, but decays exponentially in the diffuse space charge. Adapted from [27].

immobile ions and water dipoles strongly attached to electrode surface by electrostatic attraction. The C_{diff} from equation 3.2 is the diffuse layer capacitance per area formed by partially immobile hydrated ions, being the surface that comes just above Helmholtz plane. And at last, L_D or λ_{Debye} from equation 3.3 is the Debye length, which is the distance from electrode surface towards the bulk electrolyte where the potential at the ionic cloud drops to $1/e$ of its interface value.

The first term in the calculation of C_{DL}, namely C_H, is simply a capacitor separated by a distance d_{OHP}. The second term, i.e. C_{diff}, is a capacitor separated by a distance L_D. The hyperbolic cosine that appears in equation 3.2 is to compensate for the mobile charges. The double layer or interfacial capacitance C_{DL} will be the series combination of C_H and $C_{diffuse}$. An extensive and detailed review of all steps to obtain equations 3.1 to 3.3 is given in [10, 34, 35].

TABLE 3.1: Parameters to calculate double layer capacitance.

Variable	Value	Description	Reference
ε_0	$8.854 * 10^{-12}$ F/m	Vacuum permittivity	[36]
ε_{OHP}	$6 < \varepsilon_{OHP} < 78$	OHP relative permittivity	[27]
ε_{diff}	≈ 1	Diffuse space charge relative permittivity	[27]
d_{OHP}	0.5 nm	Length of OHP	[27]
L_D	0.1 nm $< L_D <$ 10 nm	Debye length	[27]
V_0	14 mV rms	Potential at electrode surface	Exp
q	$1.6 * 10^{-19}$ C	Elementary charge	[36]
K_B	$1.38 * 10^{-23}$ J/K	Boltzmannn constant	[36]
n_0	ions/Liter	Bulk number of ions in electrolyte	Exp
T	298.15 K	Experimental temperature	Exp
V_T	26 mV	Thermal voltage	[27]
z	E.g: $+1$ for Na^+, -1 for Cl^-	Valence of the ion	Exp

3.1.2 Charge Transfer Resistance

Apart from the double layer space charge that develops at electrode-electrolyte interface and along a few nanometers apart from it, an additional faradaic current in general flows from the electrode towards the electrolyte and vice-versa. This current is strongly dependent on electrode material and electrolyte and is specific for each combination electrode-electrolyte making its calculation difficult. Nevertheless, if an overpotential smaller than 50mV is assumed, a simplified equation for the charge transfer resistance can be obtained [27]:

$$R_{CT} = \frac{V_T}{J_0 z} \tag{3.4}$$

The J_0 is the so called exchange current density, z is the valence of the ion exchanged between electrode and electrolyte and V_T is the thermal voltage as defined in table 3.1. In general R_{CT} is experimentally determined by means of cyclic voltammetry and from R_{CT} the current density J_0 is calculated. It is important to mention that equation 3.4 is only valid for small perturbations, namely $v < 50mV$, as it was derived assuming a linear

relationship between applied voltage and measured current. As electrochemical systems are highly non-linear such assumption is only valid for very small potentials.

3.1.3 Warburg Impedance for Diffusion Modelling

At very low AC frequencies, ions have enough time to move from one side to the other following the variation of the electric field. In this situation, charge has time to accumulate close to electrodes. Apart from the interfacial capacitance C_{DL} and charge transfer resistance R_{CT}, a new element to represent the frequency dependence of the diffusional impedance, namely Warburg impedance Z_W, is used. It is mathematically defined as [10, 27]:

$$|Z_W| = \frac{k}{\sqrt{j\omega}} \tag{3.5}$$

Where k is the Warburg coefficient, ω is the angular frequency and j the imaginary unit. Observe that, differently from a capacitor that has a frequency dependent impedance proportional to $1/f$, the Warburg element has a frequency dependency proportional to $1/\sqrt{f}$. Borkholder in his Thesis gives a visualization of Warburg element as possibly being represented by a resistance R_W due to diffusion in parallel to a capacitance C_W caused by diffusion and with an angle of $45°$ between the two of them in the Nyquist plot. In his Thesis he also gives three analytic expressions to calculate the values of Z_W, R_W and C_W [27]. Alternative formulations for Z_W depending on the quantity of ionic species involved and the type of the diffusion process are extensively detailed in [10, Chap. 5]. In practice, the value of Z_W is determined by fitting the experimental data to an equivalent circuit model.

3.1.4 Solution Resistance

The last circuit element in the equivalent circuit model to represent the electrode-electrolyte interface is the spreading resistance, solution resistance or bulk resistance R_s or R_{bulk}. As

the name says, this resistance is used to model the effects of currents flowing from one electrode to a distant one. For a parallel plate configuration an uniform current is flowing between the electrodes. For this case, the solution resistance can be calculated by the means of [10, 27]:

$$R_s = R_{bulk} = \rho \frac{d}{A} \tag{3.6}$$

Or in terms of the conductivity σ as:

$$R_s = \frac{1}{\sigma} \frac{d}{A} \tag{3.7}$$

Or by last, in terms of the mobility and concentration of ions composing the electrolyte [10]:

$$R_s = \frac{d}{AF} \frac{1}{\sum z_i u_i C_i} \tag{3.8}$$

The variable d represents the distance between the two electrodes, A the electrode's area, ρ the resistivity of the solution and σ its conductivity. Observe that the conductivity of the electrolyte σ depends on the Faraday's constant F, the ionic valence z_i and mobility u_i of each ion composing the electrolyte and its concentration C_i. Observe also that $\rho = 1/\sigma$. The solution or spreading resistance in electrochemical cells is used to model the mobility of the ions in the electrolyte, which is dependent of several factors like temperature, type of dissolved ions and their concentration. Therefore, solutions with higher concentrations will have a lower R_s and with lower concentrations a higher R_s as fewer ions contribute to the conduction of currents.

3.1.5   Equivalent Circuit of Electrode-Electrolyte Interface

Figure 3.3 shows the complete circuit used to model electrode-electrolyte interface. Observe the presence of the double layer or polarization capacitance C_{DL} in parallel with

the charge transfer resistance R_{CT} to model the Faradaic current exchange between electrode-electrolyte, the Warburg element represented by Z_W to model the diffusion of ionic species in very low frequency ranges and the solution resistance R_s to model the ionic currents in high frequencies.
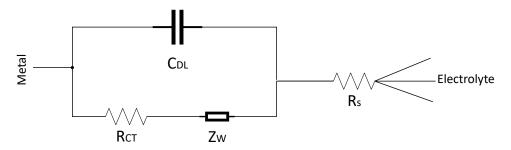
FIGURE 3.3: Equivalent circuit to model the electrode-electrolyte interface. Adapted from [10, 27].

3.2   Measurement Systems and Electrodes Setup

Electrochemical systems can be measured in several ways: by using two-electrodes-terminals (2T), three-electrodes-terminals (3T) or four-electrodes-terminals setup (4T). The choice of which setup to use will depend on what needs to be observed in the experiment. For instance, if electrode's corrosion rate is to be observed a 3T is preferred. When batteries or supercapacitors are analyzed to measure its polarization capacitance, a 2T setup will be used. In the analysis of biological cells suspensions and tissues a 4T setup is the recommended for frequencies below 1 kHz.

Figure 3.4 shows a simplified schematic view of the potential drop in an electrochemical cell. The two parallel grey bars represent the parallel plate electrodes. Each point highlighted with a letter is a possible connection point for one electrode terminal. The black line represents the potential drop along the electrochemical cell at one instant of time when a sinusoidal wave is applied. Observe that at the highlighted instant of time the potential is maximum at the electrode connected to point A and it decreases along the electrochemical cell. Important to mention is that for a sinusoidal wave the signal

amplitude is varying constantly therefore the potential drop along the electrochemical cell also changes.
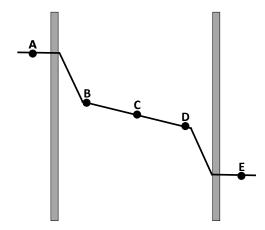
FIGURE 3.4: Potential drop in an electrochemical cell. Each capital letter represents a possible connection point of a potentiostat's terminal. Redraw from original based on [37].

Figure 3.5 shows a simplified circuit diagram of a potentiostat and its possible connections with an electrochemical cell (EC). The CA stands for Control Amplifier and it is the amplifier which controls the potential drop at the electrochemical cell (EC) by keeping it constant. It basically sums up the small input voltage (V_{in}) to the voltage output (V_{out}) and applies it again to the system. The acronym CE stands for counter electrode, RE for reference electrode, WS for working sense electrode and WE for working electrode. The V_{out} is the measured potential drop in the electrochemical cell (EC) and $V \propto I_{out}$ is a voltage output proportional to the current flowing into the electrochemical cell (EC). Observe that the electrochemical cell has four possible connection points (CE, RE, WS and WE) in the figure not connected for illustration purposes. Worthwhile noticing is that the two reference electrodes (RE and WS) are connected to the electrochemical cell (EC) by two high impedance (HiZ) buffers which have an input impedance in the order of Tera Ohms [38]. That is essential in order that no current flows neither through RE nor WS. If currents flow through RE and WS, the RE electrode potential cannot be kept constant, what makes impossible the EIS experiment. A pre-requisite for a good EIS experiment is a very stable and constant potential in the RE electrode. The current flowing into the electrochemical cell (EC) is sensed by measuring the potential drop in a resistor bank in

the figure represented by R_m in parallel with a variable capacitance. The value of R_m is automatically adjusted by the potentiostat circuit according to the impedance of the load (in this case the electrochemical cell). The potential proportional to the current flowing into the cell $V \propto I_{out}$ can be easily converted to current by means of Ohm's Law and knowing the value of R_m. The DA stands for Differential Amplifier.
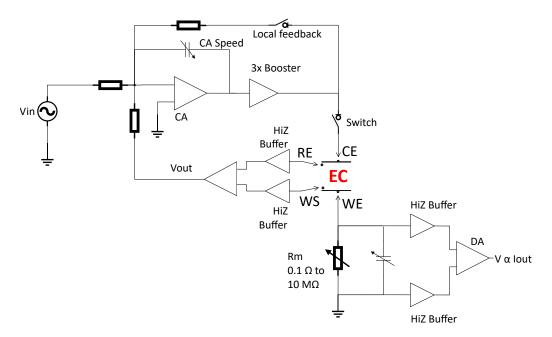
FIGURE 3.5: Simplified circuit diagram of a pontentiostat and its possible connections to an electrochemical cell. Adapted from [38].

3.2.1 Two-Electrode Measurement System

A potentiostat is a precise instrument used to measure the impedance of electrochemical cells. It has five shielded cable leads for measurements, namely working (WE), counter (CE), reference (RE), working sense (WS), counter sense (CS) electrodes plus a floating ground. In a 2T measurement system the WE and WS cable leads are shorted together and connected to point A in figure 3.4, while CE and RE are shorted and connected to point E. Therefore only two measurement points exist on the electrochemical cell. Compared to 3T and 4T setups, 2T is simpler and easier to be implemented. The drawback is that

36

the impedance increase in frequencies < 1 kHz due to electrode polarization is always present in 2T measurements.
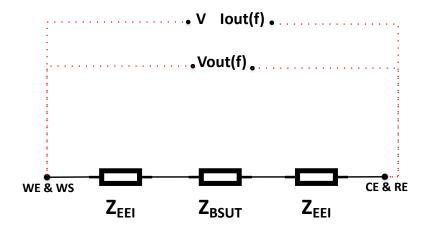
FIGURE 3.6: Simplified equivalent circuit model of an electrochemical cell connected in a 2-electrodes-terminal setup (2T). The electrochemical cell connections with the potentiostat leads are highlighted by means of red dotted lines; in reality a special shielded cable is used. The acronym Z_{BSUT} represents the impedance of the biological system under test and Z_{EEI} the impedance of the electrode-electrolyte interface. Observe that $V_{out}(f)$ is the measured output voltage and the $V \propto I_{out}$ represents the measured potential proportional to the current flowing into the electrochemical cell, both shown in figure 3.5. A substantial part of the measured impedance value in low frequencies ($f < 1kHz$) is due to polarization effects at electrode-electrolyte interface.

3.2.2   Three-Terminal Measurement System

The 3T measurement experiments are used in general to observe the reactions of the working electrode (WE) in a specific electrolyte or medium, for instance in battery experiments. In this case three connection points are used, namely, WE and WS electrodes are shorted and connected to point A, RE is connected to B, and CE is connected to point E in figure 3.4. The potential drop between WS and RE is measured and the current flowing into the electrochemical cell is collected at CE. This setup is specially interesting to study corrosion effects at electrode's surface. The RE electrode should be placed as close as possible to WE electrode in order to minimize electrolyte influence in the experiment. Still several potentiostas offer the possibility to compensate for electrolyte or solution resistance and subtract it from the experiments.
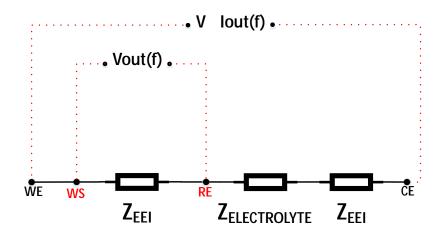
FIGURE 3.7: Equivalent circuit model of a 3T measurement system. Observe now that only the impedance of one electrode Z_{EEI} is measured. In practice a small part of the solution resistance will be also present in the measurement and must be compensated by the potentiostat. In the figure the $Z_{ELECTROLYTE}$ is the impedance of the electrolyte where the electrodes are immersed to observe the reaction; $Z_{ELECTROLYTE}$ is in general of ohmic nature (resistive).

3.2.3 Four-Terminal Measurement System

As already mentioned, in the four-electrodes-terminal setup (4T setup) the interest lies in measuring the behavior of the substance that is placed in the electrochemical cell without the effects of electrode-electrolyte interface. Therefore, in this setup four connection points are used, namely WE is connected to point A, WS to point B, RE to point D and CE to point E in figure 3.4. The equivalent circuit model of a 4T setup is shown in figure 3.8. Apart from all the impedances mentioned before, two additional ones appear, namely twice Z'_{EEI}, due to the needle reference electrodes used to measure the potential drop in the electrochemical cell. As those electrodes are made of metal (Pt-Ir) they also create a new electrode-electrolyte interface impedance (Z'_{EEI}) much smaller than the original Z_{EEI} due to their smaller area. Nevertheless, as at the end of the RE and WS electrodes there are two high impedance buffers connected in a differential amplifier configuration the input impedance seen by the current flowing into WS and RE is in the order of Tera-Ohms [38]. Thefore, the current flowing into those two reference electrodes

can be neglected as it is appromately zero. In practice, one can consider that the current flowing in the electrochemical cell flows mainly in the direction WE → CE or vice-versa; therefore the impedance "seen" by the potentiostat in a 4T setup is mainly Z_{BSUT}.
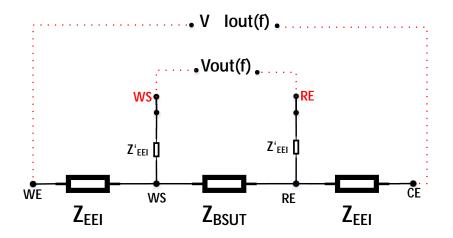
FIGURE 3.8: Equivalent circuit model of a 4T measurement system. In the 4T setup the impedance of the electrodes can be neglected and the measured impedance is equals to Z_{BSUT}.

3.3 Detailed ECM of the Experimental Setup

The complete ECM that represents the experimental setup is shown in figure 3.9. Observe the presence of the electrode-electrolyte interface impedace (Z_{EEI}) elements as the R_{CT}, Z_W and C_{DL} from both electrodes. The charge transfer resistance R_{CT} appears when electrodes are in equilibrium with electrolyte and are not corroding; in case corrosion is occurring R_{CT} is replaced by R_P, the polarization resistance. The impedance of the biological system Z_{BSUT} and the geometric capacitance CG are also shown. Two additional elements appear: C_{stray} and R_{leak}. The stray capacitance C_{stray} occurs due to the proximity of the WE and CE cables in the experimental setup which cause a mutual capacitance between them. The leak resistance R_{leak} should have a theoretical infinite value, i.e, for

a 4T setup that should not be a conductive path between WE-WS and RE-CE electrodes. In practice when the chamber is very small and get wet during experiments, the ionic solution used to suspend the cells can form a conductive path between the WE-WS and RE-CE electrodes, leading to equipment instability and experimental errors.
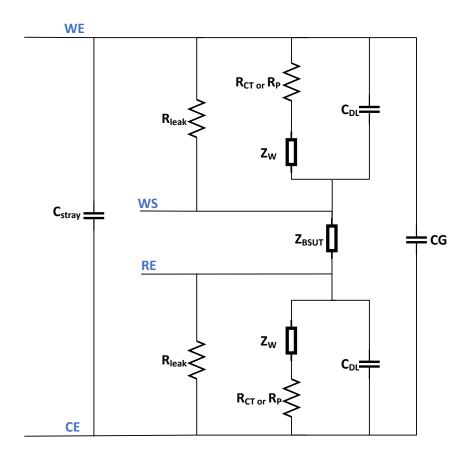
FIGURE 3.9: Detailed ECM of the experimental setup.

The current flows from WE to CE and vice-versa and the potential drop between WS and RE electrodes is kept constant by the potentiostat, which is constantly adjusting the applied potential. While in a 4T setup the impedance will be calculated by the potential drop between WS and RE divided by the current flowing through the cell, in a 2T setup the potential drop between WE and CE will be used instead. Observe that in both cases the current flowing through the cell is the same, the difference is only where the potential variation along the cell is measured.

Table 3.2 show typical values for the elements of the ECM of figure 3.9 calculated using the equations shown in previous sections of this chapter and also the experimental values.

TABLE 3.2: Typical values of the circuit elements composing the ECM.

Element	Description	Value	Comments
C_{stray}	Stray capacitance	443 fF	Assuming area $\approx 2.5 cm^2$ for crocodile clamps forming the capacitance.
R_{leak}	Leak resistance	∞	Desirable to be infinite.
R_{CT}	Charge transfer resistance	$13\ M\Omega$	Assuming Au in buffered saline [27]; otherwise fit.
Z_W	Warburg impedance	$28.3/\sqrt{(f)}$	Extracted by ECM fitting from experiments.
R_S	Solution resistance	$35\ \Omega$	For PBS. Chamber volume = 320 μl.
C_{DL}	Double layer capacitance	$10\ \mu$F	Assuming a C_{DL} typically of 30 μF/cm^2 [10, 27].
CG	Geometric capacitance	10 pF	Assuming $\varepsilon_{PBS} \approx 80$.

3.4   Designed System

The chamber was conceived as parallel plate electrodes system in order to have an uniform electric field distribution. The uniform field facilitates the interpretation of the experimental results and the extraction of information from it. In such a system, one electrode is used to apply the harmonic potential and the other to collect the current. Additional two reference electrodes are used to measure the potential drop along the electrochemical cell. Figure 3.10 illustrates the idea of the conceived system.

During the last five years several designs were fabricated. The first design had a total volume of 12.4 ml, big reference and active electrodes with an area of approximately 225 mm^2 [39, 40]. It was used to measure the impedance of two healthy cell lines, namely human keratinocytes HaCaT and mouse fibroblasts L929. The drawbacks of this version was its large size which required a large quantity of cells, making the experiments time consuming and expensive, and also it introduced an artifact in low frequencies due to the large width of the reference electrodes.

A second version was fabricated with a total volume of 1.6 ml; a reduction in volume of almost eightfold [23, 41]. It had smaller active electrodes of 64 mm^2 area and reference

electrodes of 1 mm^2. The chamber total length is 32 mm and the distance between the two reference electrodes is 24 mm. This version does not introduce artifacts in the experiments and it was used to measure the impedance of four cancer cell lines, i.e. PC-3, DU145, EOL-1 and MOLM13.

A third version of the chamber was fabricated by decreasing the distance between the two active electrodes (WE and CE) from 32 mm to 5 mm. It has a total volume of 320 μL. The objective of this version was to increase the strength of the electric field applied in the biological cells by decreasing the distance between the electrodes and therefore give a better signal. The second objective was of course the reduction of the chamber volume, which makes the experiments cheaper and faster as less cells are needed. The area of the active electrodes was maintained as 64 mm^2 for compatibility reasons. For the reference electrodes platinum needles were used instead of the 1 mm wide electrodes. Figure 3.11 shows the designed chamber. It was successfullly used to measure the impedance of several cancer cell lines, namely HT29, DU145, PC-3, MCF-7, SW620, T47D and
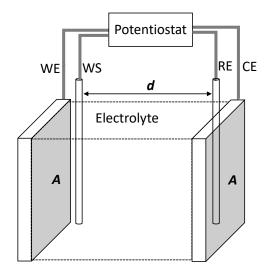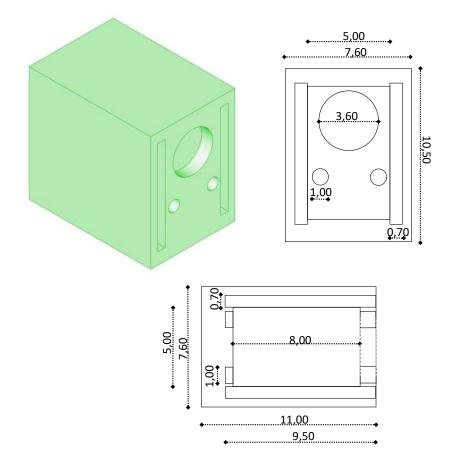
FIGURE 3.10: Conceived 4T chamber system. The WE and CE electrodes are used to apply the potential and collect the current, respectively. The two reference electrodes WS and RE are used to sense the potential drop throughout the electrochemical cell. The WS electrode must necessarily be placed close to WE and the RE electrode close to CE. The distance between WS and RE is indicated by the letter d and is equals to 5 mm in the final design. The area of the electrodes is indicated by A and is equals to 64 mm^2.

CaCo2. Details regarding the different cell types will be given in future chapters as the experimental results are presented and analyzed.

FIGURE 3.11: CAD view of the last version of the 4T chamber designed. On the top left-side the 3D view is shown, on the top right-side the upper view and on the bottom the side view. All dimensions are in milimeters. The chamber was conceived as a parallel plate electrodes system with distance between CE and WE of 5 mm. The circular opening on the top is used to insert the liquid with cell solutions and also remove it for cleaning. The small holes on the top and bottom are used to insert and fix the platinum needle reference electrodes (WS and RE). The squared holes on the sides are used to insert the two active electrodes (CE and WE). The chamber was rotated to the side by an angle of $270°$ for a better quality of the 3D printing. The total volume of this chamber is 320 μL.

A fourth version of chamber system was fabricated by decreasing further the distance between the active electrodes from 5 mm to 3 mm, the area of both electrodes was preserved as $64\ mm^2$. With this version it was not possible to measure a 4T setup, but it was

used in a 2T setup to measure the impedance of cells in high frequencies.

The chambers were fabricated with 3D printing techniques using the 3D printer *PreForm 2* from Formlabs. The clear resine V4 FLGPCL04 was used to print all the chambers and the printing resolution was set to its maximum, namely 25 μm, due to the small dimensions. Starting from the second version, all electrodes used were made of pure platinum for biological compatibility as platinum is a highly unreactive metal and release less ions in the solution. As cells are very sensitive to the metals they come in contact to, materials such as copper, silver, iron, among others should be avoided to prevent killing the cells during the experiments. Additionally, Pt offers a very stable potential at electrode-electrolyte interface, what is essential for good EIS experimental results.

3.5   Comparison 4T vs. 2T Measurements

Figure 3.12 shows the impedance measurement of DU145 cancer cells in the concentration 3 million cells/ml using a 2T setup. The same experiment was repeated three times with the same cell seed. The legend shows each experiment in different colors. Figure 3.13 shows the impedance measurements of the same cells using a 4T setup. Observe that in figure 3.12 electrode polarization effects in $f < 1$ kHz was hiding cell's response. When a 4T setup is used the response is clearly visible. The impedance response of phosphate buffer saline solution (PBS) is plotted for comparison. Observe that PBS has an approximately flat response in all measured frequency range. A small sinusoidal voltage amplitude of 14 mV was applied in all experiments and the frequency was varied from 1 MHz down to 100 mHz in steps of 10 points per decade.
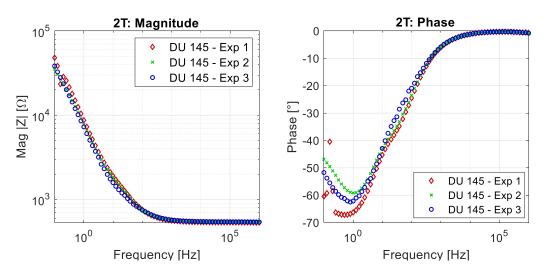
FIGURE 3.12: Bode plot showing magnitude and phase of impedance of DU145 prostate cancer cells measured in the concentration of 3 million cells/ml with the chamber of 1.6 ml volume using a 2T setup. Observe the strong DL effects due to electrode polarization at $f < 1$ kHz.
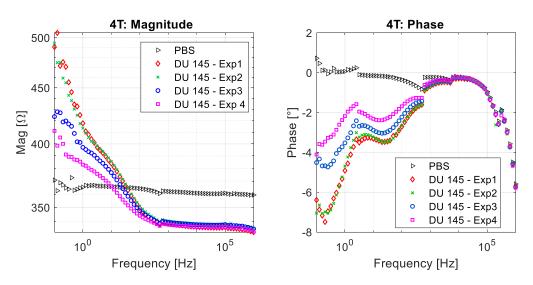
FIGURE 3.13: Bode plot showing the experimental impedance magnitude and phase of the same cells now measured using a 4T setup with the same chamber of 1.6 ml. The PBS impedance magnitude and phase is plotted for comparison.

3.6 Source of Artifacts in Low Frequency Impedance Experiments

Although being very powerful to analyse cells suspensions in low frequencies, the 4T experiments are also very sensitive and prone to errors. Apart from electrode polarization due to DL effects, several other artifacts can appear, e.g. due to reference electrodes distortion of electric field, cables, electromagnetic interferences from external devices or even malfunctioning of cables and instruments. A discussion of artifacts introduced by the electrodes can be found in [42]. In order to avoid external electromagnetic interference it is strongly recommended to place the experimental setup inside a Faraday cage to shield it. Special-purpose short and shielded cables are offered with good potentiostats and together with instrument calibration and cable capacitance compensation are able to disappear with cable effects. An appropriate way to observe whether the experiment has artifacts or the response comes really from the cells is to measure a known ionic conductivity solution, e.g. PBS or KCl, and observe the impedance magnitude and phase. As being purely ionic such solutions in a 4T setup should have a flat impedance magnitude in frequencies below Giga-Hertz range and a close to zero phase also in the same frequencies.

Dirty electrodes full of fat, fingerprints and other biological materials, e.g. rest of cells, can also insert artifacts in low frequency experiments due to the high sensitivity of the measurement in those ranges. Therefore a careful cleaning of electrodes surface with special detergent to remove biological particles is mandatory. Additionally, scratchs, corrosion and imperfections in the electrodes surface and size differences also influence the experiments therefore it is recommended to use very well polished and new electrodes. The better the electrodes used, the better will be the results obtained.

Chapter 4

Applying Electrical Impedance Spectroscopy to Cancer Cells Suspensions

4.1 Introduction

Live cells suspensions and biological tissues show a variation in their dielectric properties when submitted to frequency variable electric fields. Typically, a decrease in the dielectric constant $\varepsilon(\omega)$ and an increase in the conductivity $\sigma(\omega)$ of the biological material is seen as the frequency of the applied electric field increases. Alternative representations commonly used are the impedance magnitude $|Z|$, impedance phase $\angle Z$, real Z' and imaginary parts Z'' of impedance and also the Nyquist plot. In chapter 2, a detailed introduction was given to the topic and in the present chapter a large set of experimental results from different cell lines will be shown as impedance magnitude and phase. Table 4.1 shows a list with all measured cell lines and which type of cancer they are. Figure 4.1 shows the classification of the cell lines. In the experimental results section only the results of the cells measured with the chamber of 320 μL are shown, namely: PC-3, DU145, HT29, MCF-7, SW620 and T47D. The experiments with CaCo2 cells were performed only once and discarded as only DL effects were visible. Hospital staff had

47

TABLE 4.1: Measured cell lines and their status.

Cell Type	Description	Status
DU145	Prostate adenocarcinoma	cancer
L929	Mouse fibroblasts	normal
PC-3	Prostate small neuroendocrine cell carcinoma	cancer
EOL-1	Acute myeloid eosinophilic leukemia	cancer
MOLM-13	Acute myeloid leukemia	cancer
HT29	Human colorectal adenocarcinoma	cancer
MCF-7	Breast cancer adenocarcinoma	cancer
SW620	Human colorectal adenocarcinoma	cancer
T47D	Ductal carcinoma	cancer
HaCaT	Human keratinocytes	normal
CaCo2	Coloretal adenocarcinoma	cancer

a large difficulty cultivating CaCo2 cells, therefore such experiments were not repeated. The experimental results of HaCaT and L929 cells were published elsewhere [39].
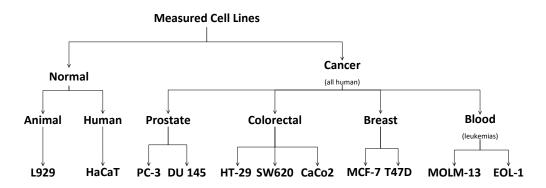
FIGURE 4.1: Hierarchy of measured cell lines.

4.1.1 Normal Cell Lines

4.1.1.1 L929: Mouse Fibroblasts

Fibroblasts are the most numerous cells encountered in connective tissues. They are resposible for maintaining the integrity of stroma, i.e., the structural framework that supports the organs. They produce all precursors of extracellular matrix, namely the ground substance and several types of fibers, e.g, collagen, reticular and elastic fibers. They also produce glycosaminoglycans. They have an important role in immuno system and wound healing as they initiate the inflamation process when external microorganisms invade the body. In general fibroblasts can be found in two states: active where they have a large endoplasmatic reticulum and an inactive state, also called fibrocytes, with a reduced size of rough endoplasmatic reticulum [43]. Their life expectancy is in average 57 ± 3 days [44].

Cancer associated fibroblasts (CAF) also play a central role in creating the tumor microenviroment (TME), basically the extracellular matrix (ECM) that supports the tumor. The TME influences the penetration, distribution and metabolism of anti-cancer drugs injected in patients, and also produces signals that allow the tumor to communicate with the external world influencing its metastatic behavior [45]. Therefore, the TME and the CAF are often target of anti-cancer treatments.

The L929 cell line was the first cell line to be immortalized in the 1940s from subcutaneous and areolar adipose tissue from a C3H mouse that was 100 days old [46]. It is commonly used in DNA transfection studies and to develop novel drugs for cancer treatment.

4.1.1.2 HaCaT: Human Skin Keratinocytes

Keratinocytes are the most abundant cells present on the epidermis, i.e., the outermost layer of human skin. Their main function is to protect our organism from external microbes, UV sunlight, loss of water, among others. They produce several proteins, e.g. keratin, in their process of differentiation or cornification, where they lose the nucleous

and organelles and become gradually filled with keratin. This makes them strong against stress and close to waterproof, which is an important characteristic of the skin as a protection barrier against water loss. Other substance which gives strength and elasticity to skin is collagen, also found in keratinocytes.

In the final stage of differentiation, most keratinocytes undergo programmed cell death and become hard and stratified, filled with collagen and keratin forming the skin barrier. Old cells are constantly replaced in the skin by new ones. In human the replacement process takes in average 40-56 days [47]. Keratinocytes are also important in wound healing as they migrate towards each other to fill the gap of cells once a wound is established [6].

HaCaT cells are an aneuploid sponteneously immortalized cell line stablished from a 62-year-old male adult skin [48]. They are often used in research as models to study the behavior of human skin cells, one example is the process of vitamin D3 production and metabolism [49].

4.1.2   Prostate Cancer Cell Lines

Prostate cancer (PC) is the most common cancer type in males and the second leading cause of cancer associated deaths in the United States [50]. The majority of PCs are classified as adenocarcinomas characterized by an absence of basal cells and uncontrolled proliferation of tumor cells with features of luminal differentiation including glandular formation and the expression of androgen receptor (AR) and prostate-specific antigen (PSA) [51].

4.1.2.1   DU 145: Prostate Adenocarcinoma

DU 145 cancer cells are one type of prostate adenocarcinoma. The cell line is commonly used in laboratory to study the behavior of non-aggressive types of prostate cancer. The cells were originally derived from a central nervous system metastasis of a 69-year-old Caucasian male. They are hormone insensitive and do not express PSA [52]. They are an

example of a non-aggressive type of PC with no (in xenogragraft mouse models) or very low (in humans) metastatic potential.

4.1.2.2   PC-3: Prostate Small Neuroendocrine Cell Carcinoma

PC-3 cells have several features that are characteristic of prostate small cell neuroendocrine carcinoma (SCNCs). They were originally established from a bone metastasis grade IV in 1979 from a 62-year-old Caucasian male patient [53]. They are extremely aggressive unlikely most PCs, and metastatic in xenograft mouse models. PC-3 cells do not express PSA and are androgen independent. They have high metastatic potential and are commonly used in biochemical investigations and in xenograft (immunodeficient) mouse models to evaluate cell response to chemotherapeutic treatments. Researchers commonly use them as a model to study aggressive types of PCs.

The PC-3 cells are normally observed as a recurrent cancer in patients that had a less aggressive type of prostate cancer and were treated and cured with hormone therapy and several years later appear with this new type of very aggressive cancer. In United States less than 2% of prostate cancer patients have small neuroendocrine prostate carcinoma [52].

4.1.3   Leukemia Cell Lines

4.1.3.1   MOLM-13: Acute Myeloid Leukemia

The cell line was established in 1995 from a 20-year-old male patient as a relapse of acute myeloid leukemia (AML) which evolved from myelodysplastic syndrome MDS [54]. The cancer develops from myeloblasts or myeloid stem cells, which are an immature stage between stem cells and monocytes and granulocytes white blood cells [55, 56]. Due to genetic mutations the cells do not differentiate and turn into mature white blood cells. Therefore, they are not able to perform the normal immune system defense as normal white blood cells do. The cells of the line MOLM-13 are normally round and grow as single cells in suspension.

They grow rapidly, accumulate on blood and bone marrow interfering with normal white blood cells functions [57]. As they grow in bone marrow, they cause the replacement of normal bone marrow cells by leukemic cells, which leads to a drop in red blood cells count, platelets and normal white blood cells. Symptoms of AML include tiredness, shortness of breath, easy bleeding and increased risk of infection due to the reduction on the number of normal white blood cells. The cancer normally spreads to skin, brain and gums [57].

If untreated, AML progress fast and kill the patient within weeks or months. The prognostic is better for patients under 60 years old where 35% are cured, than for patients above 60 years old, where only 10% will be cured. For patients above 60 years old the typical survival time is between 5 - 10 months after diagnosis [58]. In the United States approximately 1.8% of cancer deaths are due to AML [57]. Risk factors include smoking, chemotheraphy, radiation theraphy, myelodysplatic syndrome (MDS) and exposure to benzene. The diagnosis is made through blood tests or bone marrow aspiration. It is typically treated with chemotheraphy, radiation theraphy or stem cell transplantation [54, 58]. In 2015, one million people suffered from AML and in the same year $147,000$ people died of it [59, 60].

4.1.3.2 EOL-1: Acute Myeloid Eosinophilic Leukemia

The EOL-1 cell line is a human blood cell line originally established in 1985 from the peripheral blood of a 33-year-old man with acute myeloid eosinophilic leukemia (AEL). It is described as a rare variation of AML. The cells are relatively small round cells growing in suspension as single cells or small clusters, and they have a doubling time of approximately 48 hours [61]. They are pro-inflammatory granulocyte white blood cells that develop in bone marrow and fight multi-cellular parasites such as worms and flukes [61]. They constitute from 1% to 3% of white blood cells circulating [62]. Most cells will be found in blood or bone marrow. EOL-1 cells are used to develop treatment and study B/T-cells malignancies. Symptoms of AEL include bronchospasm, heart failure, eosinophil-based endomyocardial fribrosis and several symptoms of acute coronary syndrome [63, 64].

4.1.4 Colon Cancer Cell Lines

Colorectal adenocarcinoma is the most common form of colorectal cancer with 95-98% of all colorectal cases [65, 66]. It is initially discovered by a CT scan, PET or MRI, and confirmed by microscopial examination of sampled tissue through colonoscopy or sigmoidoscopy [67]. From 75-95% of colorectal cancers occurs in people with no genetic predisposition. Factors which have been appointed to increase its risk is old age, high sugar intake, high alcohol consume, smoking, lack of physical activity, obesity and large consume of red and processed meat. Inherited disorders like familial adenomatous polyposis also cause this type of cancer. It starts as a benign polyp in the colon and if not removed by colonoscopy it evolves into malignant cancer. Symptoms include weight loss, blood in stool and tiredness. Colorectal cancer is the third most common type of cancer with about 10% of all cases. Treatments include surgery, chemotheraphy, radiation theraphy and targeted theraphy [68, 69].

4.1.4.1 HT29: Human Colorectal Adenocarcinoma

The HT29 human colorectal adenocarcinoma cell line was established in 1964 from a 44-year-old woman, directly from the primary tumor. This cell line is extensively used as xenograft tumor model for colorectal cancer and also to study the transport, secretion and absorption in intestinal cells [70]. The cells are able to proliferate within 3-4 days in serum-free medium, while this time reduces to 1 day if fetal calf serum is added [71]. They resemble enterocytes from the small intestine and grow forming a compact monolayer [72]. They are eager consumers of glucose and if glucose is exchanged by galactose in cell culture they terminally differentiate into enterocytes. Given its ability to differentiate they are commonly used as a real model of in-vitro colon tissue [73].

4.1.4.2 SW620: Human Colorectal Adenocarcinoma

The cancer cell line SW620 human colorectal adenocarcinoma was derived from a metastatic lymph node of a 51-year old Caucasian patient. It consists mainly of individual

small and spherical bipolar cells lacking microvilli [74]. They are strongly invasive in vitro; in vivo however they proved to be less invasive than HT29 cells [75]. The SW620 cells are commonly used in research as a model to study metastatic undifferentiated cancers, as they were derived from a metastatic site.

4.1.4.3   CaCo2: Human Colorectal Adenocarcinoma

The CaCo2 cell line is a human epithelial colorectal adenocarcinoma, originally stablished from a 72-year-old male Caucasian patient. They grow as adherent cells in flask forming a heterogeneous monolayer easily seen in microscope [76]. Given their heterogeneity, CaCo2 cells are normally used as monolayers of cells instead of individual ones to study the absorption of orally administered drug by the human small intestine mucosa [77].

Even when they were originally derived from a colon cancer, when cultured with certain substances CaCo2 cells differentiate and polarize in a way that they resemble morphologically and functionality the normal enterocytes lining the small intestine [78, 79].

4.1.5   Breast Cancer Cell Lines

4.1.5.1   MCF-7: Invasive Breast Ductal Carcinoma

The MCF-7 breast cancer cell line was stablished in 1970 from the metastasis of a pleural effusion from a 69-year-old Caucasian woman and it is the most commonly studied xenograft model of breast cancer [80]. The original tumor was a primary invasive breast ductal carcinoma. Despite being derived from a metastasis, the cell line is non-invasive in xenograft models and represents a model of early-stage disease [81].

4.1.5.2   T47D: Breast Ductal Carcinoma

The cell line T47D was originally derived from a pleural effusion of a ductal carcinoma of a 54-year-old female patient whose primary tumor was in the mammary gland [82]. The T47 cells are widely used to study the effects of progesterone on breast cancer.

4.2   Experimental Procedure

All cancer cell lines were unfrozen and cultivated in RPMI 1640 culture medium with 10% Fetal Calf Serum (FCS) plus 50 U/mL Penicillin and 50 $\mu g/mL$ Streptomycin at 37 $^{\circ}C$, 5% CO_2 in a humidified incubator. They were grown in culture medium and harvested weekly. When they reached the desired concentration the culture medium was removed, cells that grow as adherent were detached by 0.05% trypsin-EDTA (gibco), washed twice in phosphate buffer saline solution (PBS) and re-suspended in PBS for the impedance measurements. The two leukemia cell lines already grow in suspension, therefore the step of detachment for them was skipped and they were directly washed twice in PBS and then re-suspended in PBS for the measurements.

Before experiments, cells were placed in a four-electrode-terminal (4T) chamber especially designed for such measurements and fabricated using 3D printing techniques. The cell lines L929 and HaCaT were measured with the chamber of 12.4 mL and their experimental results are shown elsewhere [39, 40]. The cell lines DU145, PC-3, MOLM-13 and EOL-1 were measured with a smaller version of the chamber that had a total volume of 1.6 mL and their results are described in [23, 41]. The latest version of the chamber which is described in chapter 3 had a total volume of 320 μL and was used to measure the following cell lines: MCF-7, SW620, CaCo2, T47D, HT29, PC-3 and DU145. For impedance measurements, pure platinum (Pt) electrodes were used for all cell lines, except L929 and HaCaT, which were measured with a special type of stainless steel electrodes corrosion resistant (V4A).

The potentiostat Gamry Interface 1000 *from Gamry Instruments Inc.* was used to perform all experiments. It works as a precise, two-, three- and four-terminal potentiostat. Cable

leads are shielded against electromagnetic interference. An amplitude voltage varying between 14 mV up to 70 mV was applied to the system in the majority of the experiments and the frequency was varied from 1 MHz down to 100 mHz in steps of ten points per decade. In the cases where a large potential was applied that is explicited in the results. Given the long experimental times for the very low frequencies, all experimental data below 1 Hz were discarded. The reason is that a pre-requisite for good 4T experiments is that electrodes and system are stable throughout the complete time taken to measure one frequency point and such condition is rarely achieved in frequencies below 1 Hz, given the dynamic nature of biological systems. All experiments were repeated from three up to five times on a row for each concentration. Most experiments were also repeated at different days with different cell seeds.

4.3 Experimental Results

4.3.1 Impedance Magnitude and Phase Curves Using the 320 μL Chamber

In this section the experimental results of different cancer cell lines measured with the chamber of 320 μL are shown as impedance magnitude and phase plots. The results of CaCo$_2$ cells were discarded as experiments were performed only once and had a strong double layer effect.

Figure 4.2 shows the experimentally measured impedance magnitude and phase of PC-3 cancer cells as a function of the frequency. An interesting observation from the plots is that the impedance magnitude in low frequencies depends (but not only) on the volume fraction of suspended alive cells. Another point worth mentioning is that the impedance magnitude decreases as the frequency increases, showing a possibly mechanism of charge movement associated with the frequency. From the figure it can be seen that two samples were measured for all three experimental days.

Figure 4.3 shows the experimental results for DU145 prostate cancer cells. Experiments were performed in three different days with the chamber of 320 μL in concentrations

varying from 3 up to 9 million of cells/mL. The experimental results from one day were discarded due to a bad electrode-electrolyte interface. Therefore the plots in figure 4.3 are the experimental results of two different days where no DC potential was applied to the electrodes and the AC potential varied between 10 mV up to 50 mV.

Comparing the characteristics of the plots with the experimental conditions very interesting conclusions can be drawn. The first observation is the same as for PC-3 cells, that the
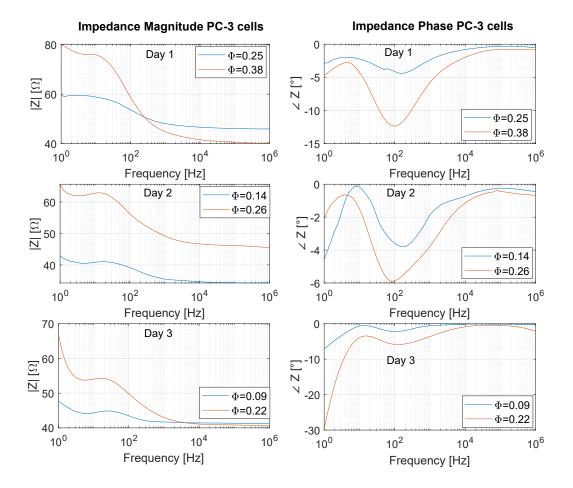
FIGURE 4.2: Experimentally measured impedance magnitude and phase of prostate PC-3 cancer cells suspended in PBS. Plotted curves are the average of repeated experiments in the same day with the same cell seed. For each curve, experiments were repeated 2-4 times. The variable Φ indicates the volume fraction of suspended cells on the chamber. A value of $\Phi = 0.13$ indicates that 13% of the volume was filled by cells the rest being buffer solution and cell's excretes.

impedance magnitude of DU145 cancer cells in low frequencies increases with cell concentration, namely, the volume fraction of suspended alive cells. The higher the volume fraction of cells, the higher the impedance magnitude in low frequencies.

Another point worth mentioning is that the curves of day 1 with the concentrations of $\Phi = 0.15$ and $\Phi = 0.08$ correspond to the 6 and 9 million of cells per mL. The experiments of the concentration with $\Phi = 0.15$ were performed two hours later after the cells were detached and suspended and the experiments with $\Phi = 0.08$ were performed six hours later. From the plots it can be seen that a large percentage of the cells died during
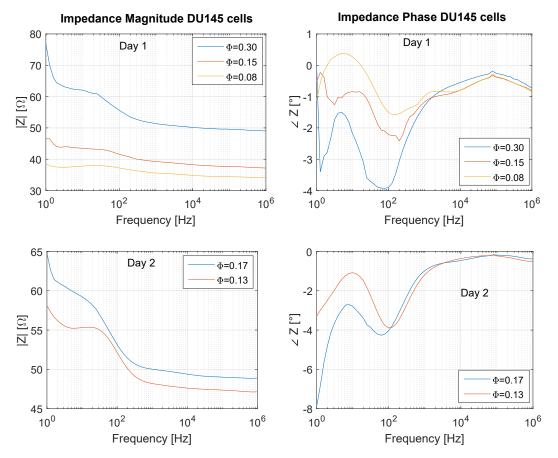
FIGURE 4.3: Experimentally measured impedance magnitude and phase of prostate DU 145 cancer cells suspended in PBS. Similar to the previous figure, plots are the average of repeated experiments in the same day with the same cell seed, and for each curve experiments were repeated 2-4 times. The volume fraction of suspended alive cells is represented by Φ.

this period, increasing the conductivity of the suspension medium, clearly seen by the flatter curves in low frequencies and lower impedance magnitudes in higher frequencies. When cells die, they disintegrate their cell membranes releasing their contents into the suspending medium, decreasing the capacitive effects at low frequencies, and increasing supernatant conductivity, what translates into a lower R_s in higher frequencies and a lower capacitance in low frequencies, as capacitive effects are caused by cell membranes, if no artifacts are present. The curves which were measured first (3 million of cells per mL) in general for all experiments showed a larger percentage of alive cells. That is important to observe for future experiments. One possible explanation for the fast cell death during the measurements was the large temperature difference between the temperature of cell cultivation (37 $^\circ C$) and the temperature of the experiments (approximately 25 $^\circ C$). For future studies it is recommended to use a temperature controlled box and measure the cells at 37 $^\circ C$ to minimize cell death.

Figure 4.4 shows the experimental results of impedance magnitude and phase of T47D cancer cells. The abbreviations D1 and D2 refer to the experimental days (day 1 and day 2) and Φ indicates the volume fraction of suspended alive cells. The same behavior as observed for PC-3 and DU145 cells, namely, the dependence of the impedance magnitude in low frequencies from the volume fraction of suspended alive cells is now observed again. The curve with the concentration of 4% of alive cells has a very flat impedance magnitude and a close to 0° impedance phase. And the larger the Φ the larger is the impedance magnitude at lower frequencies.

The experiments with SW620 cancer cells were repeated in three different days, with three different cell seeds that varied in concentration from 3 up to 9 million cells/mL. All experiments from the first day were discarded due to bad electrodes. In the second experimental day a DC potential of 250 mV was applied for testing and this also caused a very unstable system and therefore those results are not shown. In the third day, new electrodes were used and a 0 DC potential was applied together with a 10 mV AC amplitude potential. This time good results were obtained and are shown in figure 4.5. The same trend as observed for the previous cell lines was again observed.

Figure 4.6 shows the impedance magnitude and phase of MCF7 cancer cells. From the plots it can be seen a behavior similar to the other cell types, namely, an impedance
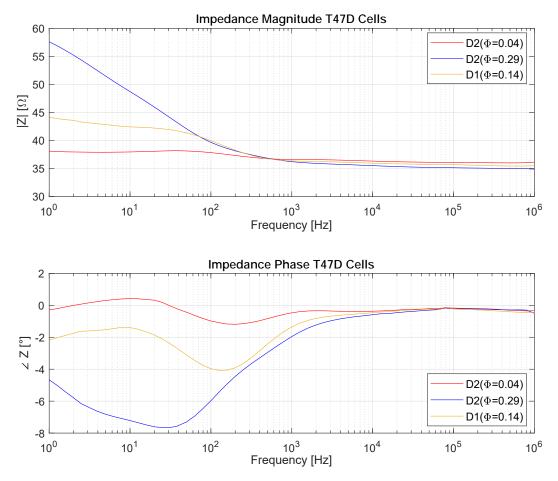
FIGURE 4.4: Experimentally measured impedance magnitude and phase of breast carcinoma T47D cancer cells suspended in PBS. Each plot is the average of repeated experiments in the same day with the same cell seed, and for each curve experiments were repeated 2-4 times; D1 and D2 refers to day 1 and day 2 and means that the experiment was repeated in two different days. The volume fraction of alive suspended cells is expressed by Φ.

magnitude clearly dependent on the volume fraction of suspended alive cells and a strong frequency dependency of the impedance magnitude and phase.

Figure 4.7 shows the impedance magnitude and phase of HT29 cells. Analyzing figure 4.7 interesting conclusions can be drawn to understand the impedance behavior of live cancer cells suspensions. First, if the plots with day 3 $\Phi = 0.27$ and day 2 $\Phi = 0.27$ are compared, it can be seen that they have the same amount of suspended alive cells (27%), the impedance phase of both plots is very similar and the impedance magnitude
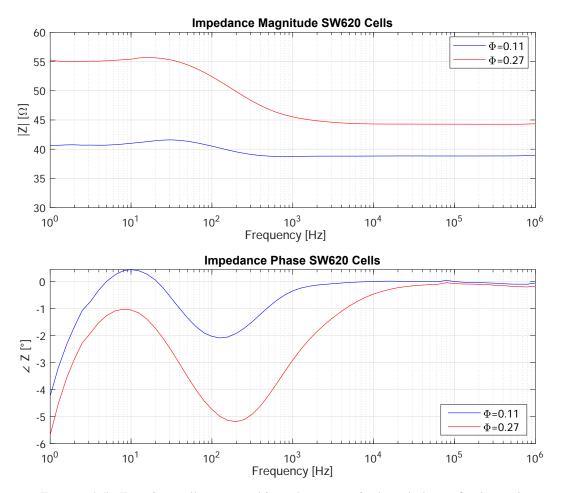
FIGURE 4.5: Experimentally measured impedance magnitude and phase of colorectal carcinoma SW620 cancer cells suspended in PBS. Plots are the average of three repeated experiments in the same day with the same cell seed. The variable Φ indicates the volume fraction of cells for each experiment.

curves have exactly the same shape, but are dislocated 20 Ω from each other in y-axis. Factors that are able to shift the impedance magnitude curve in y-axis are the temperature of the experiment, the conductitivy of the supernatant, namely, the fluid where cells are suspended and the open circuit potential of electrode-electrolyte. For higher supernatant conductivities, the impedance magnitude plots shift downwards in the y-axis and for lower upwards. The same happens with temperature, higher temperatures shift $Mag|Z|$ upwards and lower temperatures shifts it downwards. As the two experiments were performed in different days two weeks apart from each other, with different cell
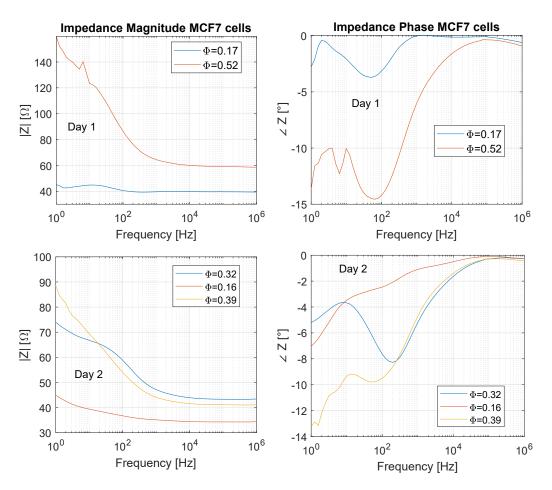
FIGURE 4.6: Experimentally measured impedance magnitude and phase of breast carcinoma MCF7 cancer cells suspended in PBS. Plots are the average of repeated experiments in the same day with the same cell seed, and for each curve experiments were repeated 2-4 times. The variable Φ indicates the percentage of alive suspended cells.

seeds, the three factors which are interdependent (temperature, conductivity and open circuit potential) explain the shift on the curves.

4.3.2   Metastatic versus Non-Metastatic Cancers

In this section the spectral response of highly metastatic prostate and colorectal cancers is compared to non-metastatic or cancers with low metastatic potential. The objective is
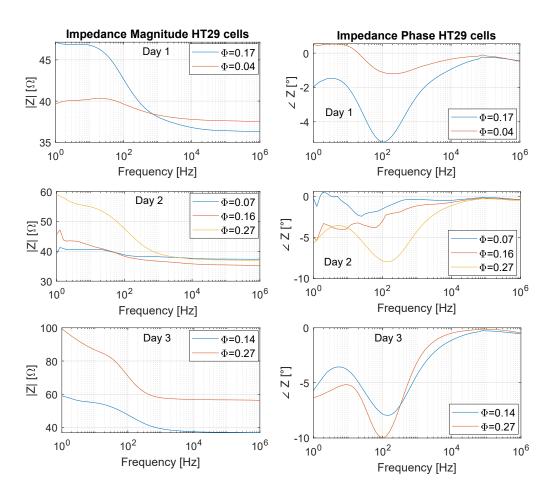
FIGURE 4.7: Experimentally measured impedance magnitude and phase of colorectal carcinoma HT29 cancer cells suspended in PBS. Plots are the average of repeated experiments in the same day with the same cell seed, and for each curve experiments were repeated 2-4 times. The variable Φ indicates the percentage of suspended alive cells.

to observe whether or not the metastatic behavior of the cells also affect their impedance spectrum.

4.3.2.1 Prostate Cancers

In this section the spectral response of the small cell neuroendocrine prostate carcinoma PC-3 cells (highly metastatic in xenograft mouse models) is compared with the spectral

response of prostate carcinoma DU 145 cells (non-metastatic in xenograft mouse models) measured using the chamber of 1.6 mL. The experimental results here shown were the first experiments performed with cancer cells using the chambers described in Chapter 3 and results were published in [23].
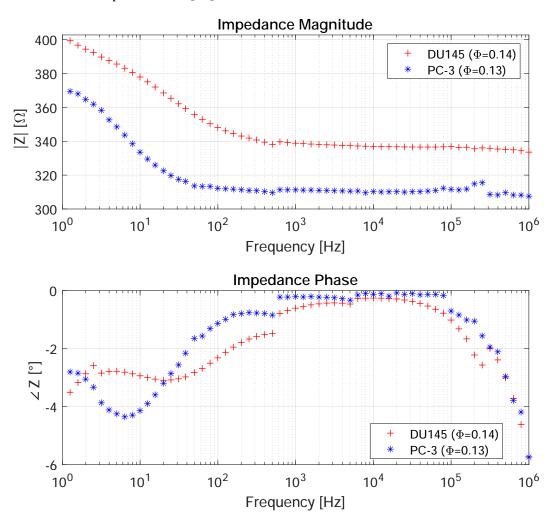
FIGURE 4.8: Experimentally measured impedance magnitude and phase of small cell neuroendocrine carcinoma PC-3 cancer cells (metastatic) compared to the impedance spectrum of prostate carcinoma DU145 cells (non-metastatic) suspended in PBS. Both cells where measured at the same concentration (3 million cells per mL), same temperature (25 °C) and had a similar volume fraction of suspended alive cells (13% and 14%), in the figure indicated by the variable Φ.

Figure 4.8 shows that the spectral response of the two prostate cancer cells suspension are different. The PC-3 cells have a steeper frequency dependency, with their impedance magnitude decaying faster when compared to DU145 cells as the frequency of the applied signal increases. While the frequency dependent behavior of DU145 cells decreases significantly above 500 Hz, the PC-3 cells cease on this behavior already below 100 Hz (approximately at 70 Hz). Notice that above 100 kHz a second effect is causing a new frequency dependent behavior in the impedance curves not related with the cells itself, but caused by the imperfections of the measuring equipment and cables.

Important to highlight is that the two cell lines PC-3 and DU145 were both measured at the same temperature, at the same concentration (3 million cells per mL) and had almost the same percentage of suspended alive cells (14% and 13% respectively). Therefore the results shown in figure 4.8 are interesting, considering that both cancer cell lines have a very different metastatic behavior. A possible reason for the observed behavior of PC-3 cells can be correlated to its larger radius when compared to DU145 cells. The capacitance of PC-3 cells will be approximately equal to $4\pi\varepsilon_0\varepsilon_r R_{cell}$, therefore cells with larger radius will also have a larger capacitance. As the imaginary part of the impedance is inversely proportional to the capacitance size, the impedance magnitude decreases steeper for the larger cells than for the smaller ones.

Nevertheless, the capacitance observed experimentally is not generated only by the cells itself, but also by the disequilibrium between the ionic cloud deformation caused by the electric field and the chemical gradient generated by charge imbalance and its attempt to restore the charge equilibrium, not to forget the friction forces. Therefore, to one side there is the electric field force pushing the charges far away from the cell surface and opposite to this force the electrochemical gradient and the friction forces. At the end what is seen on the impedance graphs are all effects summed together: the effect of the larger capacitance due to the larger cell size and the imbalance between electrostatic, chemical gradient and friction forces.

4.3.2.2 Colorectal Cancers

In this section the spectral response of two different human colorectal adenocarcinomas, SW620 (non-metastatic) and HT29 (highly metastatic), measured with the chamber of 320 μL is compared. A similar behavior as observed for prostate cancers in the previous section is seen here again. While for the non-metastatic cells SW620 the frequency dependent behavior decreases significantly above 10 kHz, for the highly metastatic cells HT29 this frequency dependency diminishes significantly already below 2 kHz.
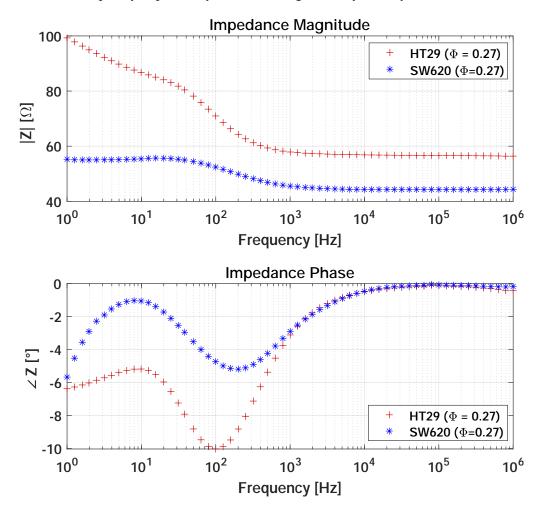
FIGURE 4.9: Impedance magnitude and phase of HT29 (metastatic) vs. SW620 (non-metastatic) cancer cells. The HT29 cancer cells have a high metastatic potential while SW620 are non-metastatic [83].

The same explanation applied for the two examined prostate cancers to explain their frequency behavior can also be extended here, as HT29 are more metastatic than SW620 and also have a larger radius.

A question that may arise is why for the prostate cancer cells the frequencies at which the frequency dependent behavior ceased to be observed were below the kHz range, and for the colorectal cancers they were observed above the kHz range. Notice that the two experiments were performed with different chambers and that the electric field strength in the colorectal cancer cells experiments was 6.4 times stronger than in the experiments with the prostate cancers[1]. Such result also shows the dependence on the impedance magnitude of the cancer cells from the strength of the external electric field applied, one more confirmation that the observed behavior is of electrostatic nature.

Although the results here are promising, it is hard to make a definitive statement whether or not this behavior will be observed in all cancer cell types. The topic of metastatis is very complex and extra substances or molecules attached to the cancer cell membrane or present in the tumor microenviroment surrounding the cancer cell can shift the equilibrium and influence the results. Nevertheless, suspicion goes into the direction that metastatic and non-metastatic cancers have a very different spectral behavior caused by the charge present at the cancer cell. The results shown here point out in the same direction of studies performed by other authors [7, 84], namely, that the charge and the ability/inability of the cancer cell membrane to separate charges between the intra- and extra-cellular medium plays an important role in the metastatic behavior of the cells.

4.3.3 Comparison of the Impedance Spectrum from Different Cell Lines

Figure 4.10 shows on the same plot the spectral response of several cancer cell lines with similar volume fractions, i.e., approximately the same quantity of suspended alive cells on

---

[1] The prostate cancer cells experiments shown in the previous section were performed with a chamber which distance between the two active electrodes was 32 mm. The colorectal cancer cells experiments were performed with a chamber where the distance between the electrodes was 5 mm. Considering that the same potential was applied into both experiments, the decrease in the distance is equivalent to applying an electric field 6.4 times stronger in the colorectal cancer cells experiments.

the chamber. Notice that the impedance spectrum of some cell types overlap, while other spectrums are completely separated. Distinguishing cell types by the sole impedance spectrum can be quite challenging. Nevertheless, several characteristics derived from the spectral response of the cells can be used to distinguish uniquely the different cell types. One example of such characteristic is shown in the next chapter, the external cell surface charge. Other characteristics which are cell specific can be certainly found. The main
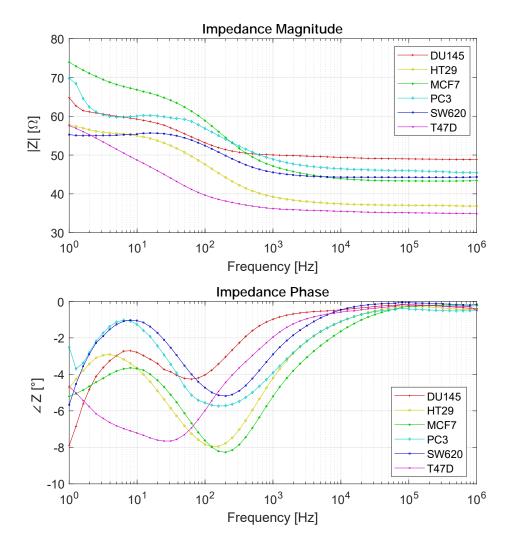
FIGURE 4.10: Impedance spectrum comparison for different cancer cell lines. The following experimental days and volume fractions are plotted: DU145 cells D1($\Phi = 0.30$), HT29 cells D2($\Phi = 0.27$), MCF7 cells D2($\Phi = 0.32$), PC3 cells D1($\Phi = 0.26$), SW620 cells D3($\Phi = 0.27$) and T47D cells D2($\Phi = 0.29$).

difficulty in using the sole complete spectrum to distinguish cells is that the spectrum is too wide; a lot of different physical and biological phenomena is occurring in different frequency ranges. In low frequencies, the electric fields are mainly confined outside the cell membranes and the results of those frequencies are reflecting the surrounding of the cells. As frequency increases, the cell membranes start being short circuited and the results reflect more and more the internal status of the cells. In the limits of very high frequencies the status of the cells organelles can be observed.

Performing impedance spectroscopy experiments in very high frequencies is challenging as the signal from the cells decrease by several orders of magnitude and the interference from the cables, PCB's, reflexion of waves in unmatched loads degrades the signal quality significantly. In this sense it is recommended to use the high frequencies only where they are extremely necessary and use small frequencies to characterize biological cells and tissues as good results in low frequencies were obtained.

Figure 4.10 shows the impedance spectral response of several cancer lines, with similar volume fractions, namely, approximately the same volume of alive cells suspended in order to facilitate the comparison. The frequency at which the spectrum starts to raise seems to show a direct dependence on the cell diameter, when one compares the spectral curves with the cells sizes. Possibly, also the strength of the electrostatic attraction of the cells with the ionic charge in the ionic cloud surrounding the cell plays a role in defining the transition frequency from a flat to an increasing curve. And the strength of this attraction force can eventually be one more distinguishing characteristic of the cells themselves. Nevertheless, worthwhile to mention is that the spectral curve is a combination of all the factors affecting the electric behavior of the cells and the system, namely, the electrochemical chamber.

4.3.4   Cell Sizes

The dimensions of the cells suspended (spherical format) was photographed and measured in microscope. Table 4.2 shows the average cell radius, the standard deviations and the number of measured cells (N) for all cell lines. Exp. Meas. in table 4.2 represents the experimentally measured values. Figure 4.11 shows the same information as a graph. In

the figure 4.11 the average of the cell radius is presented with a cross, the median appears as a continuous line. The bottom line of the box represents the mediam of the bottom half and the same for the top half. The vertical lines that extend outside the boxes highlight the minimum and maximum values. From the figure it can be seen that the majority of cells have a radius that lies between 6 μm and 13 μm, with PC-3 cells showing the second largest average radius among all measured cell lines (just below HaCaT cells).

TABLE 4.2: Cell radius and standard deviations for all measured cell lines.

Cell Line	Cell radius [μm]	Metastatic behavior	N
PC-3	10.90 ± 2.93	Highly metastatic	25
DU145	9.10 ± 1.88	Low or non-metastatic	14
EOL-1	7.07 ± 0.75	Highly metastatic	10
MOLM-13	7.66 ± 0.66	Moderate metastatic	10
MCF7	9.33 ± 1.25	Highly metastatic	22
T47D	8.99 ± 0.90	Moderate metastatic	19
HT29	7.64 ± 0.77	Highly metastatic	20
SW620	6.98 ± 0.98	Non-metastatic	21

4.4 Suggestions for Future Experiments

Performing such eletrochemical impedance experiments of live cancer cells suspensions is a very challenging task. The main reason is that several dynamic and complex variables interfere with the results. After working five years with such experiments and performing thousands of them, some useful advices I will give for future studies follows.

4.4.1 Use a Temperature Controlled Box

In order to be able to compare and distinguish different cell types, the same experimental conditions must be present in all experiments. Given the sensitivity of the method, even 1° or 2° can already affect the results. Therefore, the suggestion to use a temperature
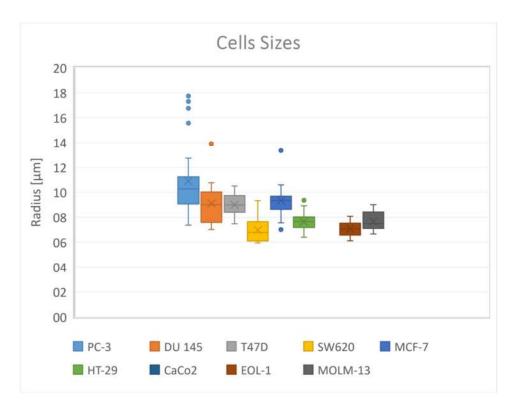
FIGURE 4.11: Cells radius experimentally measured and their standard deviations. The dots above the boxes on the graphs are the outliers,i.e., cells which were so large that their sizes deviated significantly from the mean and are outside the standard deviation. The average value is represented by a cross and the median by a continuous line.

controlled box where cells are maintained at 37 $^\circ C$ (the same temperature as they are cultivated) is strongly recommended. This temperature is also suitable to keep cells longer alive; in several experiments the percentage of dead cells was large, with one of the possible reasons the difference in temperature between cell cultivation (37 $^\circ C$) and experimental temperature (approx. 25 $^\circ C$).

4.4.2 Measure Cells Shortly After Detachment

In order to facilitate the work for medical personal at the hospital, often the cells were prepared in all concentration (3, 6 and 9 million of cells/mL) at once and left at my disposal to perform the experiments. As the sequence of measuring one cell concentration

can take up to 1 hour, often the highest concentration was measured 3 hours after detachment. Not by coincidence, in several of the experiments performed later after 2-3 hours of detachment, a large percentage of cells were dead. Therefore for future experiments it is highly recommended, although being not the best for medical personal, to prepare only one concentration, measure the impedance, prepare another concentration, measure again, and so on. In this way the percentage of cell death can be reduced.

4.4.3   Perform Only Few Experiments per Day

Although it may be more comfortable to perform a large set of experiments per day to decrease the number of visits to hospital, there are also some drawbacks of this practice. The first is the quality of the electrodes. After several repeated experiments, electrodes get hardly stable, making it difficulty to perform the experiments. One way to overcome this issue is to have more than one pair of new electrodes, both for the active and reference electrodes. The second drawback is the equipment itself. After a large set of repetitions the equipment started showing undesirable behavior, and sometimes was not able to keep the potential constant in the electrochemical cell and burned it completely. In this sense as the equipment is quite old it may be appropriate to replace it by a newer one. The last drawback is the difficulty of the experiments itself. The experiments need a lot of attention, and after several hours (10-12 hours) working without an interval one can get tired and make mistakes, having to discard the results afterwards.

4.4.4   Use Preferably New Electrodes

In order for good impedance spectroscopy experimental results in low frequencies it is essential to have a very stable electrode-electrolyte interface. When electrodes are new, well-polished and are very regular (same size and shape) the potential generated at the interface of both WE and CE almost cancel each other, leaving a very small open circuit potential. That is optimum for good experimental results. Ideally the potential should be zero, but I have never seen in any experiment a zero open circuit potential; there was always a small residual open circuit potential left.

Using new electrodes can be challenging due to their high price as they are made of pure platinum. In reality, electrodes can be reused a couple of times. After the experiments they should be cleaned with special detergent to remove biological particles and carefully dried to avoid scratches. When they get too used and are not suitable for further experiments they can be resold for a lower price in the same jewelry where they were purchased.

It may be worth to test other metal alloys for the electrodes to try to find cheaper solutions. I tested myself a very large number of metals, and the majority of them were not useful. Still it may be worth to have one or more students working on the topic to find cheaper options of electrodes for the experiments.

4.4.5   Use Small Voltage Signals

Electrochemical systems are highly non-linear, therefore using large voltage signals in impedance spectroscopy experiments will not improve the results, on the contrary will make them worse. This point is highlighted in several books specialized on the topic [10, 31] and was also strongly recommended by specialists which have several years of experience on the topic. A large AC amplitude signal will also increase the rate of corrosion at electrode's interfaces damaging electrodes faster. Throughout this Thesis most of the signals used were on the order of 14 mV Vpp or 10 mV RMS.

4.4.6   Do not apply a DC potential to impedance experiments

Applying a constant DC potential to an electrochemical system can be very useful for some types of experiments, for instance dielectrophoresis (DEP). Nevertheless, applying a large DC potential on top of an AC potential for impedance spectroscopy experiments disturbs the open circuit potential (OCP) and therefore the equilibrium of the system. By this way, OCP does not stabilize, which is a pre-requisite for good EIS experiments. Therefore, it is recommended not to apply any DC potential for EIS experiments; for other types of electrochemical experiments a DC potential can be one excellent solution to separate different types of biological entities by their charges.

4.5 Conclusions

In this chapter the impedance magnitude and phase of several cancer cell lines was shown and analyzed. Some observations can be drawn from the experimental results presented here. The first is that, possibly there is a direct dependence of the impedance magnitude in low frequencies from the volume fraction of suspended alive cells. In the experimental results presented in this chapter, the larger the volume fraction of suspended alive cells, the larger was the impedance magnitude of the cell suspension in low frequencies. A second observation was that, a pattern for the spectral response of the cancer cells suspension can only be obtained under very controlled experimental conditions, namely, the same amount of suspended alive cells, the same temperature, the same supernatant conductivity, among others. Lastly, important insights were obtained for performing new experiments, which may be useful for further studies. As science evolves with trial and errors and with the experience from others, especially in a new complex field as this one, learning from the past helps to develop and speed up the new advancements on the same topic.

Chapter 5

Measuring the Cell Surface Charge

5.1   Introduction

Charge plays a fundamental role in biological organisms. It is in the core of several important biological functions, for example the heart beat that keeps all of us alive, the neuronal communication between brain and peripheral muscles and in the tightly controlled resting potential of the cell membrane, among others. Basically charge control and flow is ubiquitous in our whole organisms. During skeletal muscle action potential firing, charge movement of three major ions namely Na^+, K^+ and Cl^- through specific ionic channels [11, Ch. 4] is on the core of all our movements since raising an arm, moving the legs or sitting. It is all controlled by a beautiful and delicate charge balance well described and mathematically documented initially by Hodgkin and Huxley [11, 85–88] in their famous experiments with Giant Squid Axon that earned them a Nobel prize in Physiology and Medicine in 1963 [89] and thirty years later developed into a human model by other authors [90–92]. Without a proper charge control and flow we would not be able to seat, move, speak and even breathe.

Charge imbalance and incorrect distribution is also associated with several disorders. The so called channelopaties are genetic diseases caused by a mutation in the genes encoding the correct behavior of the ionic channels transpassing cells membranes, for instance

mutations in sodium, potassium, chloride or calcium channels. Those diseases can cause deafness, heart attacks, renal insufficiency, among others. In general the gating properties of those channels are changed, for instance they open or close slower than normal channels and the equilibrium of charge between the intra- and extra-cellular media is altered affecting the correct firing of the action potential in nerve cells and cardmyocytes with severe and painfull consequences for patients [93].

This chapter is dedicated to analyse the charge encountered in the surface of cancer cells. As charge plays important functions in healthy biological organisms it is also possible that it plays an important role in cancers too. Several authors have been pointing out that the charge distribution and balance/imbalance in the surroundings of tumor cells inside the tumor microenvironment may play a significant function in the metastatic behavior of different cancer cell types [7, 84]. Therefore the objective of the present chapter is to calculate the charge of different cancer cells and investigate whether or not it shows any correlation with the metastatic behavior of the cells.

5.2 Low Frequency Dispersion of Colloidal Particles Suspended in Electrolyte Solutions

Throughout the last seventy years several authors have been studying and modelling the dielectric characteristics of colloidal charged particles, some with special focus on biological cells suspensions, to understand their dielectric behavior and derive useful information from it [2, 14, 17, 94–97]. The first developed model was the Maxwell-Wagner or β-relaxation theory that explains the dispersion characteristics of biological cells suspensions by the so-called interfacial polarization due to the buildup of charges at the interface of two materials of very different dielectric properties [9, 10]. This model was good to explain the relaxations observed in late kHz-MHz but failed by several order of magnitude to predict the very high relaxations values observed in low frequency ranges.

It was Gerhard Schwarz in 1962 [13] that developed the first new theory and mathematical model to explain the relaxation values observed in the low frequency ranges. According

to him, the low frequency dielectric dispersion observed in colloidal particles suspended in electrolyte solutions was caused by the polarization and movement of a counterion atmosphere surrounding the colloidal charged particles, for instance biological cells, by an externally applied electric field. In his theory, an infinitesimal double layer of charge is formed around the external surface of the charged particle similar to the double layer formed at the surface of electrodes when inserted in electrolytes. The externally applied AC electric field causes the displacement of the charges in the double layer creating a polarization effect and as the charges can move laterally in this ionic cloud by diffusion to reestablish the charge equilibrium a dispersion occurs. This effect is named as α-dispersion.

Schwarz offered analytical expressions to calculate the value of the relaxation parameters of the α-dispersion based on physical parameters. According to his theory [10, 13] the relaxation time of α-dispersion can be calculated by:

$$\tau_\alpha = \frac{l_D^2}{D} = \frac{R_{col}^2 e_0}{2u_{ic} K_B T} \tag{5.1}$$

Where l_D is the diffusion length of the particle in the double layer, D is its diffusion coefficient given by Einstein equation, R_{col} is the radius of the large colloidal particle, u_{ic} the mobility of ions inside the ionic cloud surrounding the large charged colloidal particle, K_B is the Boltzmann constant, e_0 the elementary charge and T the temperature in Kelvin.

The counterionic charges surrounding the large colloidal particle are strongly bound to it by electrostatic forces and need to overcome a high potential barrier in order to leave the ionic cloud and move freely in solution. This potential barrier or activation energy E_A can be estimated as [10, 13]:

$$E_A \sim \frac{e_0^2}{\delta \varepsilon_M} \tag{5.2}$$

Where ε_M is the dielectric constant of the suspending medium and δ is the minimum distance between the counterion and its counter charge on the surface. The value of

E_A has been estimated to be approximately 1 kcal/mol [98]. With the value of E_A it is possible to calculate the mobility of ions inside the ionic cloud as given by [10, 13]:

$$u_{ic} = u e^{-E_A/K_B T} \tag{5.3}$$

Where u is the mobility of the ion in free solution, i.e., its mobility when not subject to any electrostatic force due to the large colloidal particle. The lateral mobility of the ions in the ionic cloud surrounding the large colloidal particle u_{ic} is smaller than their mobility in solution u where they are free to move. The value of u is given by [10]:
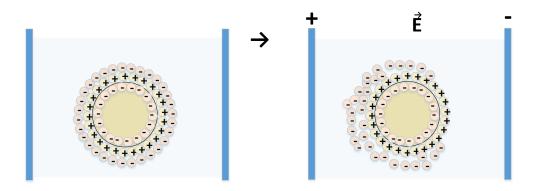
FIGURE 5.1: Illustration of the ionic cloud that surrounds suspended colloidal biological cells in electrolyte solutions. In the absence of an electric field the ionic cloud does not deform and charges are equally distributed around the cell membrane. In the presence of a polarizing electric field ions move laterally in the ionic cloud orienting themselves in the direction of the electric field deforming the cloud. As they are tightly attracked to the cells by electrostatic forces, ions closer to cell membrane do not escape. Similar to the double layer formed close to electrode's surface, surrounding the cell membrane the first layer is formed of a compact immobile layer of charge, here arbitrarily represented by positive ions. The next layer is partially mobile and ions can move in the layer laterally to the electric field, still being trapped by the electrostatic forces. The charges above this partially mobile layer are free to move and they are being attracted and repelled all the time by the ionic cloud of the cells. Note that the outermost charged layer making up the ionic cloud around the cell membrane is very unstable as charges are all the time joining and leaving it. Here only two layers of charges were represented; in reality possibly more layers exist.

$$u = \frac{ze_0}{6\pi\eta r_{ion}} \qquad (5.4)$$

The value of η is the viscosity of the suspending medium (PBS) that for the present situation was assumed equal to the viscosity of the water with a negligible error. The variable r_{ion} is the radius of the ion and z its ionic valence. The value of the α-relaxation frequency can therefore be calculated from [10, 13]:

$$f_\alpha = \frac{1}{2\pi\tau_\alpha} = \frac{u_{ic}K_BT}{\pi R_{col}^2 e_0} = \frac{zK_BTe^{\frac{-E_A}{K_BT}}}{6\pi^2\eta R_{col}^2 r_{ion}} \qquad (5.5)$$

And the permittivity increments in the dielectric constant of the colloidal particle due to the counterion relaxation can be calculated from [10, 13]:

$$\Delta\varepsilon_\alpha = \varepsilon_{low} - \varepsilon_{intcells} = \frac{9}{4\varepsilon_0}\frac{\phi}{(1+0.5\phi)^2}\frac{e_0^2 R_{col}N}{K_BT} \qquad (5.6)$$

The value of ϕ indicates the volume fraction of suspended colloidal particles, namely the biological cells, calculated through eq. 6 or 8, depending on the concentration of the cell's suspension, from reference [95]. The value of N is the average counterion density on a typical cell surface and has units of number of charges per area. Solving equation 5.6 for N, the following is obtained:

$$N = \Delta\varepsilon_\alpha\frac{4\varepsilon_0}{9}\frac{(1+0.5\phi)^2}{\phi}\frac{K_BT}{R_{col}e_0^2} \qquad (5.7)$$

Equation 5.7 basically states that the average charge density on a typical cell surface is directly proportional to the amplitude of the alpha dispersion $\Delta\varepsilon_\alpha$ experimentally observed, the temperature of the suspension medium T and inversely proportional to the radius of the colloidal particle R_{col}, i.e., the biological cell.

While equation 5.7 is hard to grasp, equation 5.6 statements have been observed experimentally several times. When measuring L929 cells, which are mouse fibroblast cells

with small radius, no dispersion could be observed at all. Even after the cell concentration was increased several times, no dispersion could be observed. The same happened while measuring yeast and pure ionic solutions. In contrast, while measuring several cancer cell lines which have a larger diameter, α-dispersion could be observed, showing a direct dependence on the amplitude of the dispersion $\Delta\varepsilon_\alpha$ observed experimentally to the cell radius. The dependence on the volume fraction ϕ of suspended alive cells was also observed several times during experiments with all cancer cell lines. For low concentrations, no dispersion was observed at all and for higher concentration that was clearly observed. The term $e_0 * N$ is also intuitive and is simply the amount of charge in the external surface of the cell, not a surprise if $\Delta\varepsilon_\alpha$ is of electrostatic nature. The question is why $\Delta\varepsilon_\alpha$ has squared dependency on the charge e_0^2 instead of single dependency. If equation 5.6 is rewritten in terms of thermal voltage V_T the following is obtained:

$$\Delta\varepsilon_\alpha = \frac{9}{4\varepsilon_0} \frac{\phi}{(1 + 0.5\phi)^2} \frac{e_0 N R_{col}}{V_T} \tag{5.8}$$

And for simplication replacing $e_0 N$ by Q:

$$\Delta\varepsilon_\alpha = \frac{9}{4\varepsilon_0} \frac{\phi}{(1 + 0.5\phi)^2} \frac{Q R_{col}}{V_T} \tag{5.9}$$

Where Q is the charge density at the external surface of the cell. Now, analysing equation 5.9 it can be seen that the amplitude of the alpha dispersion depends on the volume fraction of suspended cells, the charge of the cells, the radius of the cells and is inversely proportional to the thermal voltage V_T a much simpler and intuitive result. Still both equations 5.6 and 5.9 have the same information presented in a different way. For a rigourous mathematical proof of equation 5.6 see reference [13]. Table 5.1 summarizes all the variables from equations 5.6 up to 5.9. All constants used have the value indicated together with their units. Values indicated with "Exp" are extracted from the experimental results. Observe that $\Delta\varepsilon_\alpha$ and ϕ have no units as they are the ratio between two values with the same unit, indicated by empty brackets. The $\Delta\varepsilon_\alpha$ is the ratio between the cell suspension permittivity ε_{susp} and the vacuum permittivity ε_0. The volume fraction of

suspended cells ϕ is the ratio between the total volume occupied by the cells per the volume of the suspension.

TABLE 5.1: Variables and parameters from equations 5.6 up to 5.9.

Variable	Description	Value	Units
$\Delta\varepsilon_\alpha$	Magnitude of α-dispersion	Exp	[ ]
ϕ	Volume fraction of suspended cells	Exp	[ ]
T	Cell's suspension temperature	Exp	[K]
R_{col}	Colloidal particle i.e. biological cell radius	Exp	[$10^{-6}\ m$]
K_B	Boltzmann constant	$1.38 \text{x} 10^{-23}$	[J/K]
ε_0	Vacuum permittivity	$8.85 \text{x} 10^{-12}$	[F/m]
e_0	Elementary charge	$1.60 \text{x} 10^{-19}$	[C]
N	Average counterion charge density	Exp	[$1/m^2$]
Q	Charge density at the cell's external surface	Exp	[C/m^2]
V_T	Thermal voltage	$K_B T/e_0$	[V]

5.3   Dimensional Analysis of Equation 5.7

In order to verify the final measurement units of equation 5.7 an analysis was performed. Solving equation 5.7 only with the units the following is obtained:

$$N = [] * \frac{F}{m} * [] * \frac{K * J/K}{mC^2} \tag{5.10}$$

$$N = \frac{F}{m^2} * \frac{J}{C^2} \tag{5.11}$$

And remembering that:

$$V = \frac{J}{C} \tag{5.12}$$

$$F = \frac{C}{V} \tag{5.13}$$

Follows:

$$N = \frac{F}{m^2} * \frac{V}{C} \tag{5.14}$$

$$N = \frac{F}{m^2} * \frac{1}{F} \tag{5.15}$$

$$N = \frac{1}{m^2} \tag{5.16}$$

Where the units are Volts (V), Farads (F), Couloumbs (C), meters (m), Kelvin (K) and Joules (J). Equation 5.16 shows that the cell surface charge will be given as the number of charges per square meter. By using equation 5.7 the value of the cell surface charge can be calculated directly from the experimentally measured parameters, namely $\Delta \varepsilon_\alpha$, R_{col} and ϕ.

5.4   Correction of Schwarz Model to 4T Experiments

Gerard Schwarz and his colleagues [13, 99] were the first research group to develop a mathematical model to explain the low frequency dispersion observed in suspensions of colloidal particles due to ionic cloud relaxation; the original model was developed in 1962. Although they did a large progress on mathematically equating the phenomena and relating it to the physical parameters of the system, the limitations in experimental techniques prevented them from making an accurate estimate of the values of the low frequency dispersion amplitude, namely, $\Delta \varepsilon_\alpha$. At first, they did not use a four-electrode-terminal setup [99] which is proven to decrease by orders of magnitude electrode polarization effects [1, 23, 33, 39, 40, 42]. The techniques used to bypass electrode's polarization

were to coat the electrodes with platinum black and measure the same sample at different distances and subtracting the values from each other [99]. In the paper, it is not shown any analysis of the accuracy of using such techniques in the estimation of $\Delta\varepsilon_\alpha$.

Schwarz when developed the model for the cell surface charge estimated a low frequency dispersion magnitude $\Delta\varepsilon_\alpha$ in the order of 10^4 [13] based on experimental results of impedance measurements of polysterene spheres [13, 99]. As the experimental techniques at that time did not allow to circumvent electrode polarization effects accurately in order to measure the real values of $\Delta\varepsilon_\alpha$, he and his colleagues used the methods described above to estimate the magnitude of the $\Delta\varepsilon_\alpha$. The reality is that with a proper use of the four electrode terminal setup as described in chapters 3 and 4 of this doctoral thesis, experimental values in the order of 10^6 have been observed and those values are confirmed by other authors [14]. Another mistake made by Schwarz was to assume an inverse-square force-law dependence on the charge, a simplification from Coulomb interaction. In reality, the net electrostratic interaction of dissolved ions in liquids is much more complex, harder to estimate and of shorter range than the inverse square pair potential suggested by Schwarz [100, Chaps. 3, 14 and 22]. Therefore, the Schwarz equation was corrected to:

$$ N = \Delta\varepsilon_\alpha \frac{4\varepsilon_0}{9} \frac{(1+0.5\phi)^2}{\phi} \frac{K_B T}{R_{col} e_0^\beta} \tag{5.17} $$

Where:

$$ \beta = 1.861 \tag{5.18} $$

The value of β was estimated from the cell membrane potential V_{mem} and the cell membrane capacitance C_{mem} from PC-3 cells. From literature, $V_{mem} = 54mV$ [7] and the cell membrane capacitance per area is equal to $C_{mem} = 1.07\mu F/cm^2$ or multiplying by the area of PC-3 cells, the cell capacitance $C_{cell} = 16pF$ for one single cell [101]. Therefore by assuming the cell as a charged capacitor where the dielectric is the cell membrane, the potential is V_{mem} and the capacitance is C_{cell} the following charge can be calculated:

$$Q_{cc} = V_{mem} * C_{cell} \tag{5.19}$$

And for PC-3 cells the charge obtained is:

$$Q_{cc} = 0.054 * 16 * 10^{-12} = 8.63 * 10^{-13} C \tag{5.20}$$

Observe that the value of Q_{cc} is given in Coulombs; to convert it to unit charges this value must be divided by the value of the elementary charge, namely $1.6 \text{x} 10^{-19}[C]$. The value of Q_{cc} extracted from the experimental results and calculated with Schwarz equation can only be $8.63 * 10^{-13}$ when $\beta = 1.861$. Table 5.2 shows by using a simple parametric analysis how varying the value of the parameter β affects Q_{cc} and V_{mem}; in this case C_{mem} was kept constant. The value of V_{mem} is expressed in volts [V]. The values of the charge of one cell in Coulombs Q_{cc} and the membrane potential V_{mem} are extremely sensitive to the value of β; small variations in β cause large variations on both values. With this corrected equation the experimental results observed by this and other works are aligned with the typical cell parameter values (cell membrane capacitance, cell charge, cell membrane potential).

TABLE 5.2: Parametric analysis to identify the β parameter.

β	$Q_{cc}[C]$	$C_{mem}[\mu F/cm^2]$	$V_{mem}[V]$
1	$5.67 \text{x} 10^{-29}$	1.07	$3.55 \text{x} 10^{-18}$
2	$3.54 \text{x} 10^{-10}$	1.07	22
1.5	$1.42 \text{x} 10^{-19}$	1.07	$8.86 \text{x} 10^{-9}$
1.6	$1.07 \text{x} 10^{-17}$	1.07	$6.72 \text{x} 10^{-7}$
1.7	$8.13 \text{x} 10^{-16}$	1.07	$5.09 \text{x} 10^{-5}$
1.8	$6.16 \text{x} 10^{-14}$	1.07	$3.86 \text{x} 10^{-3}$
1.85	$5.33 \text{x} 10^{-13}$	1.07	$33.57 \text{x} 10^{-3}$
1.861	$8.63 \text{x} 10^{-13}$	1.07	$54.00 \text{x} 10^{-3}$

5.5 Experimental Results: Calculation of the Cell Surface Charge

This section shows the results of the calculation of the cell surface charge by using equation 5.17. The parameters of the equation which are not constant were extracted from the experimental results. The constant parameters have their values described in table 5.1. The method for extracting $\Delta\varepsilon_\alpha$ from the impedance measuremens is described in Appendix D. Table 5.3 shows the results. Observe that the number of unitary charges N per cell surface area is expressed in unit of charges per cm^2. Therefore to obtain the charge in Coulombs this value should be multiplied by the value of the elementar charge of one electron. Figure 5.2 shows the same information plotted as a graph to permit the visualization of the standard deviation. All experiments were repeated several times and most of them in different days. In order to keep the readability of the table, the standard deviations were removed; for a complete table with standard deviations and the number of experiments and experimental days please check the last section of this Doctoral Thesis.

Table 5.3 shows the amount of unitary charges per area N calculated based on equation 5.17 and its comparison with the cell's metastatic potential. The values of the cell radius R_C, volume fraction of suspended cells ϕ and the permittivity increments in the cell spectrum due to $\Delta\varepsilon_\alpha$ were experimentally measured. Standard deviations were removed from the table for readability. For a complete table with all standard deviations please check Appendix G. The values of C_{mem} were either extracted from the literature (PC-3 cells [101], EOL-1 and MOLM-13 cells [102], HT29 cells [104]) or calculated based on equation 5.21). The value of C_{mem} for DU145 cells was assumed to be equal to the capacitance of normal healthy cells ($C_{mem} = 1\mu F/cm^2$) as DU145 are non-metastatic. The value of C_{mem} for SW620 cells is estimated to be between 1.5 and 2.32 $\mu F/cm^2$, therefore a value of 2 $\mu F/cm^2$ was assumed as no value in literature is available. The values of V_{mem} for PC-3 cells [7], MCF7 cells [7] and T47D cells [103] where extracted from the literature; all the other values of V_{mem} where calculated by using equation 5.21 and C_{mem}. The amount of unitary charges of one single cell N_c is equal to the value of N multiplied by the cell area. The value of Q_{cc} is the charge of one single cell in Coulombs

TABLE 5.3: Cell surface charge, membrane potential and capacitance.

Cell Line	$R_C[\mu m]$	$\Delta\varepsilon_\alpha[10^6]^a$	ϕ	$N[10^{11}/cm^2]$	$N_c[10^6]$	$Q_{cc}[10^{-13}C]$	$V_{mem}[mV]$	$C_{mem}[\mu F/cm^2]$
PC-3	10.90	4.67	0.26	3.61	5.39	8.63	54	1.07^b
DU145	9.10	4.73	0.26	4.25	4.42	7.08	68	1.00^c
EOL-1	7.07	0.15	0.07	0.48	0.30	0.48	3.9	2.00^d
MOLM-13	7.66	0.16	0.06	0.56	0.42	0.66	4.5	2.00^e
MCF7	9.33	5.33	0.28	4.19	4.58	7.34	38^e	1.75^f
T47D	8.99	5.25	0.22	5.42	5.50	8.82	43^g	2.00^h
HT29	7.64	5.27	0.32	5.41	3.97	6.35	37	2.32^i
SW620	6.98	4.77	0.20	7.72	4.73	7.58	62	2.00^j

[a] For a definition which frequencies $\Delta\varepsilon_{alpha}$ is defined please check Appendix C.
[b] Extracted from [101].
[c] For DU145 cancer cells a cell membrane capacitance of $1\mu F/cm^2$ was assumed.
[d] Extracted from [102].
[e] Extracted from [7].
[f] Calculated based on equation 5.21.
[g] Extracted from [103].
[h] Calculated based on equation 5.21.
[i] Extracted from [104].
[j] Unfortunately no values for C_{mem} or V_{mem} were found in literature for SW620 cancer cells. Therefore the value of C_{mem} was estimated to be approximately $2\mu F/cm^2$. While it is hard to say the exact value of C_{mem} for SW620 cells, it is definitely between 1.5 and $2.32\mu F/cm^2$.

and is equal to N_c multiplied by the unitary charge of one electron. Observe that for all measured cell lines the more metastatic cells have a smaller amount of unitary charges per area when compared to their less metastatic counterparts. The last column shows the source from where the metastatic potential of the cells was obtained. The acronym "INT" means internal source, from hospital experiments. In order to calculate V_{mem} the following equation was used:

$$V_{mem} = \frac{e_0 N}{C_{mem}} \tag{5.21}$$

Where N and C_{mem} are as described in table 5.3 and e_0 is the unitary charge of one electron. Observe that the equation is balanced and has the units of volts [V][1].

---

[1] In this case C_{mem} was converted to F/cm^2 so equation 5.21 is correctly balanced.

Interesting is to compare the amount of unitary charges per area with the cells's metastatic potential as done in Table 5.4. From the table it can be seen that for the measured cancer cell lines the more metastatic cells showed a lower amount of unitary charges per area when compared to their less metastatic counterparts. This is a very interesting correlation not so far mentioned in literature. The acronym "INT" stands for results obtained internally in experiments at the hospital UKE[2].
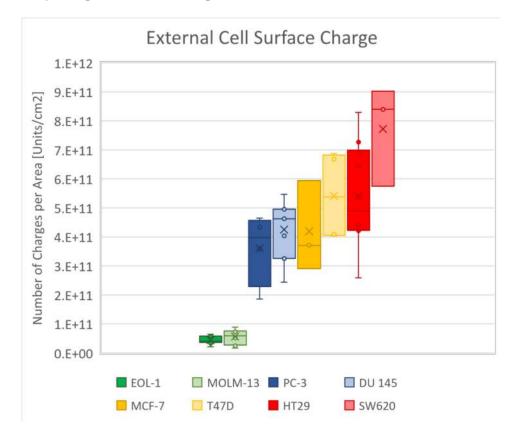
FIGURE 5.2: Cell surface charge for all measured cell types (cancers and non-cancer). The value is expressed as unit charge per cm^2. Average values are represented by a cross, median values by a continuous line, the bottom line of each box represents the median of the bottom half and the same for the top line. Vertical lines extending above and below indicate the maximum and minimum values respectively. Outliers, i.e., values which deviate significantly from all the averages are plotted as dots.

---

[2]The observation that EOL-1 cells shows a higher metastatic potential than MOLM-13 was done by Dr. Daniel Wicklein from UKE, in experiments performed with xenograft mouse models in 2014. Dr. Wicklein is specialized in analyzing the mechanisms that lead to metastasis formation in different types of cancers.

TABLE 5.4: Amount of unitary charges per cm^2 and its comparison with the cell's metastatic potential.

Cell Line	Num. Met.	Met. Pot.	N [$10^{11}/cm^2$]	Cancer Type	Source
PC-3	NA	High	3.61	Prostate	[51]
DU145	NA	Low	4.25	Prostate	[105]
EOL-1	NA	High	0.48	Leukemia	INT
MOLM-13	NA	Moderate	0.56	Leukemia	INT
MCF-7	196	High	4.19	Breast	[83]
T47D	176	Moderate	5.42	Breast	[83]
HT29	230	High	5.41	Colorectal	[83]
SW620	0	Non-metastatic	7.72	Colorectal	[83]

5.6   Comments on Schwarz Theory

Schwarz, Schwan, Pauly and Maczuk [13, 99] were the first research group to observe and model the relaxation phenomena occurring in cell's suspensions in very low frequency ranges (f < 1 kHz). Schwan observed it first in muscle tissues and later on in cell's suspensions [14]. Although their work was published in 1962, no significant progress has been done so far in mathematically analyzing the α-dispersion phenomena and very few works were published afterwards [19, 106–108]. The challenge in analyzing those frequency ranges lies in circumventing electrode polarization effects, getting a stable and error free electrode-electrolyte interface and reproducible experiments. Therefore, most authors just avoid those frequencies.

Even if their work was a steep progress in explaining the α-dispersion phenomena, the absence of having stable experimental setups to allow the correct measurement of impedance values in those extremely low frequencies made the correct estimation of the value of $\Delta\varepsilon_\alpha$ imprecise. The use of the 4T setup combined with signal processing techniques as described in Appendix C enabled the correct extraction of the $\Delta\varepsilon_\alpha$ value. Still a correction had to be made to Schwarz theory to account for the under estimation of the value of $\Delta\varepsilon_\alpha$.

5.7 Conclusions

In this chapter the cell surface charge which is encountered in the external surface surrounding suspended cancer cells was calculated in the light of the theory from Schwarz, Schwan, Pauly and Maczuk [13, 99]. As this charge causes the attraction of counterion charges suspended in the medium, a charged layer is formed around the cells. When the cells are submitted to very low frequency variable AC electric fields, a dispersion in the low frequency range occurs, the so called α-dispersion and from the analysis of the parameters of this dispersion the charge can be calculated.

Interesting to highlight is that a relationship between the metastatic behavior of the experimentally measured cells and the external cell surface charge was further found. For all analyzed cancer cells, the more metastatic cells showed a lower average cell surface charge (N) than their less metastatic counterparts.

Chapter 6

Measuring Adherent Cells

6.1 Introduction

In this chapter the analysis of adherent cells through impedance measurements is performed. Differently from suspended cells which acquire spherical shape and can move at least partially with the electric field, attached cells are immobile as they are fixed by attachment proteins in the substrate where they are grown. This has some significant impact in the measured impedance results. First the reproducibility of the results is better, i.e., when measurements are repeated one after the other the standard deviation error in the measurement values is negligible. Second, the shape of the cells varies enormously when compared to suspended cells. As the cells spread into the substrate, connect to each other and fix themselves, they acquire different formats. Third, more sensitive electrodes need to be used to read information from the cells as only one single cell layer is measured. In comparison to the 4T measurements of suspended cells where millions of cells are measured, in adherent cells experiments the number of cells in the measurement chamber system is in the order of thousands; that has an impact in the amplitude of the measured signal. Lastly, for the impedance measurements using interdigitated electrodes (IDE) which are by definition 2T measurement systems, the presence of the electrode polarization affects significantly the measured signal in low frequencies (f < 1 kHz). Therefore,

instead of having a defined curve for the cell's spectral impedance behavior, 2T measurements with interdigitated electrodes are useful for qualitative evaluations and to observe the variation from an initial to a final state or the response to a drug or treatment. They are also more sensitive than the 4T parallel plate electrode system as IDEs amplify the signal due to the large amount of electrode's fingers.

6.2   Theoretical Background

Interdigitated electrodes (IDEs) are a set of two interlaced comb-structured metal electrodes, individually addressable and printed in a non-conducting substrate [109], where to one electrode is applied the positive potential and to the other the negative or ground. Figure 6.1 shows an example of a simple IDE.
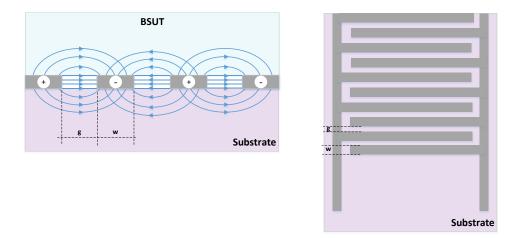
FIGURE 6.1: Illustration of the comb-like structure of interdidigitated electrodes. On the left figure a side view of such electrodes is illustrated showing the electric field lines orientation and on the right side the top view of the IDE. The acronym BSUT stands for biological system under test. In the final used IDEs the value of g and w was equal to 5 μm and the thickness of the metal layer was 200 nm.

The interesting about IDEs is that while in parallel plate electrodes the electric field lines are parallel to electrodes and are confined in the area between them, in IDEs the fringing field lines are the ones stimulating the biological material under test (BSUT) which is placed on the upper side of the electrodes in direct contact with them. They are especially

useful to have one interface of electric contact with the BSUT while the other interface is used to observe the material [109, 110]. IDEs are widely used in applications as biological and chemical sensors, for instance for the detection of the presence of the bacteria Schecheria Coli [111]. They can be capacitance based, resistance based or impedance based.

6.2.1 Working Principle

Interdigitated electrodes have a simple working principle given by their geometry. As the stimulating electrodes are printed in a flat surface parallel to each other and facing the BSUT they create bended ellipsoidal electric field lines distribution which are confined to a maximum height h from the substrate interface which is dependent on a variable known as electrode spatial wavelength λ. The electrode's λ is mathematically defined as [110]:

$$\lambda = 2(w + g) \tag{6.1}$$

Where w is the width of the IDE's fingers and g is the gap or spacing between them. The ratio of sensitivity of IDEs is a direct function of the height of the sensitive layer h and the spatial wavelength λ, which normally is a constant given by [110]:

$$r_{sens} = \frac{h}{\lambda} \cong 0.5 \tag{6.2}$$

In other words, the IDEs will be mainly sensitive to changes in an interface layer that starts at the surface of the electrodes and goes up to a maximum height equal to $w + g$ [109]. This has important implications when choosing the fingers width and gap distance according to the desired height of sensitivitness. For example, for the observation of biological cells as described in the results section the used electrodes had a finger width and spacing equals to 5 μm. This translates into a sensitive height, i.e. the height to which

variations in the BSUT are perceived and measured by the electrodes, with a maximum value of 10 μm. This characteristic is especially important for the experiments described in this chapter as the interest lies in the observation of the cells response to chemotherapy and other treatments with a minimum of medium effects.

6.2.2 Presence of the Double Layer

Differently from the four terminal setup used to measure suspended cells, interdigitated electrodes are by definition two terminal electrodes, therefore in low frequencies the double layer effect due to electrode polarization is always present. Figures 6.2 and 6.3 shows the experimentally measured impedance results using an ionic solution phosphate buffer saline (PBS) of low concentration (approximately 0.2 M). In the plot the eight channels of the measurement system (micrux chips, described in the experimental procedure) are shown. Observe in the figures the straigth ramp behavior of impedance magnitude for frequencies below 10 kHz and the phase close to $90°$ characteristic of the presence of the double layer.

6.2.3 Equivalent Circuit Model to Analyse the Cells Attached to Interdigitated Electrodes

As already explained in previous sections, during impedance measurements using IDEs the double layer effects will always be present in frequencies below 10 kHz. Nevertheless, the value of the impedance that it inserts in the measurements can be subtracted from the experiments by fitting with a proper equivalent circuit model (ECM). Alternatively only frequencies above 10 kHz can be chosen where the double layer effects have already vanished. Figure 6.4 shows a simplified drawing of cell attachment to electrodes and to each other and figure 6.5 shows the equivalent circuit model (ECM) to represent the experimental situation. The circuit parameters are: the double layer capacitance (C_{dl}), the charge transfer resistance (R_{ct}), the medium resistance (R_{med1}), the attachment proteins resistance (R_{prot}), the cell membrane capacitance (C_{mem}), the cell membrane
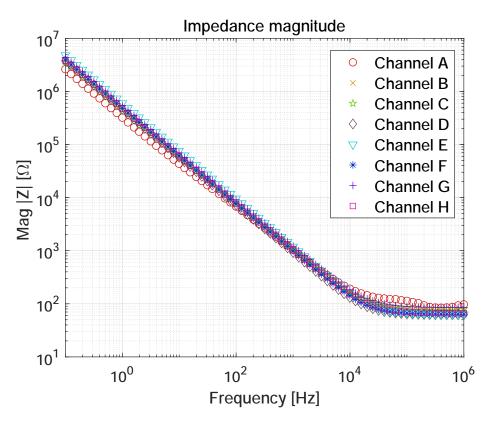
FIGURE 6.2: Bode plot of impedance magnitude measurements results of ionic solution phosphate buffer saline. Observe the strong double layer effect for frequencies below 10 kHz.

resistance (R_{mem}), the cell's junctions resistance (R_{junc}) and again the medium resistance ($R_{medium2}$). If the parallel resistances are combined the circuit can be simplified to the version on the bottom of figure 6.5 where R_{sol} is the equivalent of R_{med1} // R_{prot} and R_{eq} is the equivalent of R_{mem}//R_{junc}//R_{med2}. Remembering that the cell membrane resistance R_{mem} is very large one can write:

$$R_{eq} \approx R_{junc}//R_{med2} \tag{6.3}$$

And if cells are grown to confluence, namely, they fill completely the bottom of the chamber leaving no empty spaces among them, equation 6.3 can be rewritten as:
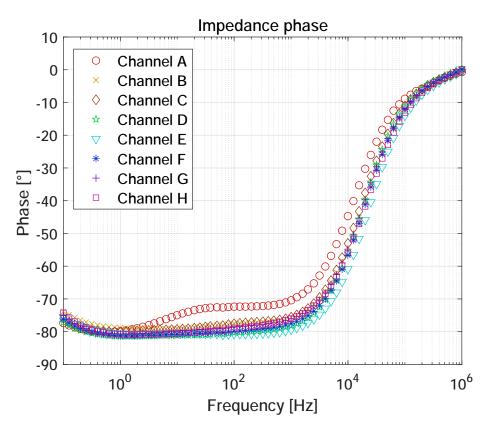
FIGURE 6.3: Bode plot of impedance phase measurements of ionic conductivity solution phosphate buffer saline. A phase equal to or close to 90° at low frequencies is a strong indicative of the double layer effect.

$$R_{eq} \approx R_{junc} \tag{6.4}$$

The results of equation 6.4 are of great importance. That is due to the role played by the resistance between the cell's junctions. Oncologists from UKE and other authors [112] believe strongly that the value of R_{junc} plays a crucial role in the metastatic behavior of the cells. Namely, that more metastatic cells have a smaller R_{junc} when compared to less metastatic ones, making easier for the cells to detach from the tumor and places where they are attached and walk through patient's body. That makes all sense. If experiments
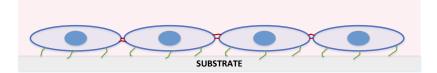
FIGURE 6.4: Simplified representation of the experimental situation of adherent cells. Cells are attached to the substrate and electrodes by means of binding proteins, in the figure represented by green lines. Cells are also attached to each other through cell junctions, in the figure represented in red color.

are performed in higher frequencies, namely, frequencies f >10 kHz, C_{dl} and R_{ct} disappear becoming a short circuit and the other elements R_{sol}, C_{mem} and $R_{eq} \approx R_{junc}$ can be determined from the fitting of the experimental data.

Unfortunately the experimental results shown on the next section such fitting was not possible and the main reason is that cells did not grow to confluence. The cells had a large difficulty in attaching to the Micrux IDE electrodes and that disturbed the observation of R_{junc}; still it was possible to observe and measure cell's growth and response to chemotheraphy. In order to measure R_{junc} a better electrode-system must be fabricated. Figure 6.6 illustrates the actual problem in Micrux IDE electrodes which prevented the proper attachment from the cells to grow to confluence and also a possible better electrode-system solution for the cells[1]. Another possible solution is to cover electrodes with a very thin layer of glass and create instead of an electrochemical cell, a capacitive cell.

6.3 Experimental Procedure

In order to perform the impedance experiments, circular interdigitated electrodes with a thin metal layer composed of 150 nm platinum on top of 50 nm titanium were purchased from *Micrux technologies*. The electrodes width and gap were both 5 μm. They had a sensitive area of 154 mm^2 and were composed of 180 pairs of fingers, leading to a

---

[1]To be fabricated. Such electrode system is not available on the market.
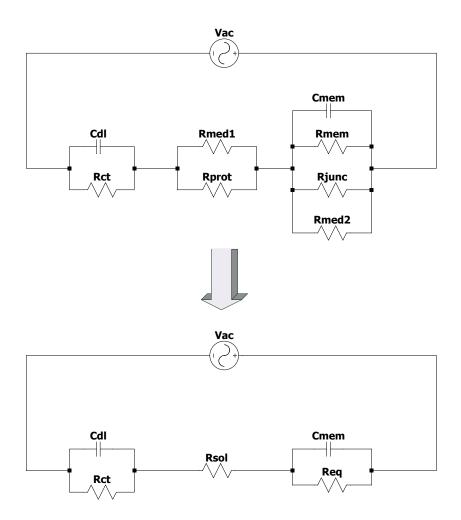
FIGURE 6.5: Equivalent circuit model for adherent cells attached on electrodes. On the left side the cell membrane resistance, cell junctions resistance and medium resistance is separated as it is in real experimental situation. On the right side, all three parallel resistances are combined together as electrically it is not possible to distinguish between them in a single experiment.

total number of 360 interlaced electrodes. Figure 6.7 shows the platinum IDE. Additionally, a platform called Multi8x All-In-One plus the add-on for multi-batch-cell was also purchased from the same company to allow the simultaneous measurement of up to eight samples with a total volume of 400 μl per channel. The multiplexer ECM8 from *Gamry Instruments* combined with the potentiostat *Interface 1000* was used as a measuring device to measure the impedance of the eight channels from Multi8x All-In-One
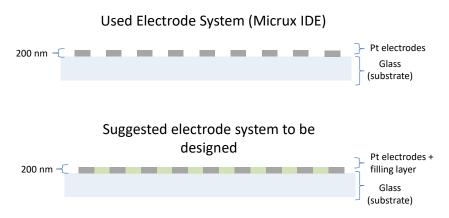
FIGURE 6.6: Lateral view (top) of used the system (Micrux IDE). Observe that the thickness of the metal patterned on the glass substrate (200 nm) was already enough to disturb complete cell attachment. Therefore the system below is proposed where the empty spaces between the patterned IDEs are filled with another material. It is very important that the surface for cell attachment is completely flat in order that cells manage to grow to confluence, then R_{junc} can be measured.

cell.
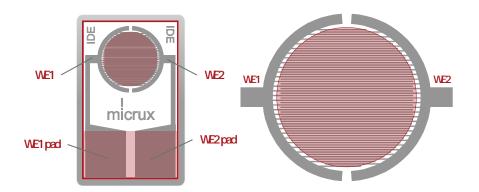
FIGURE 6.7: Micrux IDE electrodes chips used to measure the impedance of adherent cells. On the left side the complete chip is shown and on the right side a zoom only in the sensitive area. The acronyms WE1 and WE2 refer to working electrode 1 and working electrode 2. Figure extracted from [113].

In the first experiment, prostate cancer PC-3 cells were seeded on the electrodes in the numbers 7500, 15000 and 30000 at different channels and the impedance was monitored during two days to observe the cell attachment and growth. This step was important to decide the correct cell number to be seeded in the following experiments with chemo-theraphy, as the chemotheraphy only works when cells divide and grow. Therefore if a

large cell number is seeded too early, cells would stop growing due to lack of space in the electrode substrate and the effects of chemotheraphy could not be observed. After the analysis of the first experimental results, medical personnel decided to follow the next experiments with a cell seed of 6500 cells per Micrux channel.

Following, the experiment was repeated in another week for the same prostate cancer PC-3 cells during five days to observe the cell growth and response to chemotheraphy. The objective was to evaluate whether the electrode system was sensitive enough to follow cell death. A total of 6500 cells were seeded in several channels of micrux Multi8X All-In-One platform. One channel was left untreated without chemotherapy (only cells) as a control channel. Several channels were treated with different concentrations of the drug Docetaxel ranging from 1 μM up to 100 μM. Chemotheraphy was applied approximately 15 hours after cell seed and all channels were monitored for more four days regarding cell growth.

6.4 Experimental Results

6.4.1 Cell Attachment and Growth

The first objective of this part of the experiments was to test whether the platinum inter-digitated electrode system from Micrux was sensitive enough to track cells attachment and growth through impedance spectroscopy. That is important as compared to the suspension method where millions of cells are measured, in the impedance measurement of adherent cells the number of cells measured is in the order of thousands as only one layer of cells is formed on the electrodes.

The second objective of this part of the experiments was to decide the best cell number to be seeded for the chemotheraphy experiments. As chemotheraphy only works when cells divide and they stop dividing when they run out of space in the petri dish, different cell numbers that ranged from 7500 to 30000 were seeded in different channels and the impedance of the system was monitored during two days. Important to highlight is that as the used electrodes had 5 μm width and gap, a maximum height of 10 μm beginning from

electrode surface was monitored. Therefore, everything above 10 μm was not measured. This is desired as the interest lays mainly in monitoring cells behavior and not medium.

Figure 6.8 shows the magnitude of impedance for all cell's seed, namely 7500, 15000 and 30000. Observe that as expected large cell numbers give a higher impedance magnitude. As the cells do not attach directly to electrodes, but use specific proteins to fix themselves in the electrode and substrate, there will be a small layer of water with size in the order of nanometers between the electrodes and cells. This will show in the results as a double layer in frequencies below 10 kHz. Therefore, a frequency of 20 kHz was chosen to plot the impedance magnitude as at this frequency the double layer effects in the results are already vanished. From the figure it is clear that as cells attach to electrodes and grow the impedance magnitude increases. Lower frequencies are more sensitive to changes than higher frequencies, as they show in general larger values of impedance during the monitoring, but they also represent the situation in the surroundings and outside the cells. In higher frequencies the electric field is able to penetrate the cell membrane and enters inside the cell.

6.4.2   Evaluating Chemotheraphy Effects

In this part of the experiment 6500 PC-3 cells were seeded to micrux IDE microelectrodes one to five, all channels with approximately the same quantity of cells, and left to attach and grow for approximately 12 hours. Following, the chemotheraphy drug Docetaxel was given to the cells in the channels two to five in different concentrations (see figure 6.9). After that all the channels were monitored for more 25 hours and compared regarding cell growth. Figure 6.9 shows the results. In order to facilitate the comparison, curves were normalized in respect to their measured impedance by the following formula:

$$norm Z = \frac{z_{exp} - z_{min}}{z_{max} - z_{min}} \qquad (6.5)$$

Where $norm Z$ is the normalized impedance magnitude value shown in figure 6.9, z_{exp} is the experimentally measured impedance magnitude value, z_{min} is the minimum value of
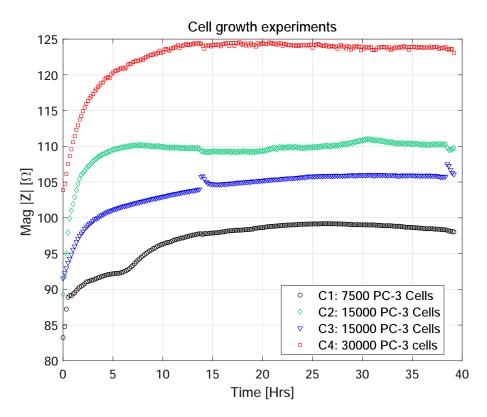
FIGURE 6.8: Magnitude of impedance monitored during two days when 7500, 15000 and 30000 cells are seeded in the IDE electrodes platinum electrodes. The plotted impedance results are for the frequency of 20 kHZ.

the measured impedance magnitude and z_{max} is the maximum value. This was done because although medical personnel tried to seed the same amount of cells in each channel it always showed some variation, i.e, in some channels a slightly larger number of cells was seeded than in others. Therefore in order to compare equally all the channels the experimental results were normalized. As in the beginning the impedance manitude is low because cells have not attached to electrodes and started growing yet, only the results after 5 hours are presented.

From figure 6.9 it can be seen that the quantities of 1 μM and 10 μM are not enough to prevent cell growth. For channel two, where 1 μM Docetaxel was applied cells stopped growing temporarily but after five hours they started growing again. For channel three, the 10 μM Docetaxel applied was not enough to prevent cell division and cells continued
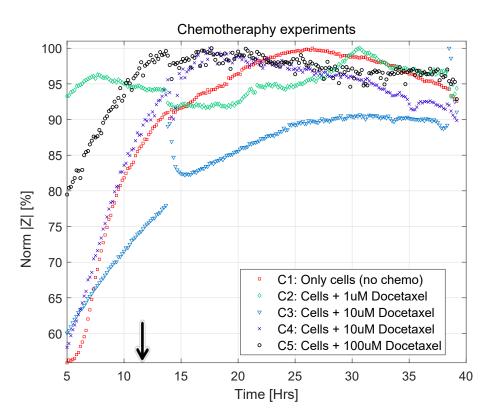
FIGURE 6.9: Normalized impedance magnitude comparison of cell growth with and without chemotherapy treatment. All channels were seeded with the same amount of 6500 cells and channel 1 (C1) was left untreated. Channel 2 (C2) was treated with 1 μM of Docetaxel, channels 3 and 4 (C3 and C4) with 10 μM and channel 5 (C5) was treated with 100 μM Docetaxel. The point in time where chemotheraphy was applied to the cells is highlighted with an arrow.

growing normally. In channel five, after Docetaxel was applied cells stopped growing and started slowly dying after 20 hours.

In a next experiment, the capacitance of 6500 PC-3 cells seeded in micrux IDE was measured and compared against the same amount of cells when the chemotherapy drug cisplatin is given. Figure 6.10 shows the results. While in channel two the capacitance raises during all the experimental period showing that cells continue growing, channel one where chemotheraphy was applied at 17 hours, after chemo application the capacitance decreases sharply showing the effect of cisplatin preventing cell growth and leading to cell death.
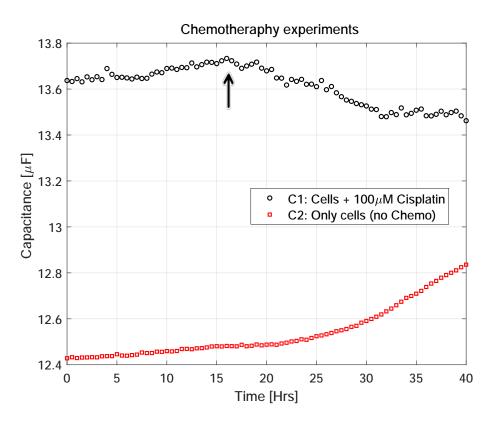
FIGURE 6.10: Comparison of the capacitance growth of PC-3 cells seeded in IDE micrux microelectrodes when cells are treated with the chemotherapy drug cisplatin (channel 1: C1) and no treatment (channel 2: C2). The same amount of 6500 cells were seeded in both electrodes. The point in time where cisplatin was applied is highlighted by an arrow.

6.5   Conclusions

In this this chapter, Time Domain Dielectric Spectroscopy (TDDS) was evaluated as a possible technique to automate cancer protocol screenings, for instance in a tumor-spheroid environment, to evaluate the best chemotherapy agent to be administered to a patient. In such a setting, different concentrations and/or different chemotherapy agents are applied to cell cultures formed directly from biopsies extracted from the primary tumor of the patients and TDDS is used to monitor the impedance magnitude or other variable, for instance, the capacitance of the cell culture for a long period of time in a single frequency. By comparison the trend whether cells are dying or not can be found, as when

cells die their membranes break and the overall capacitive effects decrease. Based on the percentage of cell death physicians can have a better idea of which type of treatments are more or less effective to a specific patient. Currently, such screenings are rarelly performed due to their high costs, as a lot of manual work is involved and one laboratory technician should be dedicated to the this single task during a couple of weeks, not to say the fact that such screenings are not paid by most healthy insurances.

Limitations of using TDDS to automate cell screening protocol are the need to use frequencies above 10 kHz to avoid double layer effects in low frequency ranges as two terminal interdigitated electrodes (IDE) are used. Although the development of a four electrode terminal is theoretically possible, it is certainly not the best setup for such experiments as the larger distance between the current carrying electrodes make the electric field lines go higher in the medium instead of staying confined close to the cells, in this case making the results worse.

The system used here from the company Micrux Technologies (Multi8x All-In-One Platform) combined with the multiplexer ECM8 from Gamry Instruments has the advantage of providing several channels at the same time (up to eight) for comparison, having very narrow gaps and finger sized electrodes (5 μm) and being made of platinum, but lacks specificity and accuracy. Often experiments had to be repeated or provided innacurate results due to innacuracy in the electrodes already from the fabrication process. A second limitation is that cells had difficulty attaching to the places where the IDE electrodes were patterned. In microscopic figures taken from the micrux chips, in many of them cells attached better to the places where there was no metal only the glass. Even when the metal thickness is in the order of 200 nm it seems already enough to disturb good cell attachment. In this case for a long term use inside a hospital another system is recommended as previously described and envisioned in figure 6.6.

Chapter 7

Spectral Response of Healthy Tissues and Solid Tumors

7.1 Theoretical Background

Cells are the building blocks of multicellular organisms; they are all enclosed by a cellular membrane. They are the basic unit forming the tissues. Animal tissues are organized and well-coordinated and cooperating collection of cells. In general, four types of tissues are distinguished in animals: connective, epithelial, nervous and muscular. Nevertheles, the large structural differentiation is made between connective and non-connective tissues.

Tissues are composed of cells and extracellular matrix (ECM) secreted by the cells around themselves. Extracellular matrix gives supportive tissues, e.g. bone, its mechanical strength. The extracellular matrix also allows cells to be connected together. Nevertheless, cells can also be directly connected by cell junctions.

Connective tissues are rich in extracellular matrix which holds the mechanical load. In other tissues, extracellular matrix is rare and cells hold the load directly. In non-connective tissues cells are joined directly together through cell junctions. Examples of connective tissues are tendons, bones, dermis of the skin and cartilage. The extracellular

matrix constitutes the bulk of the connective tissues and cells responsible for producing the ECM are scarcely spread on it.

The tensile strength of connective tissues comes mainly from collagen. The different types of connective tissues will have different types of collagens, different quantities and different molecules connecting collagen. Collagen constitutes approximately 25% of the total protein mass of mammalian organisms. There are 20 different types of collagen proteins found in animal cells [6].
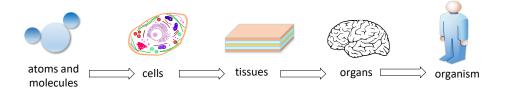
FIGURE 7.1: Illustration of the hierarchy forming mammalian organisms. In the lowest level atoms form molecules, molecules form cells, cells form tissues, tissues form organs and organs will form entire organisms.

Tissues and organs[1] are organized collections of many cell types, that live together and cooperate. Although tissues differ substantially from each other they all carry some common features. All tissues need a supportive framework that provides them mechanical strength given by the connective tissue. Also in all tissues nutrients and oxygen are provided by blood vessels formed of epithelial cells. The blood vessels also collect waste together with lymphatic vessels which collect excess of liquid. All tissues contain nerve cells or axons for sensitivity. They are also populated by macrophages that migrate from one site to the other and do the cleaning of debris. Additionally in all tissues lymphocytes for defense of the cells against foreign invading microorganisms will be found.

Therefore, all tissues are an organized and complex conjunction of many different cells types, that must remain different in order to perform their activities and that must coexist and cooperate harmonically. In all tissues cells are constantly dying and being replaced by new cells, except in nervous tissues.

---

[1]Organs are organized collection of several tissues.

One question that may appear is how the same organization of the tissue is preserved. Three factors are important to contribute for tissue organization and stability, namely: cell to cell communication, selective cell adhesion and cell memory [6]. Cells are constantly sending signals to other cells in their surroundings and also monitoring the environment to search for messages from other cells. They also adjust their behavior according to the messages received. Also cells do not adhere to each other randomly, but have specific cadherins and other adhesion molecules that attach to the same cell type or very specific other cells and the ECM. Therefore, the attachment from one cell to each other or to the ECM is very selective. This prevents the disorganization of the tissue by cell attachment. By last, cells also carry memory by means of genes since their embrionatic state and pass it on to their daughter cells to preserve their distinctive characteristics.

Summarizing, tissues and organs are organized collection of different cell types that live together and cooperate. All tissues contain nerves, blood and lymphatic vessels, macrophages and lymphocytes. All tissues except nervous ones are constantly being renewed at different rates. Figure 7.1 shows in a stepwise manner the organization of mammalian organisms, starting from the smallest level, that is the atom, up to whole organisms. Figure 7.2 exemplifies the organization of the small intestine organ showing its composing tissues and cell types.

7.2   Spectral Response of Healthy Tissues

The main features of the dielectric spectrum of tissues are well known and have been measured and parameterized for a variety of tissues [18, 114–117]. The dielectric spectrum of tissues vary in three main defined steps or dispersion regions, namely, α, β and γ [14, 115]. Minor effects of δ-dispersion can sometimes also be observed. The α-dispersion occurs due to accumulation of charge caused by ionic cloud and diffusion surrounding cellular membranes. It is observed in the lowest frequency range, approximately from few Hz up to 100 kHz [14] and it reaches high permittivity values depending on the tissue in the order of $10^6 - 10^8$ in frequencies below 100 Hz [115]. The β-dispersion is observed above hundreds of kHz and up to 100 MHz and is due to polarization of cellular membranes impeding the charge flow between the intra- and extra-cellular medium.
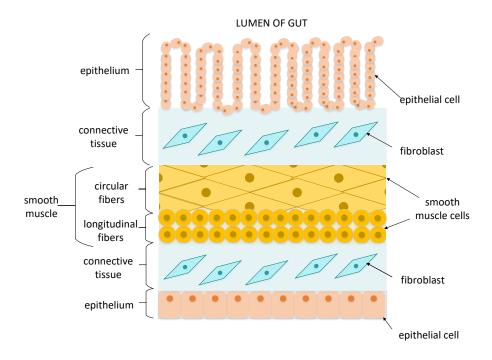
FIGURE 7.2: Simplified view of a part of the intestine of a mammal. The intestine is formed of epithelial tissue, connective tissue and muscular tissue. Each tissue by itself is formed of cells connected to each other by cell junctions or connected to the ECM.

Other mechanisms contributing to it may be the polarization of proteins and other organic molecules. The γ-dispersion is due to polarization of water dipoles inside biological material and is observed in the GHz range.

Several expressions are used to model each dispersion region, the simplest and widely known as Debye formula express the complex permittivity of the tissue as a function of the angular frequency ω, the relaxation time τ, and the dielectric constants at low (ε_s) and high frequencies (ε_∞). Mathematically:

$$\hat{\varepsilon} = \frac{\varepsilon_s - \varepsilon_\infty}{1 + j\omega\tau} + \varepsilon_\infty \qquad (7.1)$$

To model the complete spectrum of a tissue several authors report that between four to five dispersion terms are necessary [114]. Another effect commonly observed in biological

material is the broadening of the dispersions. Therefore, introducing an exponent (α_n) in the equation above to account for the broadening and representing all the dispersion regions by a sum we have the well-known Cole-Cole equation:

$$\hat{\varepsilon}(\omega) = \sum_{n=1}^{N} \frac{\Delta \varepsilon_n}{1 + (j\omega\tau_n)^{(1-\alpha_n)}} + \frac{\sigma_i}{j\omega\varepsilon_0} \qquad (7.2)$$

The capital letter N represents the total number of dispersions and small n represents the parameters for a single dispersion. With the choice of the correct parameters to each tissue type, Cole-Cole equation can be used to represent accurately the dielectric behavior for a large number of tissues in a wide frequency range. Observe that $\hat{\varepsilon}(\omega)$ is complex valued.

Figures 7.3 and 7.4 show a plot of the dielectric behavior of several tissues based on the data summarized in Table 1 of reference [114]. This is a compilation of more than fifty years of study, with data measured from animal and human tissues. For some tissues like skin and fat the variation in the dielectric spectrum is large and some authors report a range instead of average values. Several organs were also measured in transversal and longitudinal direction and in the plot the average is shown. Gabriel [117] reports values for the dielectric properties of tissues that go from 10 Hz up to several GHz. In figures 7.3 and 7.4 only the dielectric data that corresponds to the frequency range 1Hz - 1 MHz is shown.

The figures also show that the permittivity and conductivity vary significantly from tissue to tissue. That can easily been explained by tissue composition, therefore a behavior already expected. Each tissue has its characteristic curve, each one very different from each other. Although the figures show the dielectric behavior of different tissues in a wide frequency range, they do not explain the molecular and biological mechanisms behind such behavior.
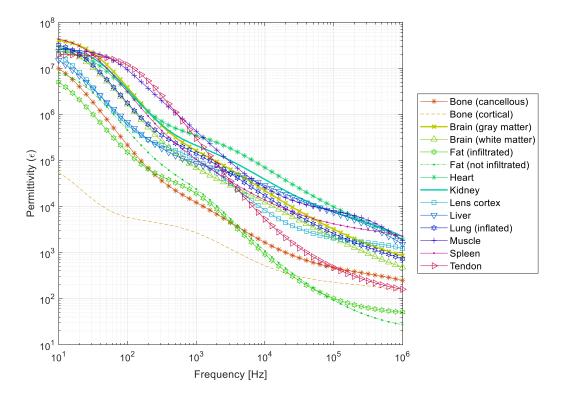
FIGURE 7.3: Permittivity (ε) of different animal and human tissues, compiled from [18, 114–117].

7.3 Tumor Composition and Organization

Organs are composed of cells and stroma. Cells are responsible for performing the main function of the organ, e.g., produce hormones, produce sweat, secrete some substance while the stroma supports the organ mechanically and provides a path for nutrients to the cells of the organ. The stroma is divided in ECM which is rich in fibrous proteins and stromal cells, like fibroblasts, adipocytes, cells of the vascular and immune system. In the stroma metabolites will also be present. As the stroma supports the normal organ functioning also the tumor stroma supports its development. Later stage cancers in general have a more supportive tumor environment than restrictive [118–120]. Examples of stromal components that are commonly associated with tumor promoting functions are carcinoma associated fibroblasts (CAF), type I collagen and some types of immune cells.
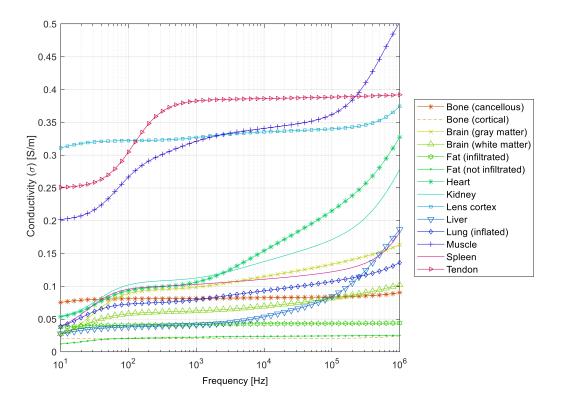
FIGURE 7.4: Conductivity (σ) of different animal and human tissues, compiled from [18, 114–117].

Solid tumors resemble and work as organs [121]. Similar to healthy organs, they are composed of cells and stroma. In the tumor organ or microenvironment several cell types are found, like tumor cells which compose the massive part of the tumor core, endothelial cells forming the blood vessels which provide oxygen and nutrients for the tumor, fibroblasts which are responsible for producing and remodeling of the tumor ECM, macrophages which promote cancer cell migration, neutrophils that can be tumor supporting or suppressing, dendritic and cytotoxic T cells [122]. Figure 7.5 shows a high level visualization of the tumor microenvironment composition. The stiffness of the tumor is related to the abundant ECM rich in fibers that surrounds it. As tumors develop they also recruit neighboring cells to grow blood vessels to vascularize them. Some unstructured and mal-functioning versions of a lymphatic system can also be found.

Tumors also interact with the other organs sending signals and receiving signals from
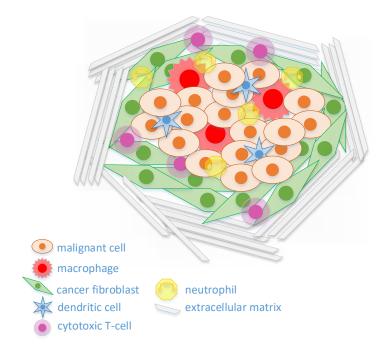
FIGURE 7.5: Simplified view of tumor microenvironment. While the core of the tumor is massively populated by tumor cells, the stroma is filled with several other cell types like fibroblasts, macrophages, neutrophils, among others. The tumor is surrounded by ECM fibers. In the drawing, blood and lymphatic vessels are not shown.

them. Nevertheless, in normal organs the interaction and products of the cells promote the survival of the organism, while in tumors their effects and wastes will at the end cause the death of the patient.

7.4 Main Structural Differences Between Tumor and Healthy Tissues

As already mentioned in the previous section, some authors [121] also define tumors as organs; others prefer to refer to tumors and its surrounding as tumor microenvironment.

As organs, tumors are also formed of tissues, but differently from normal organs where cells are orderly organized in layers to form tissues, in tumors the cell arrangement is disorganized. The organ loses its composing parts and cells proliferate and adhere disorderly. Also, in normal organs cells show uniformity in shape and size. In tumors cells are deprived of harmony, therefore cells shape and size varies significantly. In adult tissues cells are constantly dividing and forming new cells; nevertheless in tumor the rate of reproduction is surprisingly higher and increases for more aggressive types of cancer. The number of dividing cells is also significantly larger in tumors when compared to healthy tissues.

With respect to circulation, tumors differ mainly in two characteristics when compared to healthy tissues: blood vessels of tumors are leaky and tumors do not contain a properly functioning lymphatic system [123, 124]. This implies that solid tumors have a high intratumoral fluid pressure (IFP) due to the accumulation of blood and fluids inside of them [125]. The high IFP is also the reason why most cancer patients with solid tumors do not respond properly to chemotherapy. Due to Fick's law of diffusion, substances diffuse from areas of high concentration to low concentration, nevertheless due to high IFP chemotherapy agents do not diffuse deep into the tumors, but stay confined in a small area surrounding blood vessels and at the tumor margins [125–127]. An average of 75% of patients with solid tumors do not respond to any cancer treatment [128] and physicians attribute that largely to the high IFP.

Other characteristic commonly mentioned by several authors is that cancer cells have in general a large and variable nucleus size than normal cells. Cancer cells also lose their specialized functions and in general are unable to perform the activity done by the original cell that gave rise to the cancer ones. Another commonly mentioned difference is that while the boundaries of normal organs are well defined tumors have poorly defined boundaries.

In normal adult organisms, cells are constantly dying and are replaced by new cells. Cells divide when they are needed and stop to divide when not. They also must be able to "kill" themselves when they are defective or not needed, a process called cell apoptosis. Healthy cells also remain in the places and tissues where they are supposed to be respecting the surroundings. Those are exactly the two mechanisms which are lacking

in malignant cells: they divide continuously disrespecting the normal constraints of cell survival and they invade surrounding tissues. If cells multiply continuously but do not invade surrounding tissues, they form benign tumors. Otherwise, if they metastasize they are called malignant tumors. In Europe and North America it is expected in the next years that 25% of the population will die of cancer [6]. Table 7.1 summarizes the main differences between healthy and cancer cells and tissues.

TABLE 7.1: Main differences between cancer and healthy cells and tissues.

Characteristic	Cancer	Normal
Cell's arrangement	disordely	orderly
Cell's shape and size	variable	uniform
Number of dividing cells	large	small
Blood vessels	leaky and malfunctioning	normal
Lymphatic vessels	inexistent or damaged	well functioning
Interstitial fluid pressure (IFP)	high	normal
Cell's nucleus size	large and variable	normal and uniform
Boundaries	poorly defined	well defined
Proliferation	indefinite (never stops)	well defined and controlled
Specialized cell's functions	unable to perform	normal
Respect to organ's location	no (metastasize)	yes
Ability to populate and survive abnormal locations	very able	unable; cells die when moved to abnormal locations

7.5 Comparison Tumor vs. Healthy Tissues Spectral Response

Bioimpedance spectroscopy is a technique that can be used to differentiate healthy from cancer tissues based on the variation of the electrical properties of the tissues when submitted to frequency variable electric fields. In a previous publication [1], five different tissues of a healthy mice and two cancerous infected with the tumor cell lines UT-SCC-5 (tongue squamous cell carcinoma) and UM-SCC-10A (laryngeal squamous cell carcinoma) were measured with a 2T setup and compared. Our results proved that the different tissue types show a significant variation in their impedance values and that in frequencies above 1 kHz it was possible to distinguish the healthy tissues from the cancer ones.

In this section, experiments were performed with healthy tissues of six mice and tumors using a 4T setup. The same trend as observed in previous works that cancer tissues have the conductivity values amongst the highest, equivalently the lowest impedance values [1, 129] was again confirmed. More interesting is that the use of a 4T setup allowed the observation of tissues response without the interference of electrode polarization up to very low frequencies (f = 10 Hz).

7.5.1 Experimental Setup

A total of six immunodeficient mice (xenograft model) were provided by the Institute of Anatomy and Experimental Morphology of the University Medical Center Hamburg-Eppendorf (UKE) for the experiments. The mice are known as severe combined immunodeficient mice (SCID) and they were purchased from Charles River. They possess a genetic autosomal mutation which combines into a severe immunodeficiency affecting B and T lymphocytes, therefore their immune system is unable to respond to tumor formation and the implanted tumor can develop without the interference of the mouse immunosystem. A total of 1 million human cancer cells as described in table 7.2 were subcutaneously injected in each mouse in the area of the right scapula. All experiments

with animals were approved by the local animal experiment approval committee (Behörde für Gesundheit und Verbraucherschutz, Amt für Verbraucherschutz, Lebensmittelsicherheit und Veterinärwesen, assigned project No. N08/2018), supervised by the institutional animal welfare officer and performed in accordance with relevant guidelines and regulations. Mice were kept in individually ventilated cages under pathogen-free conditions, fed with sterile standard food and water ad libitum, and were regularly monitored concerning sub cutaneous tumor growth. As soon as the tumor has grown up to 1 cm^3 each animal was sacrificed and the impedance was measured $ex-vivo$ shortly after animal death. All experiments were performed with a 4T electrode setup using needle electrodes. For the experiments of the tumor HT29 stainless steel needles were used and all the others were performed with platinum-iridium needle electrodes. All implanted cancer cell lines are human cancer cells.

Organs and primary tumor were placed in phosphate buffered saline (PBS) from Dulbecco's to keep them longer alive and for nutrition. For the measurements, the organs one by one were removed from PBS and fixed in a petri dish. An array with four needle electrodes was used to perform the experiments in order to provide a four-electrode-terminal stimulation and avoid double layer (DL) effects at electrodes surfaces in low frequencies. Figure 7.6 illustrates the electrode array used. The needles used were made of platinum-iridium (M2-M6) or stainless steel (M1) and they are used normally to subdermal EMG stimulation. They had a total length of 12 mm and a diameter of 0.4 mm. After each experiment, needles were discarded.

The potentiostat Gamry Interface 1000^{TM} from Gamry Instruments Inc. was used to perform all experiments. The device measures the tissue current (perturbation) caused by the applied voltage. A 14 mV amplitude voltage signal was applied and the frequency was varied from 1 MHz up to 1 Hz in steps of ten points per decade to measure the tissues response.

7.5.2 Experimental Results

Experimental data was processed in MATLAB® for visualization and analysis. Data was plotted as permittivity ε and conductivity σ in order to be comparable with literature
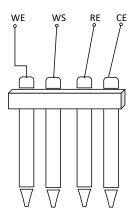
FIGURE 7.6: Illustration of the array of needle electrodes used to perform the measurements. The four needles are fixed through a small support in order that they do not move and they are also equally spaced by 2 mm distance. The acronyms WE, WS, RE and CE refer to electrodes terminals, namely, working, working sense, reference and counter. The WE and CE are the current carrying electrodes, while the WS and RE are used to sense the voltage in the tissues.

values. The value of ε was calculated as [114, 115]:

$$\varepsilon = \frac{C}{C_{air}} \tag{7.3}$$

Where C is the experimentally measured capacitance and C_{air} is the air capacitance of the array of four needle electrodes. In the present case the C_{air} experimentally measured is equal to 41.22 pF. The capacitance C is directly extracted from the experimental data by means of:

$$C = \left| \frac{1}{\omega * imagZ} \right| \tag{7.4}$$

Where imagZ is the imaginary part of the measured impedance. Important to highlight here is that differently from normal capacitors which have a constant ε, the ε of biological tissues is frequency dependent. The value of σ can be calculated as follows:

$$\sigma = G * K \tag{7.5}$$

TABLE 7.2: Measured mice with tumor types and organs.

Mouse	Implanted Cancer Cells	Cancer Type	Measured Organs
M1	HT29	Human colon carcinoma	Brain, Heart, Kidneys, Lungs, Liver, Skeletal Muscle
M2	PC3	Prostate neuroendocrine cell carcinoma	Brain, Heart, Liver, Lungs, Skeletal Muscle, Tumor
M3	PC3	Prostate neuroendocrine cell carcinoma	Brain, Heart, Kidneys, Liver, Lungs, Skeletal Muscle, Spleen, Tumor
M4	PC3	Prostate neuroendocrine cell carcinoma	Brain, Heart, Kidneys, Liver, Lungs, Skeletal Muscle, Spleen, Tumor
M5	PC3	Prostate neuroendocrine cell carcinoma	Brain, Heart, Kidneys, Liver, Lungs, Skeletal Muscle, Spleen, Tumor
M6	PC3	Prostate neuroendocrine cell carcinoma	Brain, Heart, Kidneys, Liver, Lungs, Skeletal Muscle, Spleen, Tumor

The value of K is known as cell constant and is a parameter of the geometry of the system. For a parallel plate electrode configuration it is defined as the distance of the electrodes d, divided by their area A. In the case of other geometries where it is hard to calculate it analytically, it can be experimentally determined through the measurement of a known conductivity ionic solution for instance PBS or NaCl. For the present case its value is equal to 27. The conductance G is also extracted directly from the experimental data as:

$$G = \frac{1}{realZ} \tag{7.6}$$

Where the value of *realZ* denotes the real part of the experimentally measured impedance.

Figure 7.7 shows the experimental results for the mice brain (healthy) relative permittivity ϵ_r and figure 7.8 the value of the experimentally measured conductivity σ. Brain was measured in left and right side lobes, both in transversal (tran) and longitudinal (long) directions. The values of M1 to M6 indicate the number of the mouse which the experimental result refers to. In the case of brain, the average for both right and left side lobes

120

in the longitudinal direction is shown as "Mn-long" where n is the mouse number. The same way for the transversal (Mn-tran). The average value for brain calculated from all experiments is also plotted (Mean).

Following brain, the impedance of mice kidneys was also measured. Figures 7.9 shows the ε_r and figure 7.10 the σ derived from the results. Mice kidneys were also measured both right and left sides, in longitudinal (long) and transversal (tran) directions. The plotted values are the average for both kidneys, left and right, in either longitudinal or transversal direction. The average (mean) of all the experiments is also plotted. The value of conductivity for M1 was excluded from figure 7.10 as it was unstable and incorrect in several frequencies. That is a clear indication of a poor electrode interface with the measured tissue. This can be caused by old, bad quality, corroded electrodes and also unstable metals like stainless steel. That is the reason why for the following experiments (M2-M6) platinum-iridium needle electrodes were used. Interesting to notice is that this effect is not seen in the permittivity derived from the imaginary part of the experimentally measured impedance, but only in the conductivity derived from the real part of it, indicating the possible existence of a polarization current.

In a next step mice liver was measured in longitudinal and transversal directions. Figure 7.11 show the permittivity ε_r and figure 7.12 the conductivity σ derived from the results. Skeletal muscle from the mice legs was measured afterwards. Figures 7.13 and 7.14 show the permittivity ε_r and the conductivity σ respectively. Muscle in general has a lot of salt content therefore it has higher conductivity when compared to other organs.

Differently from skeletal muscle, lungs showed a very small conductivity. Such result is expected as a substancial part of the measured organ is formed of tiny membranes and there is not much path for current flow. Figures 7.15 and 7.16 show the permittivity ε_r and the conductivity σ for the lungs.

Spleen followed, measured only in longitudinal direction as it was too narrow in transversal direction to be measured. Figures 7.17 and 7.18 show the results. Spleen had the smallest conductivity and the smallest permittivity among all compared organs. Mice heart results are shown in figures 7.19 and 7.20.

Figures 7.21 and 7.22 show the permittivity ε_r and conductivity σ of the tumors. For M1 the spread in impedance values for frequencies below 100 Hz is large, the reason is the use of stainless steel electrodes which form an unstable interface with the biological tissue under test. Contrary, for M2-M6 the spread in low frequencies is low and can be neglected. The reason is that new platinum-iridium electrodes were used to measure the tissues of those animals, which provide a much more stable interface (stable potential). For the implant and future measurements it is highly recommended to use platinum electrodes as platinum is a very stable metal for biological measurements and in general does not react with biological material. Therefore it can provide very stable reference electrodes which are essential for four-electrode-terminal impedance measurements. The disadvantage is that platinum is an expensive metal.

Very interesting is to plot the permittivity and conductivity of all organs together (figures 7.23 and 7.24) and compare them. And also the impedance magnitude and phase (figures 7.25 and 7.26). Not surprisingly, tumor showed the lowest impedance from all measured organs or equivalently the highest conductivity. The same result we also observed in a 2T measurement already in high frequencies [1] with other mice tissues and tumor types. As described in previous sections, tumors have leaky blood and mal-functioning lymphatic vessels, therefore liquids and salts accumulate inside them. This accumulation of fluids cause a decrease in tumor impedance values when compared to normal organs.

For the phase, the PC-3 cells tumors have a larger phase as the HT29 tumor, but from the phase alone it is hard to distinguish each organ. From figure 7.23 it can be seen that both tumors showed the highest average permittivity, which translates into the highest capacitance among all measured organs. This is somehow interesting and other authors found similar results [20, 130]. Observe that the larger average permittivity represents the permittivity of the complete tumor, namely, tumor cells plus tumor microenvironment. The tumor cells are surrounded by the tumor microenvironment with extracellular matrix, lots of fibers, fibroblasts, lymphatic and blood vessels, among others, and the permittivity of the tumor is a measure of everything.

7.6 Conclusions

One important contribution of this chapter to Biomedical Science was to extend the experimental data of ε_r and σ for seven different normal tissues (brain, spleen, heart, lungs, kidneys, liver and skeletal muscle) and two tumor types (HT29 human colon carcinoma and PC3 prostate neuroendocrine cell carcinoma) up to 10 Hz. Literature data for the frequency range below 1 kHz is scarce or inexistent. The curves shown by [114, 115, 117] which are the most recent compilation from the literature of the measurements performed during the last fifty years, for most tissue types are based on best fitting for frequencies below 1 kHz and as the references explain are subject to errors. This work, by using a four electrode terminal setup allows data extension for ε_r and σ up to 10 Hz. Important to highlight is that, here the experimental data is based on mice tissues, while the authors of references [114, 115, 117] used mostly porcine for their experiments.
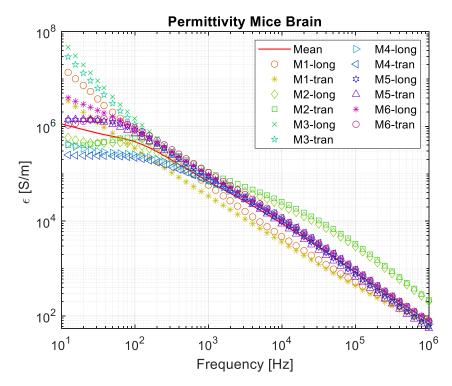

FIGURE 7.7: Experimentally measured relative permittivity ε_r of mice brain.

One interesting observation was that tumors have a tendency to show smaller impedance magnitudes and higher conductivity values than normal tissues, due to their high water content. This result was already observed by other authors in different experiments [3, 4, 20]. Nevertheless, for its generalization, a larger clinical study with at least twenty repetitions of the same experiment for each tumor type is necessary. Such clinical study is out of scope of this work.

A second important observation was that both tumors showed in average a larger ε_r, which translates into a larger capacitance, than all the other normal tissues measured. O'Rourke [20] and Pethig [130] obtained similar results in their studies; the first with hepatic tumors and the second with breast tumors. Important to highlight here is that this result represents the capacitance of the complete set of tumor and its microenvironment (extracellular matrix, lymphatic and blood vessels, other cells in the microenvironment and so on). Here again the generalization of such results requires a larger set of experiments in the context of a clinical study.
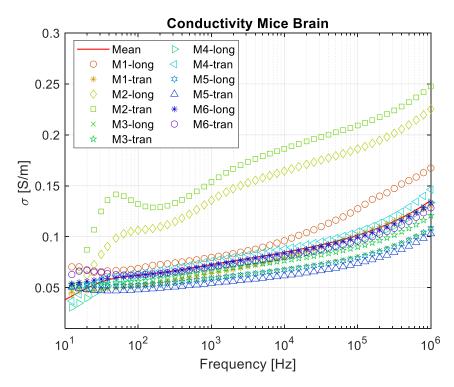
FIGURE 7.8: Experimentally measured conductivity σ of mice brain.
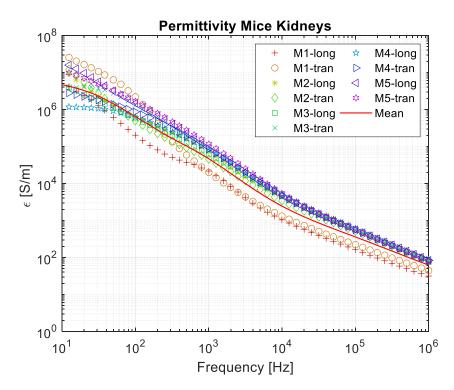
FIGURE 7.9: Mice kidneys permittivity ε_r

.
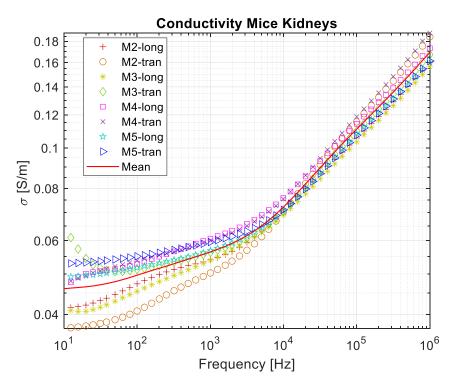
FIGURE 7.10: Mice kidneys conductivity σ.
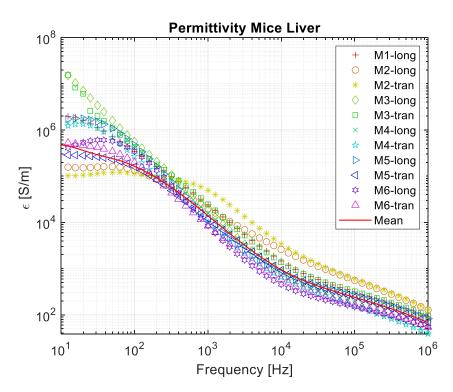
FIGURE 7.11: Mice liver permittivity ε_r.
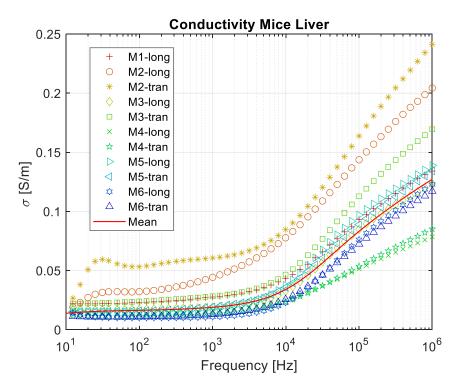
FIGURE 7.12: Mice liver conductivity σ.
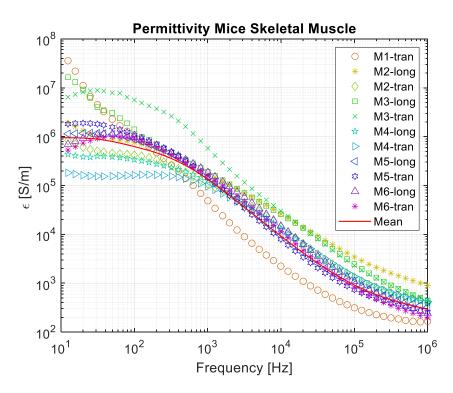
FIGURE 7.13: Mice skeletal muscle permittivity ε_r.

127
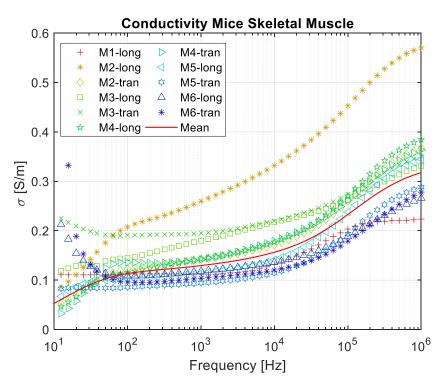
FIGURE 7.14: Mice skeletal muscle conductivity σ.
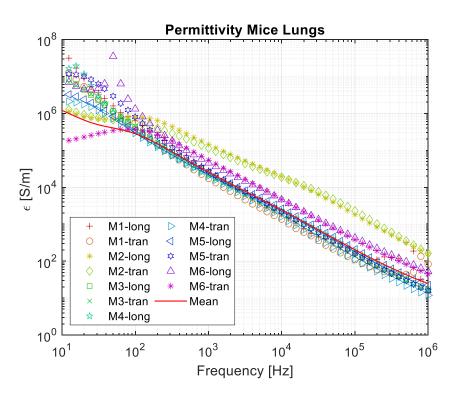
FIGURE 7.15: Mice lungs permittivity ε_r.
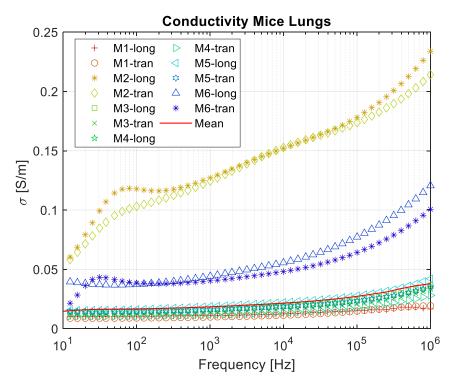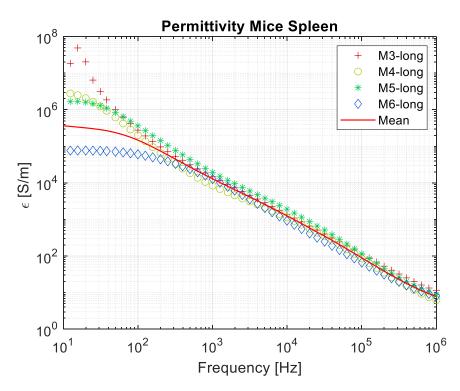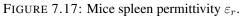
FIGURE 7.16: Mice lungs conductivity σ

.

FIGURE 7.17: Mice spleen permittivity ε_r.

129
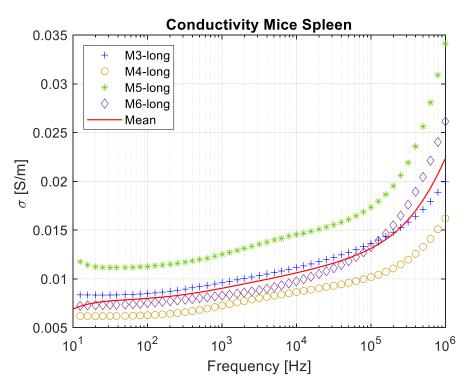
FIGURE 7.18: Mice spleen conductivity σ.
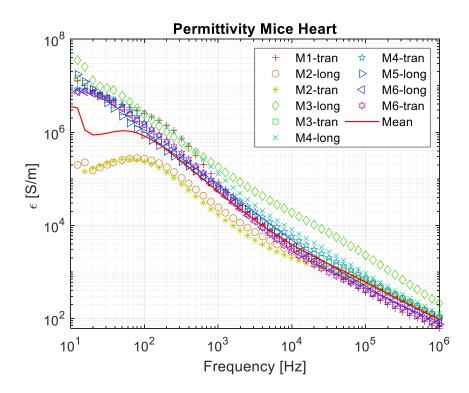
FIGURE 7.19: Mice heart permittivity ε_r.
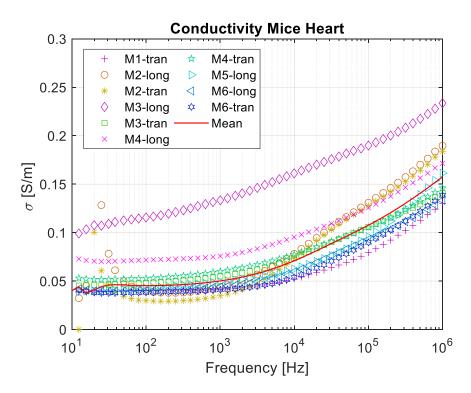
FIGURE 7.20: Mice heart conductivity σ.
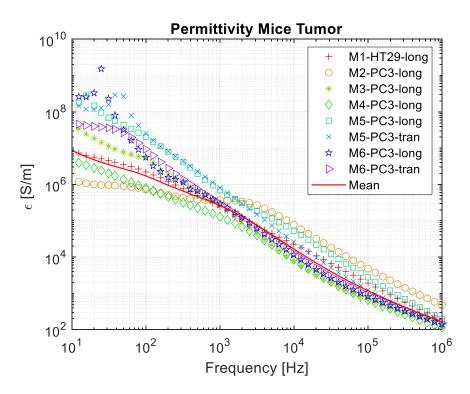
FIGURE 7.21: Permittivity of mice tumors.
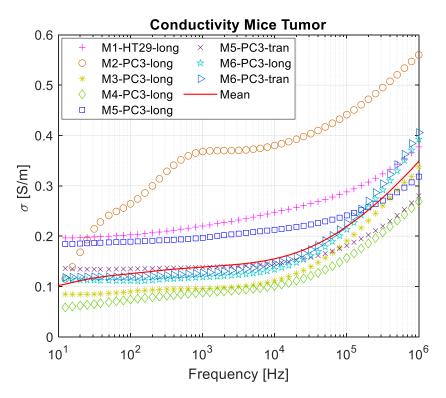
FIGURE 7.22: Conductivity of mice tumors.
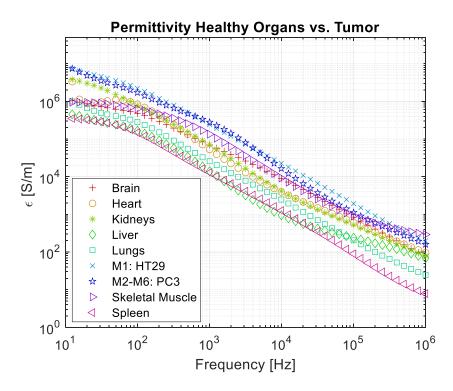
FIGURE 7.23: Comparisom of tumor and healthy organs permittivity ε_r.
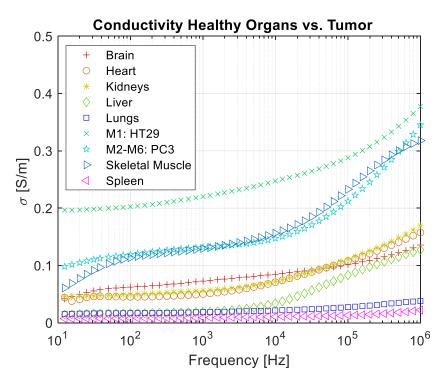
FIGURE 7.24: Comparisom of tumor and healthy organs conductivity σ.
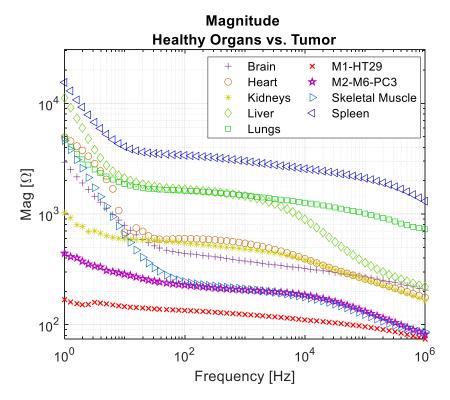
FIGURE 7.25: Comparisom of tumor and healthy organs impedance magnitude.
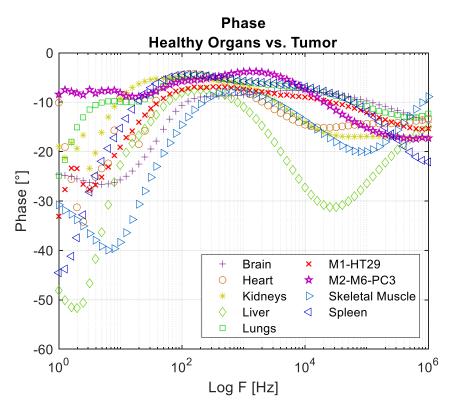
FIGURE 7.26: Comparisom of tumor and healthy organs phase.

Chapter 8

Conclusions and Future Work

8.1   Summary and Conclusions

The main research question of this Doctoral Thesis was to answer whether different cell types and tissues could be distinguished by means of BIS. Especially a large focus was given to distinguish cancer cells and solid tumors from healthy ones by means of BIS. The results of many chapters in this Doctoral Thesis pointed out in the direction of several differences in the dielectric properties of healthy and cancer tumors and cells, that potentially can be used to distinguish them. In regards to solid tumors it was observed that they in general have a lower impedance magnitude and higher conductivity than healthy organs. This characteristic can be used to aid in the development of new drugs and therapies for patients. In regards to cancer cells, it was observed that the more metastatic they are, the lower is the external cell surface charge, showing a leakier membrane. With a leakier membrane, cells have difficulty keeping the correct level of the cell membrane resting potential, shifting it towards more positive values. As the value of the cell membrane potential functions as signaling for the cells to start their division cycle [7], a leakier membrane explains at least partially the aggressiveness of the cancer.

Throughout the last year ten years, several authors found similar trends. In [131], the authors developed a microelectrical impedance spectroscopy device to measure single

cells. They scanned several frequencies starting at 5 kHz up to 1 MHz, and they found the optimal frequency of 119 kHz where the impedance difference between the healthy (SV-HUC-1) and cancer urothelial cells (TCCSUP) is maximized. In a second research [132], the authors developed an assay-based method that uses electrical impedance spectroscopy to measure the impedance of in vitro cells to distinguish between the healthy and cancer ones. In their protocol, they measured four consecutive phases and extracted 26 relevant characteristics from the cell cultures. They extracted from the set of 26 characteristics the most relevant in terms of their discriminant capacity, and through those characteristics they were able to distinguish between the healthy and cancer cells with a rate of 4.5% of false positives and no false negatives. In a third work [133], authors combined a microelectrical impedance spectroscopy device with machine learning techniques and they were able to distinguish between the normal and cancer cells with an accuracy of 91.7%. In a fourth research [134], the authors developed a microfluidic microelectrical impedance spectroscopy device to measure single prostate normal (RWPE-1) and cancer (PC-3) cells and they were able to discriminate between the cells by means of the admittance and susceptance with an average difference of more than 50%.

When this doctoral thesis started as a research there was a vision of an unique signature of cells and tissues, similar to a fingerprint, that could be used to distinguish them. Experimental results from the chapter 4 showed that possibly this signature exists for cancer cells and for one cell type (HT29) such signature was observed. The challenge here in measuring cells suspensions lies on keeping the experimental conditions in a such a controlled way, with exactly the same parameters (same temperature, same electrodes condition, same volume fraction of alive suspended cells, same supernatant conductivity) that such signature can be measured accurately. That is quite challenging, given the very dynamic nature of biological media. Nevertheless, much less challenging is to extract parameters from the spectral response of the cells and use such parameters to analyse them. Although a spread in the parameters is observed, still they permit interesting insights in the cells characteristics.

8.2 Recommendations and Guidelines

Four electrode terminal measurements are powerful to characterize biological cells and tissues, nevertheless they are very sensitive and prone to errors. As discussed throughout this Doctoral Thesis, experimental artifacts due to reference electrodes distortion of electric field, external electromagnetic interference for instance from the laptop placed close to the experiment or a laboratory lamp and a mal-functioning instrument due to inappropriate calibration can all interfere with the quality of the results.

In order to have good experimental results it is strongly recommended to place the experimental setup inside a Faraday cage which can shield it against electromagnetic interference. One Faraday cage was already developed for the purpose of such experiments and has been extensively used. It is availaible at our institute for use. Additionally, small and short cables for the potentiostat should be used and the instrument should be calibrated every six months to disappear with any cable capacitance effects.

Electrodes should also be new, well-polished, free from scratches and clean from biological parts, fat or fingerprints. It is recommended to touch the electrodes only by using disposable gloves and wash them with a special detergent to remove any fat and rest of cells which can attach to their surface during the experiments. Special care should be taken with the electrodes as they are very expensive and the quality of the experiments depends strongly on good electrodes. After each set of experiments they should be washed, cleaned and dried and placed in a special container to prevent scratches in their surface. It is also essential that they are very regular and have the same size in order that the half-cell potential developed at each electrode interface cancels as best as possible with each other. Another recommendation for electrodes is to use metals which are biocompatible and have a very stable half cell potential. Platinum showed in this sense excellent properties being the best evaluated, followed by gold.

To improve even further the experimental results and their repeatability it is recommended to use a temperature controlled box. As the experiments are very sensitive, even $1°C$ or $2°C$ can already affect the spectral curve. To decrease the speed of cell death, which also interferes with the results it is recommended to keep the cells at $37°C$ during the experiments, the same temperature as they are cultivated.

Another point worth mentioning is to measure the cells shortly after detachment. That is quite challenging for medical staff at the hospital, as they have to stop several times during the day to prepare the cells fresh. Nevertheless such practice can reduce the percentage of cell death, therefore improving the quality of the experiments.

This point was mentioned several times throughout this Doctoral Thesis, but it will be repeated here again. Use small voltage AC signals (no DC) to perform 4T setup impedance experiments. Large AC signals will not improve the quality of the 4T experiments, by the opposite, will decrease the accuracy of the results by introducing harmonics into the system, increasing the speed of corrosion from the electrodes and making electrodes less stable. Large AC voltages are certainly useful for other types of studies, but not for 4T setup impedance spectroscopy experiments.

8.3 Future Work

The first suggestion for future work is to improve the Micrux electrode system in order to allow the measurement of the resistance between the cell's junctions R_{junc}. As in chapter 6 it is already suggested, either by filling the empty spaces between the metal IDE electrodes or placing a very thin layer of glass on top of the IDE's. The importance lies in providing the cells with a flat and regular surface where they can attach and grow to confluence. After that, measuring the impedance and through signal processing the value of R_{junc} can be extracted. Such experiments can confirm whether physicians expectations that more metastatic cells have a much smaller R_{junc} than non-metastatic ones.

A second recommendation is to switch the material of the 3D printed chamber to glass instead of using the clear resin V4 FLGPCL04. Due to the porosity of the resin V4 FLGPCL04 the size of the chamber to measure the cells was limited. Several tentatives were made to decrease the size of the chamber to volumes smaller than 320 μL but all failed due to the rapid liquid evaporation and diffusion in the walls of the chamber. In this sense, 3D printed glass is more suitable to miniaturize such a device and recommended to be used for future versions of the chamber. The use of glass will allow the further miniaturization of the chamber, even to the level of the size of a microfluid channel to

measure single cells. The trade-off here lies in evaluating what is cheaper: to buy a 3D printer able to print glass or to pay an external company to fabricate such microfluid channels. If decision is made in the direction of buying a glass 3D printer certainly it will have lots of uses at the institute and the university.

Appendix A

Architecture proposal of a 4T impedance measurement system

This appendix describes the development of the architecture of a small portable 4T-potentiostat to measure the impedance of biological cells and tissues. The architecture here described can serve as the basis to be miniaturized for the implant. The specifications of such device are as follows:

- Flat gain: up to 1 MHz

- Zero phase: up to 1 MHz (desirable)

- Phase margin: minimum of $100°$

- Power consumption: smallest as possible

- Temperature of operation: $25°C$ - $40°C$

- Applied voltage: 14 mV Vpp

- Frequency range: 10 Hz - 1 MHz

The motivation of developing such a device architecture is to serve as a concept of a hardware that can be miniaturized as an implant.

A.1 Macro view of the impedance measurement system

Figure A.1 shows a macro view of the complete impedance measurement system. It is composed of an oscillator for the waveform generation, a 4T-potentiostat to measure the impedance of the biological system, a frequency mixing block to separate real and imaginary parts of impedance, filtering to remove the harmonics and front end to generate the .txt files with the results of the measurements.
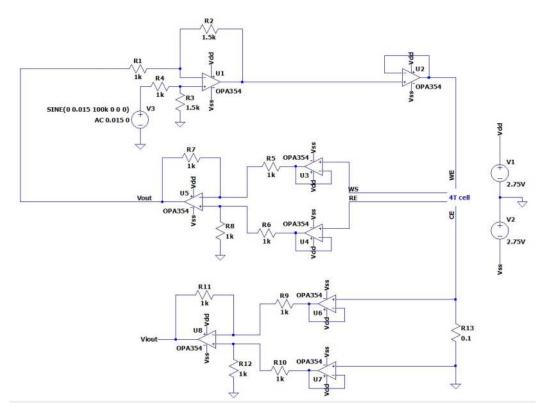
FIGURE A.1: Macro view of the portable impedance measurement system.

A.1.1 Oscillator

For the macro version of the device a PCB board with an ASIC for waveform generator from Analog Devices was used. In the implant an oscillator should be implemented which supports up to very low frequencies ($\approx$ 10 Hz). Developing such oscillator can

be quite challenging in CMOS technology. Examples of architectures of small frequency oscillators in MOS technology are described in references [135–137].

A.1.2 Potentiostat

Potentiostat is an instrument that measures the current flowing in an electrochemical cell while keeping the voltage drop along the cell constant. It can have two-, three- or four-electrodes in order to measure the cell in a two-terminal, three-terminal or four-electrode-terminal setup. Depending of what is to be observed one configuration is desired in regards to the others. For the observation of the spectral response of cells suspensions and solid tumors without the interference of the electrode polarization in frequencies below 1 kHz a four-electrode-terminal is used. The schematic of a such device developed in LTSpice is shown in figure A.2.
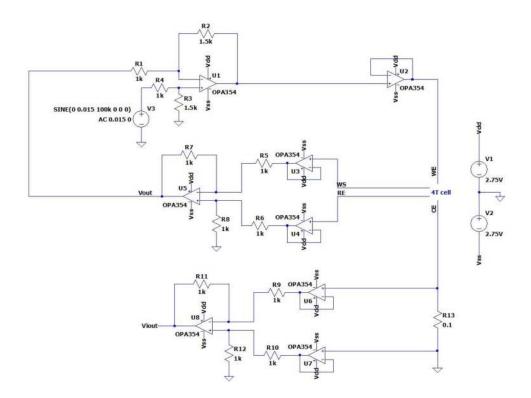
FIGURE A.2: Schematic of a four-electrode-terminal potentiostat circuit.

The circuit is composed of three differential amplifiers formed by U1, U5 and U8 and five buffers or voltage followers formed U2, U3, U4, U6 and U7. The buffers are essential to keep the voltage constant in the points of contact with the electrochemical cell. The selected amplifier must have a very high input resistance and an extremelly low output impedance, therefore the opamp OPA354 from Texas Instruments was chosen.

The potential drop in the electrochemical cell (4T cell) is measured at the points WS and RE which stand for working sense and reference electrodes. The output voltage V_{out} or $V_{WS} - V_{RS}$ is measured at the output of U5. The current which is flowing into the electrochemical cell is measured at the output of U8. The voltage feedback from the output of U4 towards R1 is essential to keep the potential drop in the electrochemical cell constant. The unknown impedance of the electrochemical cell will be given by:

$$Z_{4Tcell} = \frac{0.1V_{out}}{V_{iout}} \tag{A.1}$$

As the amplifiers are connected in a closed loop in the feeback configuration it is necessary that the loop gain of the circuit is larger than 1 to avoid oscillations; therefore R2 was chosen as 1.5 $k\Omega$. Figure A.3 shows the simulation results for the experimentally measured impedance of HaCaT cells. The top figure shows the magnitude and phase of impedance in decibels in order to facilitate the visualization of the amplifiers frequency effects. The middle figure shows the real part of impedance and the bottom one the imaginary part. The red curve shows the results as will be measured by the potentiostat with real (commercial) operation amplifiers, and the blue as they should be if the operational amplifiers composing the circuit where perfect.

The circuit works pretty well up to 1 MHz, but due to the very large load capacitances the error increases at higher frequencies.

A.1.3 Principles of lock-in detection

Lock in detectors or lock in amplifiers are instruments able to extract the amplitude and phase of signals in very noisy environments [138]. They normally use the principle of frequency mixing where a reference signal is mixed or multiplied by the noisy signal to be identified. In the multiplication a higher amplitude reference signal can be used to amplify the small amplitude noisy signal. Also, the reference signal has a pre-determined frequency to move the noisy signal to the desired bandwidth. After the multiplication or frequency mixing, there will be two copies of the signal one at $f_{ref} + f_{noisy}$ and a second at $f_{ref} - f_{noisy}$. With properly filtering the desired copy of the signal can be filtered and further analyzed. If the noisy and reference signals are in phase during the multiplication, the in phase or the real part of the signal to be measured will be extracted. If the reference signal is $90°$ phase shifted from the noisy signal the quadrature or imaginary part of the signal is extracted.

In the architecture suggested for the implant the lock in detection is used to extract the real and imaginary parts of the signal. With proper signal processing afterwards, the real and imaginary parts can be transformed in any of the other representations (polar, cartesian, etc).

A.1.3.1 Frequency mixer

Frequency mixers are non-linear circuits used to create new frequencies from two signals applied to its inputs. The signals are normally created at the sum and at the difference of the frequencies of the two applied signals. Depending on the type of mixer other frequency components may also appear.

In electronic circuits there are several types of mixers: unbalanced, single balanced and double balanced. The unbalanced mixers produce apart from the two signals at the sum and at the difference, also allow the input signals to pass to the output. The single balanced mixer will produce the two signals at the sum and at the difference of the frequencies, but also will allow either one of the input's signal frequency to appear at the output. The double balanced mixer produces only the signals at the sum and difference of the

frequencies at the output, and suppress both frequencies of the two input signals. Figure A.4 illustrates the process.

In order to develop the implant a double balanced mixer is desirable, because it will have at its output only the frequency components at $f_{LO} - f_{IR}$ and $f_{LO} + f_{IR}$, therefore facilitating the filtering. A commonly used and simple implementation of a double balanced mixer in CMOS technology is the Gilbert cell [139]. Analog Devices, NXP and other companies offers several commercially available implementations of Gilbert-cell based frequency mixers. In the PCB implementation of impedance measurement system the AD831AP from Analog Devices was used.

A.1.3.2   Filtering

In order to do the filtering of the signal an active, op-amp based filter was chosen. The main reason for choosing an active instead of a passive filter was the gain. While passive filters normally attenuate the signals at higher frequencies, the gain of active filters can be set to any value and be kept constant. The possibility of using a digital filter was also evaluated, nevertheless given its high costs as digital filters normally are implemented with the help of an FPGA, this possibility was discarded. The option of an active op-amp based filter offers already a quite good solution for a good price.

The filtering part of the impedance measurement system was developed with the help of the tool *Analog Filter Wizard* from Analog devices. A 10th order Butterworth filter, with 0 dB gain, -3 dB passband at 1 Hz, -60 dB stopband at 2 Hz was designed with the help of the tool. The filter was designed to measure the DC component of the signal and eliminate all components above. The filter response is shown in figures A.5 and A.6. The light blue highlighted area shows what would be the filter response when the passive components, namely resistors and capacitors, which are used in the filter were not perfect and varied theirs value within commercially ranges (resistors $\pm$ 1% and capacitors $\pm$ 5%).

In reality given its very narrow pass- and stopbands such a filter showed to be very slow to do a frequency sweep starting from 1 MHz and decreasing up to 10 Hz, in frequency steps

146

of 10 points per decade. A better solution is to use several filter banks with wider pass- and stopbands for higher frequencies, and changing the filter bank used as the frequency sweep progress towards lower frequencies. That is the technique used in commercially available devices, such the potentiostat from Gamry Instruments used to perform all experiments.

A.1.4   Front-end and complete system

The front-end of the implant still needs to be developed. It should contain an ADC to convert the analog signals to digital ones, a wireless transmitter to transmit the signal from the inside of the patient's body towards a receiver placed outside of it. The rest of the signal processing should be done outside of the patient's body as it is more power efficient to do it outside than inside. A SW tool, for instance Matlab, must be used for the visualization and analysis of the Magnitude and Phase response of the patient's tumor.

A.2   Conclusions

In this appendix the architecture of a prototype for the implant to be placed inside the tumor of cancer patients was proposed. The architecture comprises an impedance measurement system with five blocks, namely: oscillator, potentiostat, frequency mixing, filtering and front end. The system should be able to measure the impedance (magnitude and phase) of the tumor in the frequency range from 1 MHz up 10 Hz in steps of 10 points per decade. The front-end should comprise apart from the analog-to-digital conversion part also the wireless transmission system to transmit the signal to a receiver outside the patient's body. All signal processing afterwards should be performed by the receiver. The requirements on the potentiostat is that it has an architecture which allows for a four-terminal-setup measurement (four electrodes), uses a very small amplitude signal to avoid harmonics and heating of the tumor tissue, and keeps a constant potential. Electrodes should be made or coated with noble metals like Pt or Au, but preferably Pt.

Depending on the characteristic that wants to be observed the interval between measurements may be varied. The only recommendation is that the interval has a minimum of 10 min between consecutive measurements, as a complete frequency sweep takes between 2-7 min. In reality, as biological systems vary very slowly, a good compromise between measurements and power saving would be one measurement in intervals between 30min up to 1 hour.
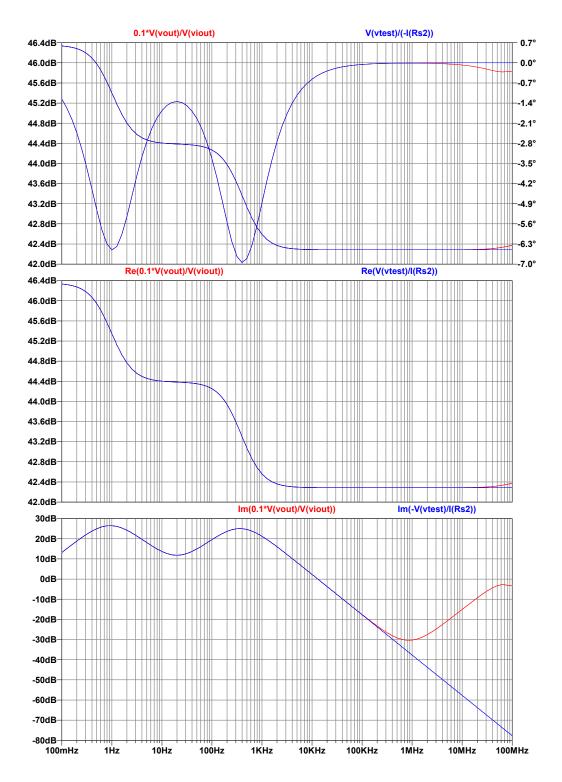
FIGURE A.3: Simulation of result of developed potentiostat for the experimentally measured impedance of HaCaT cells. Red curves represent the response of the potentiostat with commercially available operational amplifiers, while the blue curve represents the same response if the amplifiers were perfect with no parasitics.

149
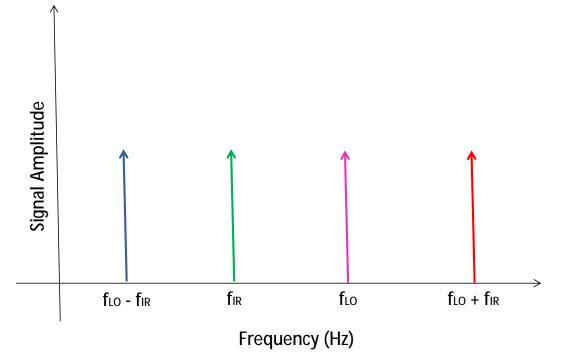
FIGURE A.4: Unbalanced, single balanced and double balanced mixer. An unbalanced mixer will have at its output all the four frequency components, namely the frequencies at $f_{LO} - f_{IR}$, f_{IR}, f_{LO} and $f_{LO} - f_{IR}$. A single balanced mixer will have the output signal with frequency components at $f_{LO} - f_{IR}$ and $f_{LO} - f_{IR}$, plus either f_{LO} or f_{IR}, but not both at the same time. A double balanced mixer will have only the two components at the sum and difference of the input frequencies, namely, $f_{LO} - f_{IR}$ and $f_{LO} + f_{IR}$.
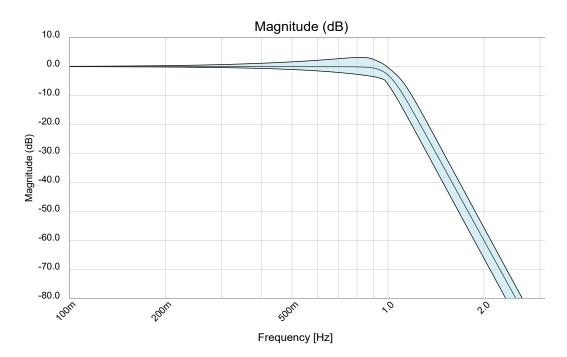
FIGURE A.5: Magnitude response of 10th order Butterworth filter.
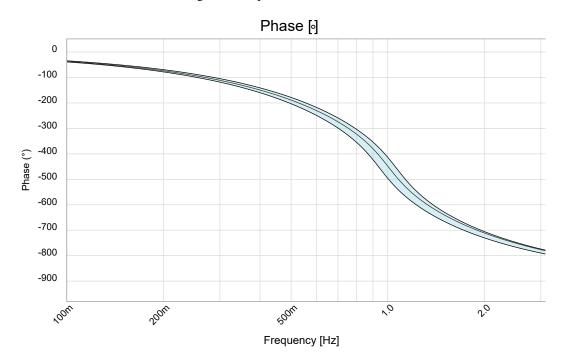
FIGURE A.6: Phase response of 10th order Butterworth filter.
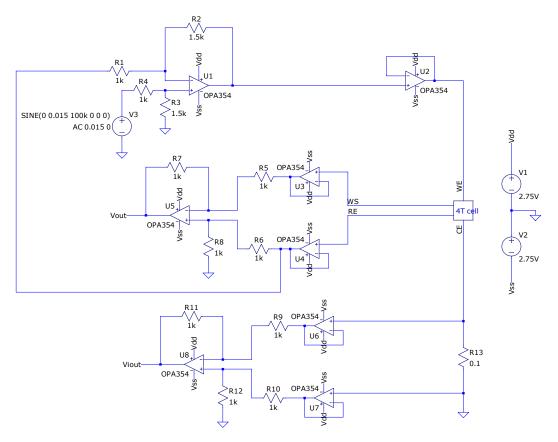
FIGURE A.7: Visualization of the complete impedance measurement system as an implant and a front-end outside of patient's body.

Appendix B

Cancer metabolites identification

Cancer metabolites or tumor metabolites are substances which are commonly encountered in tumors and serve as tumor biomarkers. Different types of tumors will express at least one, often several different types of biomarkers. As diverse as they are, they serve the purpose to understand cancer mechanisms better and also provide useful hints for physicians to possible therapies. Examples of cancer metabolites or biomarkers are citrate, lactate, uric acid, glucose, glutamin, ATP, among others. During the next sections two methods are proposed to develop a sensor to be placed inside solid tumors or cancer cells suspensions and monitor the presence and concentration of such cancer metabolites.

B.1   First method: membrane system to separate different types of ions

The procedure starts by defining the cancer metabolite that wants to be identified, e.g., citrate, lactate, uric acid and so on. The next step is to identify which body fluids and microenvironments the substance will be encountered, for instance, urine, blood, serum, sweat, inside tumors, and so on. Once identified, the membrane system should be developed for an specific body fluid, therefore it is essential to choose the body fluid which will be used to separate the desired metabolite. An example is the citrate concentration

which can be measured in the urine of prostate cancer patients. The steps which follow are mainly to identify the chemical formula of the metabolite to be measured and also other substances present in the body fluid. The idea is basically to use a nano-membrane/nano-pore system to separate substances in different compartments and by using Electrical Impedance spectroscopy measure the conductivity of the liquids separated in the different compartments one can obtain the desired concentration of the cancer metabolite.

Figure B.1 below summarizes the description in steps.

B.1.1   Step A: identify body fluids

It is common that one specific metabolite is present in more than one body fluid, for instance citrate can be found in urine and blood serum. And this happens for the majority of metabolites which can be present in several parts and fluids of the human body. Therefore some time should be spent to identify the body fluids where the specifc metabolite is encountered and the best body fluid to be used for the measurement.

B.1.2   Step B: choose one body fluid

From all the body fluids identified previously, one should be chosen to develop the membrane system. The membrane system is specific for each body fluid as the composition of body fluids vary a lot.

B.1.3   Step C: identify metabolite chemical formula

It is basically necessary to identify the exact chemical formula of the metabolite in the chosen body fluid. As the metabolites pass through a set of transformations during cell metabolism, they can vary in chemical formula throughout the process.

FIGURE B.1: Step by step suggestion of a procedure to identify cancer metabolites in body fluids by means of Electrical Impedance Spectroscopy and nano/micro-pore membrane system.
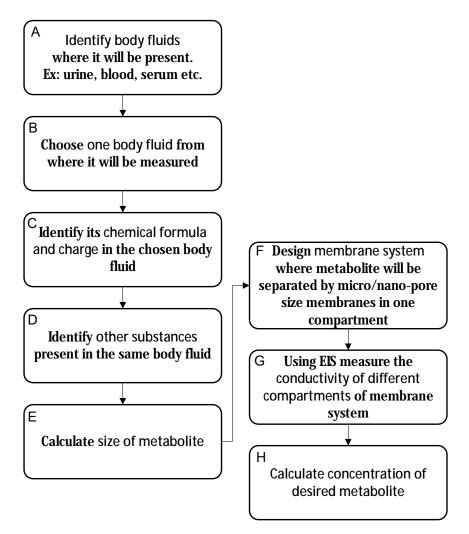
B.1.4 Step E: calculate the molecular size of the metabolite

In order to calculate the complete molecular size of the cancer metabolite, the molecular size of each one of the composing atoms should be estimated and added to the solvent accessible size, in this case water. The molecular size is calculated by assuming all atoms

as
wit
sur
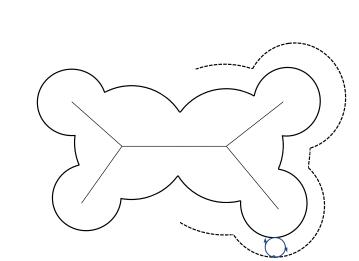
FIGURE B.2: Illustration of the Van der Walls surface of a generic molecule and its solvent accessible area. The Van der Walls surface is represented by a continuous line and the solvent accessible area by a dashed line. The water molecule which should be "rotated" around the Van der Walls surface is highlighted in blue with arrows surrounding it. Adapted from [140].

B.1.4.1 Example: estimation of molecular size of citrate

In this section an example on how to calculate the molecular surface of citrate is given. The metabolite citrate is defined as follows:

- Chemical formula: $C_6H_7O_7^{-3}$

- Van der Walls Radii

    - C (carbon): 1.77 Å

    - H (hydrogen): 1.10 Å

    - O (oxygen): 1.58 Å

- Covalent radii

- C (carbon): 76 pm

- H (hydrogen): 31 pm

- O (oxygen): 66 pm

Figure B.3 shows a 3D view of citrate molecule where each type of atom composing the molecule is highlighted in different colors: oxygen in red, carbon in gray and hydrogen in white.
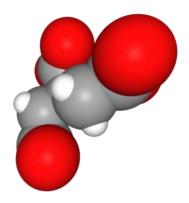
FIGURE B.3: Three dimensional visualization of citrate molecule. Extracted from [141].

Figure B.4 shows a 2D view of the same citrate molecule, but now with the values of Van der Walls radii highlighted. Observe that the approximate molecule size without hydration sheet is 1024 pm per 720 pm.

Figure B.5 shows the last step in estimating the citrate surface molecule. The molecule is approximated by an sphere of 1024 pm of diameter and the hydration sheet is added to that. At the end, it results in a molecular size of 1624 pm or 1.624 nm with hydration sheet added. Such result implicate that when developing a membrane system to separate citrate in urine or other body fluid one of the pore diameter to filter citrate will have to be approximately 1.624 nm. It should not be smaller, so citrate molecules can still diffuse through the pores, nevertheless it should not be significantly larger, so a lot of undesired molecules also flow inside the compartment.

- pm = pico meter = 10^{-12} m
- Gray = carbon
- Red = Oxygen
- Light white = hydrogen
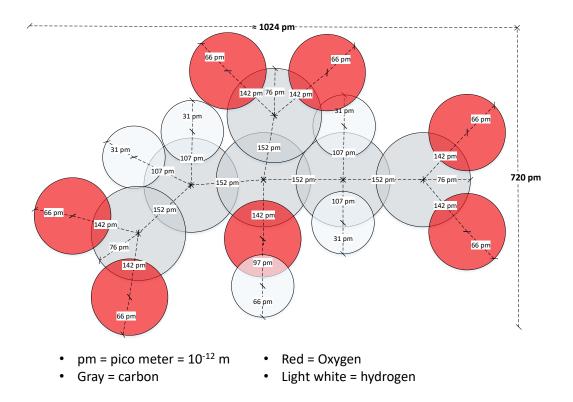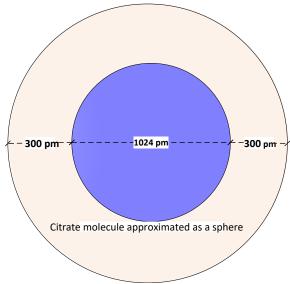
FIGURE B.4: Two dimensional visualization of citrate molecules size by using Van der Walls radii. Summing up all the diameter of the molecules in citrate a total size of 1024 pm per 720 pm can be calculated.

B.1.5 Design membrane system to separate metabolite

An example of a possible membrane system to separate lactate in body fluids is shown in figure B.6. In the first compartment highlighted by σ_1 a large pore size membrane indicated by the letter A is used, so the body fluid will be filtered from cells and other large molecules (< 50 nm). On the next compartment (σ_2) the membrane pore size at B should have approximately a diameter of 1.624 nm to allow citrate to diffuse, but to block other large molecules. The membranes at C and D should have all the same pore size, which should be smaller than 1.64 nm in order to allow for molecules smaller than citrate to diffuse to the third compartment. By diffusion law the following will occur:

- The concentration of small molecules will be the same in the three compartments.

FIGURE B.5: Last step in citrate molecular size estimation: adding hydration sheet. The hydration sheet is highlighted in light rose color and the citrate molecule approximated by a sphere by dark blue (not in scale).

• The concentration of citrate will be the same in both compartments indicated by σ_1 and σ_2.

Therefore the lactate concentration will be:

$$\sigma_{lactate} = \sigma_2 - \sigma_3 \tag{B.1}$$

Observe that the membrane pore system should be covered by a metal layer, Pt or Au, for instance, in order that the conductivity of each compartment (σ_1, σ_2 and σ_3) can be measured through EIS. Recommended is to use Pt when available, as it resists better the reaction with chloride always present in biological media. Notice that this is only one suggestion of a possible membrane separation system. Other systems with a larger number of compartments can also be designed if that facilitates the filtering process.

B.1.6   Conductivity measurement of different compartments

The conductivity measurement is simply an impedance spectrocopy experiment in a single frequency larger than 1 kHz. In general conductivity meters adjust the measurement frequency according to liquid concentration, i.e., for larger concentrations it increases the measurement frequency and for smaller concentrations it decreases it. A good suggestion is to use something between 10 kHz and 100 kHz. If the potentiostat used goes up to 1 MHz, using frequencies very close to 1 MHz can affect the accuracy by the insertion of non-idealities from cables and amplifiers from the instrument. Below 10 kHz double layer effects may still be present as the chamber setup is a two-electrode-terminal setup.
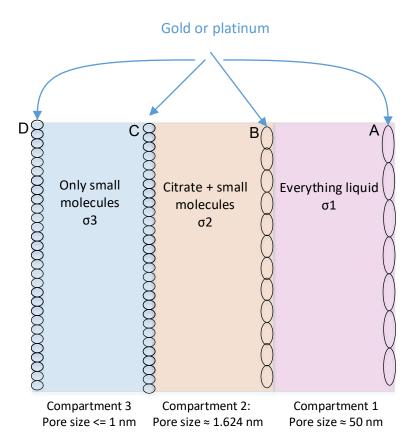
FIGURE B.6: Suggestion of possible membrane system to separate lactate in body fluids (liquid biopsy).

Notice that at least three different experiments should be performed: one to measure σ_1, one to measure σ_2 and the last to measure σ_3. The result will be then:

$$Z_1 = R_1 + jX_1 \qquad \text{(B.2)}$$

$$Z_2 = R_2 + jX_2 \qquad \text{(B.3)}$$

$$Z_3 = R_3 + jX_3 \qquad \text{(B.4)}$$

$$\text{(B.5)}$$

And remembering that:

$$R = \frac{K}{\sigma} \qquad \text{(B.6)}$$

One can also write:

$$\sigma_1 = \frac{K}{R_1} \qquad \text{(B.7)}$$

$$\sigma_2 = \frac{K}{R_2} \qquad \text{(B.8)}$$

$$\sigma_3 = \frac{K}{R_3} \qquad \text{(B.9)}$$

$$\text{(B.10)}$$

And remembering that $\sigma_{lactate} = \sigma_2 - \sigma_3$, the desired lactate conductivity can be calculated directly from the experimental results and the cell constant K. The value of K comes directly from the geometry of the experiment as defined in equation 2.7. When K can not be analytically calculated, it can also be experimentally measured by means of a known conductivity ionic solution, for instance KCl or PBS. Notice that such experiments are very sensitive to temperature.

B.1.7 Calculate metabolite concentration

To finalize the processing, the metabolite conductivity calculated in the previous step should be converted to concentration. The following steps are necessary:

- Divide the conductivity by one million to get the value in microsiemens.

- Calculate the concentration in ppm by multiplying conductivity in microsiemens per 0.64.

- Change ppm to molarity.

In the next section one example is given on how to convert lactate conductivity in concentration.

B.1.7.1 Converting conductivity to concentration

Suppose the following citrate conductivity is measured with the proposed electrode system:

$$\sigma_{citrate} = 1 S/m \tag{B.11}$$

The first step consists on dividing $\sigma_{citrate}$ to one million. Therefore:

$$\sigma_{citrate}[\mu S/m] = 1/1000000 = 1 \mu S/m \tag{B.12}$$

The next step consists on multiplying the previous value by 0.64, therefore:

$$\sigma_{citrate} = 1 * 0.64 = 0.64 ppm \tag{B.13}$$

Remembering that 1 ppm is equal to 0.001 g of solute in one liter of solution, that molarity is equal to moles/liter and that the atomic weight is given in grams/moles, the concentration of the solute in molarity will be:

$$\sigma_{citrate}[moles/liter] = \frac{\sigma_{citrate}[grams/liter]}{AW_{citrate}[grams/mole]} \tag{B.14}$$

Where AW is the citrate atomic weight and is equal to 189.10 grams/mole. Therefore:

$$\sigma_{citrate}[moles/liter] = \frac{0.001 * 0.64}{189.10} \approx 3.38 \mu M \tag{B.15}$$

B.1.8 Comments about the method

This method certainly can be used to identify a large number of cancer metabolites in body fluids. If the sensor is miniaturized, it can also be placed inside the tumors of patients to monitor the metabolites concentration in vivo. The difficulties of the method is to obtain the proper membrane pore sizes. Currently there is only one company which dominates the technology, namely Oxford Nanopore, and this company does not sell the membranes alone, but just the whole equipment. Nevertheless, by the status of 2019 there were three more companies developing and improving the same technology of nanopore sized membranes. Once such technology is developed and mature, the nanopore sized membranes can be used to develop the sensor here described and identify the desired metabolites concentration.

B.2 Second method: surface modified interdigitated electrodes

This method consists in modifiyng IDE electrodes as desbribed in chapter 6 with a trapping substance, namely, a chemical substance which is able to bind to the desired cancer metabolite dissolved in solution. Once the metabolite "gets trapped" it modifies the

electrode-electrolyte interface, therefore causing a significant change in the double layer capacitance. By means of calibration with standard solutions and calculations the correct metabolite concentration can be determined. Figure B.7 illustrates an example of a proposed system.

Several layers (from bottom up):
- − Metal layer (Au, Pt, etc)
- − Last layer (orange)-> chemically modified layer with bioreceptor

Example IDE electrodes
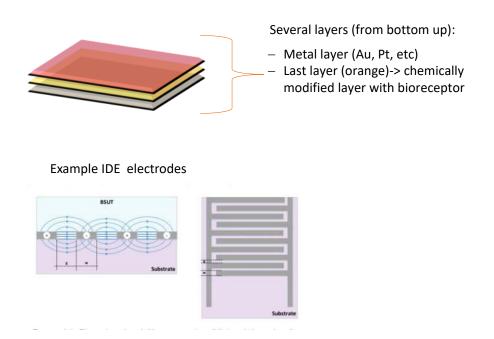
FIGURE B.7: Propose IDE system to identify cancer metabolites.

The difficulty on this method lies exactly in developing the chemical substance or the bioreceptor which is able to trap the desired metabolite. Currently in the market there are available bioreceptors for glucose[1] and lactate[2]. For more details on the topic please check references [142, 143]. Therefore for those two metabolites, glucose and lactate, it is quite straightforward to develop the sensor and by using EIS identify the desired cancer metabolite concentration. For the other metabolites the bioreceptor has to be researched and developed. Given the complexity and difficulty of developing such biosensors, that is enough work for one PhD in Chemistry or Electrochemistry.

---

[1]Glucose oxidase (GOx), Glucose dehydrogenase nicotinamide adenine dinucleotide (GDHNAD) and Glucose dehydrogenase flavin adenine dinucleotide (GDH-FAD).

[2]Lactate oxidase (LOD) and Lactate dehydrogenase (LDH or LD).

Appendix C

Extracting $\triangle \varepsilon_\alpha$ from impedance measurements

In Chapter 5 the parameter $\triangle \varepsilon_\alpha$ was used to calculate the value of the cell surface charge. Here the steps for extracting $\triangle \varepsilon_\alpha$ from the experimental results are detailed.

While 4T measurements significantly decrease the effects of electrode polarization in low frequencies, it does not disappear completely with all effects occurring at those frequencies. In some cases, the results obtained are already satisfactory, in others corrections have to be applied. Additional methods explored by other authors to decrease electrode polarization effects are described in reference [99]. It depends on the quality of electrode-electrolyte interface, basically it is desirable that the potential developed at the electrode-electrolyte interface from both electrodes cancel completely each other. In reality this rarely occurs; a small value of open circuit potential (OCP) is obtained. The larger the OCP experimentally observed, the worse is the impedance measurement, in the sense that it has more effects of electrode's polarization.

C.1 Equivalent circuit model

In order to extract the $\Delta\varepsilon_\alpha$ from the experimental results a variation of the Ladder equivalent circuit model (ECM) [10] was used as shown in figure C.1. This ECM models a frequency dependent distributed diffusion process, which showed to be the more adequate to model such experimental results as suspended biological cancer cells. Other models are suggested into the literature [10, 23, 27]. Looking at the model proposed in chapter 3 (figure 3.9), the impedance of the biological system under test Z_{BSUT} can be replaced by the circuit in figure C.1.

The model in figure C.1 is a good representation in terms of discrete electrical components, although in reality the elements which compose the experimetal setup, namely electrodes, electrolyte (PBS), biological cancer cells and the electrical and electrochemical effects cannot be discretely separated in the system, forming a whole new system. That means, cells attach to electrodes and affect their electrode-electrolyte interface behavior. Cells accumulate close to electrodes affecting the double layer. Cells and electrolyte interact; cells remove ions from the electrolyte to feed themselves and also release their wastes in the electrolyte. Cells also die. All of this affects electrolyte composition and therefore the experimentally measured impedance results.
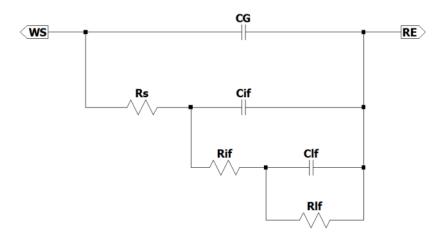

FIGURE C.1: ECM used to model the impedance of the biological system under test Z_{BSUT} as shown in figure 3.9 from Chapter 3.

The circuit elements of the figure C.1 are the low frequency resistance and capacitance (R_{lf} and C_{lf}), the intermediate frequencies resistance and capacitance (R_{if} and C_{if}), the solution resistance (R_s) and the geometric capacitance (CG). The WS and RE stand for Working Sense and Reference electrodes. In electrochemical systems all the effects of the interacting electrical, biological and chemical systems are summed up and seen in the impedance curves; nevertheless in different frequency ranges some effects are more apparent than others. In low frequency ranges the diffusion of reactants due to the electrochemical potential created by the uneven ionic distribution is the dominant effect. Remember that this uneven ionic distribution is caused by the disturbance of the external electric field, in equilibrium, this will not be observed. In intermediate frequencies double layer effects close to cell membranes of biological cells and the distortion of ionic clouds surrounding cell membranes externally is the dominant effect. Namely, electric fields interact in this range with biological cells normally outside their cell membranes. In higher frequencies (a couple of MHz, not represented in the circuit of figure C.1) the electric fields enter the cell membranes and allow a better observation of the interior of the cells. The solution resistance represents the ability of the electrolyte to conduct electric current and is inversely proportional to the electrolyte concentration, namely, the higher the ionic concentration the lower the R_s. The geometric capacitance CG represents the imperfection of the cables and measurement equipment. In all experiments performed CG was always in the range 2 pF up to 100 pF (experimentally measured).

C.2   Fitting the experimental data

The fitting of the experimental data is hard and important for the accuracy of the derived data. It was performed in several steps according to the recommendations of references [114, 115, 117] for fitting impedance data in large frequency ranges.

The problem of fitting such data is that the impedance values in low frequencies are large when compared to the high frequencies ones and tend to affect the accuracy of the fitting of the elements at high frequencies. As most fitting algorithms use the LMSE (Least Mean Squared Error) method to reduce the error between fitted and experimental curves,

the accuracy of high frequency elements suffers. Gabriel [114, 115, 117] suggests to fit by parts the impedance curves, fitting first the high frequency elements, fixing their values or limiting then into a small range, and then fitting the low frequency elements by last. This method was extensively used here.

The first element fitted was CG for being the smallest capacitance of the system. Then the CG value was constrained, and the value of C_{if} which stays in the intermediate frequencies, was fitted afterwards. Following that the value of C_{if} was constrained and the value of C_{lf} was fitted by last, for being the largest capacitance of the system. The solution resistance fitting is easy and the original guess can be directly extracted from the visual analysis of the curves. The R_{if} and R_{lf} were both calculated by the fitting algorithm. As the fitting algorithms use different convergence formulas, a good initial guess is important for an accurate fitting.

In order to do the fitting, each single experimental curve was plotted and fitted individually in the tool *Echem Analysist* from Gamry instruments. The fitting was done as described above (first CG, then C_{if} and by last C_{lf}) and at the end the average of all curves and the standard deviation was calculated. Good guesses for CG and R_s were given and the value of C_{if} was constrained based on a range of values in the literature given for a large number of biological cells. Once a good value for C_{if} was obtained, i.e, a value that minimizes the error between the fitted curve and experimental data, followed the extraction of $\Delta\varepsilon_\alpha$ detailed in the next section.

C.3   Extracting $\Delta\varepsilon_\alpha$

Extracting $\Delta\varepsilon_\alpha$ from C_{if} is straightforward. Remembering that for a parallel plate geometry as desbribed in chapter 3:

$$C = \varepsilon_0 \varepsilon_r \frac{A}{d} \tag{C.1}$$

Or written in another way:

$$\varepsilon_{low} = \frac{C_{if} * d}{A * \varepsilon_0} \tag{C.2}$$

Where ε_{low} is the low frequency relative permittivity caused by the suspended cells, A is the area of the electrodes, d is the distance between them, ε_0 is the vacuum permittivity and C_{if} is the capacitance of the cells and ionic cloud extracted as described in the previous section. The value of $\Delta\varepsilon_\alpha$ will be then:

$$\Delta\varepsilon_\alpha = \varepsilon_{low} - \varepsilon_{intcells} \tag{C.3}$$

Where the $\varepsilon_{intcells}$ is the next decay in the permittivity curve of the spectrum of the cells (see figure 2.5, or the equivalent to the beginning of the β dispersion). The value of ε_{low} is directly extracted from C_{if} by means of C.2, the value of $\varepsilon_{intcells}$ can only be extracted from the epsilon curve of the suspension by a second fitting. Nevertheless, checking the curve from Schwan in figure 2.5 one can see that the value of $\varepsilon_{intcells}$ is at least 100 times smaller than ε_{low}, therefore the value of $\Delta\varepsilon_\alpha$ was simplied to:

$$\Delta\varepsilon_\alpha \approx \varepsilon_{low} \tag{C.4}$$

C.4 Example of fitting PC-3 cells experiments to extract $\Delta\varepsilon_0$

Figure C.2 shows an example of extracting C_{if} from one experimental curve from PC-3 cells. The ECM as shown in figure C.1 was used to fit the data as described in section C.2. Observe that in the impedance curve all the summed effects of cells (C_{if}), geometry and cables (CG) and electrodes and low frequency diffusion effects of reactances (C_{lf}) are presented in the curve. To extract the effect of the capacitance caused only by the cells the C_{if} must be fitted and extracted from the experimental results.

The fitting starts always with the smallest capacitance of the system, in this case CG. A guess of CG equals to 52 pF is the starting point for the algorithm to search for the correct value. After that Autofit is pressed and the algorithm finds the closest value which minizes the Root-Mean-Squared-Error (RMSE) between experimental and fitted curve. Visually the curve is inspected to see whether the fitting is good enough. After that, CG is fixed (Locked) so its value does not change anymore. Now a good guess of Rs (the solution resistance) is given and again Autofit is pressed. The algorithm searches for the optimal point and again it is visually inspected if the fitting is satisfactory. Then the value of Rs is fixed (Locked) and C_{if} is fitted. A good guess of C_{if} is given, its value is constrained between 0 and 20 μF (which is the maximum value biologically relevant according to Schwan paper [14], a C_{if} of 20 μF is equivalent to ε_{low} of a maximum of 10^8) and the Autofit is pressed. The curve is visually inspected and when the fitting is satisfactory the value of C_{if} is Locked. Now the fitting of the other circuit elements followed through the same process. A figure of the original experimental curve for PC-3 cells and the fitting is shown below. Observe that the fitting is excellent above 10 Hz, and below 10 Hz the error increases. The main issue is that the dynamics of the biological system liquid plus cells, is faster than the measurement at those frequencies. Therefore it is very hard to get accurate measurements for the impedance values of biological systems at frequencies below 10 Hz. That is why the majority of authors restrict their curves up to 10 Hz and extrapolate the 10 Hz value to DC to get the DC values of the curves.
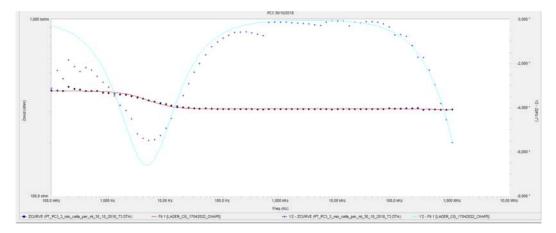

FIGURE C.2: Example of experimental data fitting of PC-3 cells to extract C_{if}.

FIGURE C.3: Fitted parameters for the experimental data from figure C.2.

The open question now is: "How from C_{if} the value of $\Delta\varepsilon_{alpha}$ is extracted?" The answer is: $\Delta\varepsilon_{alpha}$ cannot be extracted from C_{if}, but only the value of ε_{low} or in the limit when the curve is extrapolated from 10 Hz to 0 Hz or DC, the value of ε_{DC} is extracted by using equations C.1 through C.4.

The next question that can arise is: "How to be sure that C_{if} corresponds to the ε_{low} used to calculate $\Delta\varepsilon_{alpha}$?" Basically cells are charged entities and as charged entities they show a polarization when submitted to a frequency variable electric field, therefore they manifest in the system a capacitance caused by the polarization of their charge. In the system there are three clearly identifiable capacitances:[1] CG, C_{if} and C_{lf}. The CG is called geometric capacitance and depends on the geometry of the chamber system and not from the cells on suspension. It was observed experimentally several times that CG is completely independent on the cell type which is being measured, but it varies with the geometry of the chamber system used. From the other two capacitances left, namely C_{if} and C_{lf}, now the question is which one corresponds to the ε_{low}? By fitting the curves the values of C_{if} varied between hundreds of nF up to some tenths of μF while the value of C_{lf} varied between several hundreds of μF up to several mF. That means, C_{lf} is in average 100 to 1000 times larger than C_{if}. If one assumes C_{lf} as the capacitance of the

---

[1]The name given to the capacitances is irrelevant for the discussion. The important is that they are three.

α-dispersion of the cells, one would get cell membrane resting potentials in the other of several tenths of volts (30V, 50V or larger), which physically is impossible. Therefore the capacitance caused by the polarization of the cells with the externally applied electric field is C_{if}.

The last question that may arise is: "What is C_{lf}? What is causing this very large low frequency capacitance?" Several complicated physical phenomena occur in the very low frequencies (below 10 Hz), and explanation in literature so far is scarce. Certainly there are still small effects from electrode polarization as complete elimination of double layer effects is almost impossible. The fact is that in reality one never manages to fabricate two electrodes entirely equal to each other to eliminate all double layer effects. Therefore in all experiments a small open circuit potential in the order of some milivolts was observed. Other authors [10] also cite the effects of diffusion of reactants close to electrode's surfaces and the balance/counterbalance of electrochemical gradients and diffusion effects against each other to restablish chemical and electrical equilibrium at those low frequencies. The reality is that probably a combination of all those effects summed together (remnants of double layer effects, electrochemical gradients and diffusion effects) are causing the large low frequency capacitance C_{lf} observed in the experiments.

Complete Table Cell Surface Charge

In Chapter 5 the values of R_c, $\Delta\varepsilon_\alpha$, ϕ, N, N_c, Q_{cc}, V_{mem} and C_{mem} were shown, but the standard deviations were omitted for readiability. Here the complete table is presented with all standard deviations. For an explanation of each parameter and how it was calculated or measured, please refer to the above mentioned chapter.

Cell Line	R_c [μm]	$\Delta\varepsilon_\alpha$ [10^6]	ϕ	N [$10^{11}/cm^2$]	N_c [10^6]
PC-3	10.90 ± 2.93	4.67 ± 0.76	0.26 ± 0.08	3.61 ± 0.88	5.39 ± 1.32
DU145	9.10 ± 1.88	4.73 ± 0.88	0.26 ± 0.11	4.25 ± 0.86	4.42 ± 0.89
EOL-1	7.07 ± 0.75	0.15 ± 0.05	0.09 ± 0.03	0.48 ± 0.10	0.30 ± 0.07
MOLM-13	7.66 ± 0.66	0.16 ± 0.05	0.06 ± 0.08	0.56 ± 0.19	0.42 ± 0.14
MCF7	9.33 ± 1.25	5.33 ± 0.18	0.28 ± 0.08	4.19 ± 1.17	4.58 ± 1.28
T47D	8.99 ± 0.90	5.25 ± 0.21	0.22 ± 0.07	5.42 ± 1.36	5.50 ± 1.38
HT29	7.64 ± 0.77	5.30 ± 0.21	0.32 ± 0.13	5.41 ± 1.45	3.97 ± 1.07
SW620	6.98 ± 0.98	4.77 ± 0.59	0.20 ± 0.06	7.72 ± 1.32	4.73 ± 0.80

TABLE C.1: Number of charges per cell area N calculated based on equation 5.17. The values of the cell radius R_c, volume fraction of suspended cells Φ and the permittivity increments in the cell spectrum due to $\Delta\varepsilon_\alpha$ were experimentally measured. The number of charges of one singe cell N_c is equal to the value of N multiplied by the cell area.

Cell Line	Q_{cc} [$10^{-13}C$]	V_{mem} [mV]	C_{mem} $\mu F/cm^2$	NIE	NE
PC-3	8.63 ± 2.12	54 ± 13^a	1.07 ± 0.26^b	4	27
DU145	7.08 ± 1.44	62 ± 14^c	1.10 ± 0.22	4	33
EOL-1	0.48 ± 0.11	3.87 ± 0.85^d	1.53 ± 0.35	3	21
MOLM-13	0.67 ± 0.22	4.52 ± 1.53^e	1.82 ± 0.60	3	15
MCF7	7.34 ± 2.05	38 ± 10^f	1.77 ± 0.49	3	25
T47D	8.82 ± 2.21	$43 pm 11^g$	2.07 ± 0.52	3	25
HT29	6.35 ± 1.71	37 ± 10^h	2.32 ± 0.62	1	9
SW620	7.58 ± 1.29	62 ± 10^i	2.48 ± 0.42	1	9

TABLE C.2: .

Single cell charge (Q_{cc}) in Coulombs, cell membrane resting potential (V_{mem}) in mV and cell membrane capacitance (C_{mem}) in $\mu F/cm^2$. The acronym NIE stands for number of independent experiments, namely the number of different experimental days and different cell's seed. The acronym NE stands for number of experiments, including also the repitition of the same experiment. [a]V_{mem} source [7]. [b]C_{mem} source [101]. [c]V_{mem} must be larger than 54 mV. [d]V_{mem} source [102].[e]V_{mem} source [102].[f]V_{mem} source [102].[g]V_{mem} source [103]. [h]$C_{mem} = 18.5 pF/cell$; C_{mem} source [104]. [i]V_{mem} estimated; must be largen than 38 mV.

Bibliography

[1] V. S. Teixeira, W. Krautschneider, and J. J. Montero-Rodriguez. Bioimpedance spectroscopy for characterization of healthy and cancerous tissues. In *2018 IEEE International Conference on Electrical Engineering and Photonics (EExPolytech)*, pages 147–151, Saint Petersburg, Russia, 2018. IEEE. ISBN 978-1-5386-8122-0. doi: 10.1109/EExPolytech.2018.8564401.

[2] K. Asami, Y. Takahashi, and S. Takashima. Frequency domain analysis of membrane capacitance of cultured cells (hela and myeloma) using the micropipette technique. *Biophysical Journal*, 58(1):143–148, 1990. ISSN 00063495. doi: 10.1016/S0006-3495(90)82360-2.

[3] A. J. Surowiec, S. S. Stuchly, J. B. Barr, and A. Swarup. Dielectric properties of breast carcinoma and the surrounding tissues. *IEEE transactions on bio-medical engineering*, 35(4):257–263, 1988. ISSN 0018-9294. doi: 10.1109/10.1374.

[4] D. Haemmerich, S. T. Staelin, J. Z. Tsai, S. Tungjitkusolmun, D. M. Mahvi, and J. G. Webster. In vivo electrical conductivity of hepatic tumours. *Physiological measurement*, 24(2):251–260, 2003. ISSN 0967-3334.

[5] R. J. Halter, A. Schned, J. Heaney, A. Hartov, S. Schutz, and K. D. Paulsen. Electrical impedance spectroscopy of benign and malignant prostatic tissues. *The Journal of urology*, 179(4):1580–1586, 2008. doi: 10.1016/j.juro.2007.11.043.

[6] B. Alberts, D. Bray, K. Hopkin, A. Johnson, J. Lewis, M. Raff, K. Roberts, and P. Walter. *Essential cell biology*. Garland Science, New York, NY and Abingdon, 4th edition edition, 2014. ISBN 978-0-8153-4454-4.

[7] M. Yang and W. J. Brackenbury. Membrane potential and cancer progression. *Frontiers in physiology*, 4:185, 2013. ISSN 1664-042X. doi: 10.3389/fphys.2013. 00185.

[8] S. Laufer, A. Ivorra, V. E. Reuter, B. Rubinsky, and S. B. Solomon. Electrical impedance characterization of normal and cancerous human hepatic tissue. *Physiological Measurement*, 31(7):995–1009, jun 2010. doi: 10.1088/0967-3334/31/7/009. URL https://doi.org/10.1088/0967-3334/31/7/009.

[9] F. S. Barnes and B. Greenebaum. *Bioengineering and biophysical aspects of electromagnetic fields*, volume / ed. by Frank S. Barnes; Ben Greenebaum ; Vol. 1 of *Handbook of biological effects of electromagnetic fields*. CRC Press, Boca Raton, Fla., 3. ed. edition, 2007. ISBN 978-0849395390.

[10] V. F. Lvovich. *Impedance spectroscopy: Applications to electrochemical and dielectric phenomena*. Wiley, Hoboken, N.J, 2012. ISBN 978-0-470-62778-5. doi: 10.1002/9781118164075. URL http://site.ebrary.com/lib/alltitles/docDetail.action?docID=10579495.

[11] J. Malmivuo and R. Plonsey. *Bioelectromagnetism: Principles and applications of bioelectric and biomagnetic fields*. Oxford Univ. Press, New York, NY, 1995. ISBN 978-0195058239. URL http://www.loc.gov/catdir/enhancements/fy0603/93042971-d.html.

[12] Wikipedia contributors. Cell membrane — Wikipedia, the free encyclopedia, 2019. URL https://en.wikipedia.org/w/index.php?title=Cell_membrane&oldid=928901766. [Online; accessed 21-February-2020].

[13] G. Schwarz. A theory of the low-frequency dielectric dispersion of colloidal particles in electrolyte solution. *The Journal of Physical Chemistry*, 66(12):2636–2642, 1962. ISSN 0022-3654. doi: 1-0.1021/j100818a067.

[14] H. P. Schwan. Electrical properties of tissues and cell suspensions: mechanisms and models. In *Proceedings of 16th Annual International Conference of the IEEE*

Engineering in Medicine and Biology Society, pages A70–A71. IEEE, 1994. ISBN 0-7803-2050-6. doi: 10.1109/IEMBS.1994.412155.

[15] C. Grosse and K. R. Foster. Permittivity of a suspension of charged spherical particles in electrolyte solution. *The Journal of Physical Chemistry*, 91(11):3073–3076, 1987. ISSN 0022-3654. doi: 10.1021/j100295a086.

[16] M. Fixman. Charged macromolecules in external fields. i. the sphere. *The Journal of Chemical Physics*, 72(9):5177–5186, 1980. ISSN 0021-9606. doi: 10.1063/1.439753.

[17] H. P. Schwan. Electrical properties of tissue and cell suspensions. volume 5 of *Advances in Biological and Medical Physics*, pages 147–209. Elsevier, 1957. ISBN 9781483231112. doi: 10.1016/B978-1-4832-3111-2.50008-0.

[18] K. R. Foster and H. P. Schwan. Dielectric properties of tissues and biological materials: a critical review. *Critical reviews in biomedical engineering*, 17(1):25–104, 1989. ISSN 0278-940X.

[19] Q. Guofeng, W. Wei, D. Wei, Z. Fan, A. J. Sinclair, and C. R. Chatwin. Bioimpedance analysis for the characterization of breast cancer cells in suspension. *IEEE transactions on bio-medical engineering*, 59(8):2321–2329, 2012. ISSN 0018-9294. doi: 10.1109/TBME.2012.2202904.

[20] A. P. O'Rourke, M. Lazebnik, J. M. Bertram, M. C. Converse, S. C. Hagness, J. G. Webster, and D. M. Mahvi. Dielectric properties of human normal, malignant and cirrhotic liver tissue: in vivo and ex vivo measurements from 0.5 to 20 ghz using a precision open-ended coaxial probe. *Physics in medicine and biology*, 52(15):4707–4719, 2007. ISSN 0031-9155. doi: 10.1088/0031-9155/52/15/022.

[21] K. Grenier, D. Dubuc, T. Chen, F. Artis, T. Chretiennot, M. Poupot, and J-J. Fournie. Recent advances in microwave-based dielectric spectroscopy at the cellular level for cancer investigations. *IEEE Transactions on Microwave Theory and Techniques*, 61(5):2023–2030, 2013. ISSN 0018-9480. doi: 10.1109/TMTT.2013.2255885.

[22] J. Jossinet and M. Schmitt. A review of parameters for the bioelectrical character-ization of breast tissue. *Annals of the New York Academy of Sciences*, 873:30–41, 1999. ISSN 0077-8923. doi: 10.1111/j.1749-6632.1999.tb09446.x.

[23] V. S. Teixeira, T. Barth, V. Labitzky, U. Schumaher, and W. Krautschneider. Elec-trical impedance spectroscopy for characterization of prostate pc-3 and du 145 cancer cells. In *41st Annual Conference of Engineering in Medicine and Biology Society*, 2019.

[24] B. Tunstall, W. Wang, Z. Cheng, M. McCormick, and D. Rew. An analysis of systematic errors in the electrical impedance measurement of tissue characteristics during an in-vitro study in the frequency range 1 khz to 4 mhz. In *Proceedings of the 19th Annual International Conference of the IEEE Engineering in Medi-cine and Biology Society. 'Magnificent Milestones and Emerging Opportunities in Medical Engineering' (Cat. No.97CH36136)*, pages 860–862. IEEE, 1997. ISBN 0-7803-4262-3. doi: 10.1109/IEMBS.1997.757797.

[25] Gamry Instruments. What causes a cpe, 2014. URL `http://www.consultrsr.net/resources/eis/cpe2.htm`. [Online; accessed 12-February-2020].

[26] GamryInc. Basics of electrochemical impedance spectroscopy: Application notes, 2020. URL `https://www.gamry.com/application-notes/EIS/basics-of-electrochemical-impedance-spectroscopy/`. [On-line; accessed 15-February-2021].

[27] D. Borkholder. *Cell based biosensors using microelectrodes*. Dis-sertation, Stanford University, Stanford, November, 1998. URL `http://davidborkholder.com/dev/wp-content/uploads/2015/04/borkholder_thesis1.pdf`.

[28] S. Holm, T. Holm, and O. G. Martinsen. Simple circuit equivalents for the con-stant phase element. *PloS one*, 16(3):e0248786, 2021. doi: 10.1371/journal.pone.0248786.

[29] S. Westerlund. Dead matter has memory! *Physica Scripta*, 43(2):174–179, 1991. ISSN 0031-8949. doi: 10.1088/0031-8949/43/2/011.

[30] S. Holm, editor. *Waves with Power-Law Attenuation*. Springer, 2019.

[31] A. Lasia. *Electrochemical Impedance Spectroscopy and its Applications*. Springer New York, New York, NY and s.l., 2014. ISBN 978-1-4614-8933-7. doi: 10.1007/978-1-4614-8933-7. URL `http://dx.doi.org/10.1007/978-1-4614-8933-7`.

[32] Gamry Instruments Inc. Introduction to electrochemical impedance spectroscopy, 2019. URL `https://www.gamry.com/assets/Uploads/Basics-of-Electrochemical-Impedance-Spectroscopy.pdf`. [Online; accessed 03-August-2021].

[33] V. S. Teixeira, J-P Kalckhoff, and W. Krautschneider. *Impedance spectroscopy measurement of ionic solutions in order to distinguish between different ions*. Amersfoort, 2017. ISBN ISBN 978-94-92579-027. URL `http://www.ictopen.nl/content/Proceedings+2017`.

[34] A. J. Bard and L. R. Faulkner. *Electrochemical methods: Fundamentals and applications*. John Wiley, New York and Chichester, 2nd ed. edition, 2001. ISBN 0471043729.

[35] J. O'M Bockris and A. K. N. Reddy. *Modern electrochemistry: An introduction to an interdisciplinary area*. Plenum Pub. Corp, New York, 1970. ISBN 0306250012.

[36] D. R. Lide, editor. *CRC handbook of chemistry and physics: A ready-reference book of chemical and physical data*. CRC Press, Boca Raton, 84th ed. edition, 2003. ISBN 0849304849.

[37] GamryInc. Two, three and four electrode experiments: Application note, 2020. URL `https://www.gamry.com/application-notes/instrumentation/two-three-and-four-electrode-experiments/`. [Online; accessed 10-December-2021].

[38] GamryInc. Interface 1000 potentiostat/galvanostat/zra operator's manual, 2015. URL `https://www.gamry.com/assets/Uploads/Interface-1000-Operators-Manual2.pdf`. [Online; accessed 10-November-2021].

[39] V. S. Teixeira, J-P. Kalckhoff, W. Krautschneider, and D. Schroeder. Bioimpedance analysis of l929 and hacat cells in low frequency range. *Current Directions in Biomedical Engineering*, 4(1):115–118, 2018. doi: 10.1515/cdbme-2018-0029.

[40] J-P. Kalckhoff, V. S. Teixeira, and W. Krautschneider. Ionic experimentation, modelling and simulation for cell solution characterization. Master thesis, Hamburg University of Technology, Hamburg, Germany, 04.01.2018. URL `https://intranet.et5.tuhh.de/papers/intern/MT_Jan-PatrickKalckhoff.pdf`.

[41] T. Barth. Electrical impedance spectroscopy to measure biological cells solutions in low-frequency range. Mt, Hamburg University of Technology, Hamburg, Germany, 13.11.2018. URL `https://intranet.et5.tuhh.de/papers/intern/MT_Tobias_Barth.pdf`.

[42] T. Barth, V. S. Teixeira, and W. Krautschneider. Designing electrodes for electrical impedance spectroscopy in a four terminal setup: Transactions on additive manufacturing meets medicine, vol 1 (2019): Trans. ammm / transactions on additive manufacturing meets medicine, vol 1 (2019): Trans. ammm. 2019. doi: 10.18416/AMMM.2019.1909S02T01.

[43] Altogen Biosystems. Fibroblast, 2019. URL `http://www.fibroblast.org/`. [Online; accessed 02-October-2019].

[44] P. Weissmanshomer and M. Fry. Chick embryo fibroblasts senescence in vitro: Pattern of cell division and life span as a function of cell density. *Mechanisms of Ageing and Development*, 4:159–166, 1975. ISSN 00476374. doi: 10.1016/0047-6374(75)90017-2.

[45] T. Liu, L. Zhou, D. Li, T. Andl, and Y. Zhang. Cancer-associated fibroblasts build and secure the tumor microenvironment. *Frontiers in cell and developmental biology*, 7:60, 2019. ISSN 2296-634X. doi: 10.3389/fcell.2019.00060.

[46] W. R. Earle, E. Schilling, and T. H. Stark. Production of malignancy in vitro. iv. the mouse fibroblast cultures and changes seen in the living cells. *JNCI: Journal of the National Cancer Institute*, 1943. doi: 10.1093/jnci/4.2.165. [Online; accessed 07-November-2021].

[47] K. M. Halprin. Epidermal "turnover time"–a re-examination. *The British journal of dermatology*, 86(1):14–19, 1972. ISSN 0007-0963. doi: url="10.1111/j. 1365-2133.1972.tb01886.x".

[48] Expasy. Cellosaurus hacat (cvcl_0038), 2012. URL https://web.expasy. org/cellosaurus/CVCL_0038. [Online; accessed 05-October-2019].

[49] B. Lehmann. Hacat cell line as a model system for vitamin d3 metabolism in human skin. *The Journal of investigative dermatology*, 108(1):78–82, 1997. ISSN 0022-202X. doi: 10.1111/1523-1747.ep12285640.

[50] R. L. Siegel, K. D. Miller, and A. Jemal. Cancer statistics, 2019. *CA: a cancer journal for clinicians*, 69(1):7–34, 2019. doi: 10.3322/caac.21551.

[51] S. Tai, Y. Sun, J. M. Squires, H. Zhang, W. K. Oh, C-Z. Liang, and J. Huang. Pc3 is a cell line characteristic of prostatic small cell carcinoma. *The Prostate*, 71(15): 1668–1679, 2011. doi: 10.1002/pros.21383.

[52] A-C. Gaupel, W-L. W. Wang, S. Mordan-McCombs, E. C. Yu Lee, and M. Tenniswood. Xenograft, transgenic, and knockout models of prostate cancer. In *Animal Models for the Study of Human Disease*, pages 973–995. Elsevier, 2013. ISBN 9780124158948. doi: 10.1016/B978-0-12-415894-8.00039-7.

[53] M. E. Kaighn, K. S. Narayan, Y. Ohnuki, J. F. Lechner, and L. W. Jones. Establishment and characterization of a human prostatic carcinoma cell line (pc-3). *Investigative urology*, 17(1):16–23, 1979. ISSN 0021-0005.

181

[54] Y. Matsuo, R. A. MacLeod, C. C. Uphoff, H. G. Drexler, C. Nishizaki, Y. Katayama, G. Kimura, N. Fujii, E. Omoto, M. Harada, and K. Orita. Two acute monocytic leukemia (aml-m5a) cell lines (molm-13 and molm-14) with interclonal phenotypic heterogeneity showing mll-af9 fusion resulting from an occult chromosome insertion, ins(11;9)(q23;p22p23). *Leukemia*, 11(9):1469–1477, 1997. ISSN 0887-6924. doi: 10.1038/sj.leu.2400768.

[55] P. Fialkow. Clonal origin of human tumors. *Biochimica et Biophysica Acta (BBA) - Reviews on Cancer*, 458(3):283–321, 1976. ISSN 0304419X. doi: 10.1016/0304-419X(76)90003-2.

[56] P. J. Fialkow, J. W. Janssen, and C. R. Bartram. Clonal remissions in acute nonlymphocytic leukemia: evidence for a multistep pathogenesis of the malignancy. *Blood*, 77(7):1415–1417, 1991. ISSN 0006-4971.

[57] B. S. Marino and K. S. Fine. *Blueprints pediatrics*. Blueprints. Wolters Kluwer/Lippincott Williams & Wilkins, Philadelphia, sixth edition edition, 2013. ISBN 9781451116045.

[58] H. Döhner, D. J. Weisdorf, and C. D. Bloomfield. Acute myeloid leukemia. *The New England journal of medicine*, 373(12):1136–1152, 2015. doi: 10.1056/NEJMra1406184.

[59] T. Vos, C. Allen, M. Arora, et al. Global, regional, and national incidence, prevalence, and years lived with disability for 310 diseases and injuries, 1990–2015: a systematic analysis for the global burden of disease study 2015. *The Lancet*, 388(10053):1545–1602, 2016. ISSN 01406736. doi: 10.1016/S0140-6736(16)31678-6.

[60] H. Wang, M. Naghavi, C. Allen, R. M. Barber, et al. Global, regional, and national life expectancy, all-cause mortality, and cause-specific mortality for 249 causes of death, 1980–2015: a systematic analysis for the global burden of disease study 2015. *The Lancet*, 388(10053):1459–1544, 2016. ISSN 01406736. doi: 10.1016/S0140-6736(16)31012-1.

[61] Wikipedia. Eosinophil granulocyte — wikipedia, the free encyclopedia, 2019. URL `https://simple.wikipedia.org/w/index.php?title=Eosinophil_granulocyte&oldid=6547000`. [Online; accessed 30-September-2019].

[62] J. S. Ackerman, K. Ishihara, N. Hirasawa, et al. Ex vivo models for the study of eosinophils. In *Eosinophils in Health and Disease*, pages 39–71. Elsevier, 2013. ISBN 9780123943859. doi: 10.1016/B978-0-12-394385-9.00004-3.

[63] P-E. Séguéla, X. Iriart, P. Acar, M. Montaudon, R. Roudaut, and J-B. Thambo. Eosinophilic cardiac disease: Molecular, clinical and imaging aspects. *Archives of cardiovascular diseases*, 108(4):258–268, 2015. doi: 10.1016/j.acvd.2015.01.006.

[64] N. R. Rose. Viral myocarditis. *Current opinion in rheumatology*, 28(4):383–389, 2016. doi: 10.1097/BOR.0000000000000303.

[65] Colon, rectosigmoid, and rectum equivalent terms and definitions: C180-c189, c199, c209: (excludes lymphoma and leukemia m9590 – m9992 and kaposi sarcoma m9140), 2019. URL `https://seer.cancer.gov/tools/solidtumor/Colon_STM.pdf`.

[66] CTCA. : Colorectal cancer types, 2020. URL `https://www.cancercenter.com/cancer-types/colorectal-cancer/types`. [Online; accessed 04-April-2020].

[67] D. Cunningham, W. Atkin, H-J. Lenz, H. T. Lynch, B. Minsky, B. Nordlinger, and N. Starling. Colorectal cancer. *Lancet (London, England)*, 375(9719):1030–1047, 2010. doi: 10.1016/S0140-6736(10)60353-4.

[68] National Cancer Institute. Colon cancer treatment (pdq®)–patient version, 2020. URL `https://www.cancer.gov/types/colorectal/patient/colon-treatment-pdq#section/all`.

[69] B. W. Stewart and C. P. Wild, editors. *World cancer report 2014*. International Agency for Research on Cancer and Distributed by WHO Press, World Health Organization, Lyon, France and Geneva, Switzerland, 2014. ISBN 978-92-832-0443-5.

[70] F. Weis-Garcia. Ht-29: Human colorectal adenocarcinoma cell line (atcc htb-38): Sk 809, 2020. URL `https://www.mskcc.org/research-advantage/support/technology/tangible-material/human-colorectal-adenocarcinoma-cell-line-ht-29`.

[71] M. E. Forgue-Lafitte, A. M. Coudray, B. Bréant, and J. Mester. Proliferation of the human colon carcinoma cell line ht29: autocrine growth and deregulated expression of the c-myc oncogene. *Cancer research*, 49(23):6566–6571, 1989. ISSN 0008-5472.

[72] Wikipedia contributors. Ht-29 — Wikipedia, the free encyclopedia, 2019. URL `https://en.wikipedia.org/w/index.php?title=HT-29&oldid=908237716`. [Online; accessed 12-March-2020].

[73] D. Martínez-Maqueda, B. Miralles, and I. Recio. *The Impact of Food Bioactives on Health: in vitro and ex vivo models: HT29 Cell Line*. Cham (CH), 2015. ISBN 9783319157917. doi: 10.1007/978-3-319-16104-4{\textunderscore}11.

[74] ATCC. Sw620 [sw-620] (atcc® ccl-227™): Colorectal adenocarcinoma, 2020. URL `https://www.lgcstandards-atcc.org/Products/All/CCL-227.aspx?geo_country=de#generalinformation`. [Online; accessed 12-March-2020].

[75] J. Christensen, S. El-Gebali, M. Natoli, T. Sengstag, M. Delorenzi, S. Bentz, H. Bouzourene, M. Rumbo, A. Felsani, S. Siissalo, J. Hirvonen, M. R. Vila, P. Saletti, M. Aguet, and P. Anderle. Defining new criteria for selection of cell-based intestinal models using publicly available databases. *BMC genomics*, 13: 274, 2012. doi: 10.1186/1471-2164-13-274.

[76] ATCC. Caco-2 [caco2] (atcc® htb-37™), 2020. URL `https://www.lgcstandards-atcc.org/Products/All/htb-37.aspx?geo_country=de#`. [Online; accessed 31-May-2020].

[77] ReadyCell. A cell-based and ready-to-use concept for in vitro intestinal absorption evaluation, 2020. URL `https://readycell.com/cacoready/`. [Online; accessed 31-May-2020].

[78] J. Fogh. *Human tumor cells in vitro*. 1975. ISBN 030630810X.

[79] Pinto M., Robine S., Appay M-D, Robin S., Kedinger M., Triadon N., Dussanlxx E., Croix B., Zweibaum A. Enterocyte-like differentiation and polarization of the human colon carcinoma cell line caco-2 in culture. *Cell*, pages 323–330, 1983.

[80] A. V. Lee, S. Oesterreich, and N. E. Davidson. Mcf-7 cells–changing the course of breast cancer research and care for 45 years. *Journal of the National Cancer Institute*, 107(7), 2015. doi: 10.1093/jnci/djv073.

[81] J. Welsh. Animal models for studying prevention and treatment of breast cancer. In *Animal Models for the Study of Human Disease*, pages 997–1018. Elsevier, 2013. ISBN 9780124158948. doi: 10.1016/B978-0-12-415894-8.00040-3.

[82] ATCC. T-47d (atcc® htb-133™), 2020. URL `https://www.lgcstandards-atcc.org/Products/All/HTB-133.aspx?geo_country=de#`. [Online; accessed 12-February-2020].

[83] U. Schumacher and E. Adam. Lectin histochemical hpa-binding pattern of human breast and colon cancers is associated with metastases formation in severe combined immunodeficient mice. *The Histochemical journal*, 29(9):677–684, 1997. ISSN 0018-2214. doi: 10.1023/a:1026404832394.

[84] R. Binggeli and R. C. Weinstein. Membrane potentials and sodium channels: Hypotheses for growth regulation and cancer formation based on changes in sodium channels and gap junctions. *Journal of Theoretical Biology*, 123(4):377–401, 1986. ISSN 00225193. doi: 10.1016/s0022-5193(86)80209-0.

[85] A. L. Hodgkin and A. F. Huxley. The components of membrane conductance in the giant axon of loligo. *The Journal of physiology*, 116(4):473–496, 1952. ISSN 0022-3751. doi: 10.1113/jphysiol.1952.sp004718.

[86] A. L. Hodgkin and A. F. Huxley. Currents carried by sodium and potassium ions through the membrane of the giant axon of loligo. *The Journal of physiology*, 116 (4):449–472, 1952. ISSN 0022-3751. doi: 10.1113/jphysiol.1952.sp004717.

[87] A. L. Hodgkin and A. F. Huxley. The dual effect of membrane potential on sodium conductance in the giant axon of loligo. *The Journal of physiology*, 116(4):497–506, 1952. ISSN 0022-3751. doi: 10.1113/jphysiol.1952.sp004719.

[88] A. L. Hodgkin and A. F. Huxley. A quantitative description of membrane current and its application to conduction and excitation in nerve. *The Journal of physiology*, 117(4):500–544, 1952. ISSN 0022-3751. doi: 10.1113/jphysiol.1952.sp004764.

[89] Wikipedia contributors. Hodgkin–huxley model — Wikipedia, the free encyclopedia, 2020. URL https://en.wikipedia.org/w/index.php?title=Hodgkin%E2%80%93Huxley_model&oldid=951453663. [Online; accessed 9-July-2020].

[90] J. R. Schwarz, G. Reid, and H. Bostock. Action potentials and membrane currents in the human node of ranvier. *Pflugers Archiv : European journal of physiology*, 430(2):283–292, 1995. ISSN 0031-6768. doi: 10.1007/BF00374660.

[91] C. C. McIntyre, A.G. Richardson, and W. M. Grill. Modeling the excitability of mammalian nerve fibers: influence of afterpotentials on the recovery cycle. *Journal of neurophysiology*, 87(2):995–1006, 2002. ISSN 0022-3077. doi: 10.1152/jn.00353.2001.

[92] C. C. McIntyre and W. M. Grill. Sensitivity analysis of a model of mammalian neural membrane. *Biological cybernetics*, 79(1):29–37, 1998. ISSN 0340-1200. doi: 10.1007/s004220050455.

[93] V. S. Teixeira. *Circuit Modelling of Ionic Distribution and of Action Potential Propagation in Damaged Nerve Cells*. Masterarbeit, Hamburg University of Technology, Hamburg, 29.09.2014.

[94] T. Hanai, K. Asami, and N. Koizumi. Dielectric theory of concentrated suspensions of shell spheres in particular reference to the analysis of biological cells suspensions. *Bulletin of the Institute for Chemical Research, Kyoto University*, (57(4)):297–305, 1979.

[95] K. Asami. Characterization of biological cells by dielectric spectroscopy. *Journal of Non-Crystalline Solids*, 305(1-3):268–277, 2002. ISSN 00223093. doi: 10.1016/S0022-3093(02)01110-9.

[96] K. Asami, Y. Takahashi, and S. Takashima. Dielectric properties of mouse lymphocytes and erythrocytes. *Biochimica et Biophysica Acta (BBA) - Molecular Cell Research*, 1010(1):49–55, 1989. ISSN 01674889. doi: 10.1016/0167-4889(89)90183-3.

[97] I. Ermolina, Y. Polevaya, and Y. Feldman. Analysis of dielectric spectra of eukaryotic cells by computer modeling. *European biophysics journal : EBJ*, 29(2):141–145, 2000. ISSN 0175-7571. doi: 10.1007/s002490050259.

[98] M. F. Smiechowski and V. F. Lvovich. Characterization of non-aqueous dispersions of carbon black nanoparticles by electrochemical impedance spectroscopy. *Journal of Electroanalytical Chemistry*, 577(1):67–78, 2005. ISSN 15726657. doi: 10.1016/j.jelechem.2004.11.015.

[99] H. P. Schwan, G. Schwarz, J. Maczuk, and H. Pauly. On the low-frequency dielectric dispersion of colloidal particles in electrolyte solution 1. *The Journal of Physical Chemistry*, 66(12):2626–2635, 1962. ISSN 0022-3654. doi: 10.1021/j100818a066.

[100] J. N. Israelachvili. *Intermolecular and Surface Forces*. Elsevier Science, Saint Louis, 3rd ed. edition, 2015. ISBN 9780080923635. URL https://ebookcentral.proquest.com/lib/kxp/detail.action?docID=4676134.

[101] A. Mansoorifar, A. Koklu, and A. Beskok. Quantification of cell death using an impedance-based microfluidic device. *Analytical chemistry*, 91(6):4140–4148, 2019. doi: 10.1021/acs.analchem.8b05890.

[102] Q. Tan, G. A. Ferrier, B. K. Chen, C. Wang, and Y. Sun. Quantification of the specific membrane capacitance of single cells using a microfluidic device and impedance spectroscopy measurement. *Biomicrofluidics*, 6(3):34112, 2012. ISSN 1932-1058. doi: 10.1063/1.4746249.

[103] A. A. Marino, I. G. Iliev, M. A. Schwalke, E. Gonzalez, K. C. Marler, and C. A. Flanagan. Association between cell membrane potential and breast cancer. *Tumour biology : the journal of the International Society for Oncodevelopmental Biology and Medicine*, 15(2):82–89, 1994. ISSN 1010-4283. doi: 10.1159/000217878.

[104] T. Fujii, T. Shimizu, M. Katoh, S. Nagamori, K. Koizumi, J. Fukuoka, Y. Tabuchi, A. Sawaguchi, T. Okumura, K. Shibuya, T. Fujii, H. Takeshima, and H. Sakai. Survival of detached cancer cells is regulated by movement of intracellular na+,k+-atpase. *iScience*, 24(5):102412, 2021. doi: 10.1016/j.isci.2021.102412.

[105] S. M. Pulukuri, C. S. Gondi, S. S. Lakka, A. Jutla, N. Estes, M. Gujrati, and J. S. Rao. Rna interference-directed knockdown of urokinase plasminogen activator and urokinase plasminogen activator receptor inhibits prostate cancer cell invasion, survival, and tumorigenicity in vivo. *The Journal of biological chemistry*, 280(43): 36529–36540, 2005. ISSN 0021-9258. doi: 10.1074/jbc.M503111200.

[106] M. Han and K. Zhao. Effect of volume fraction and temperature on dielectric relaxation spectroscopy of suspensions of ps/pani composite microspheres. *The Journal of Physical Chemistry C*, 112(49):19412–19422, 2008. ISSN 1932-7447. doi: 10.1021/jp803530m.

[107] J. Lyklema. Fundamentals of interface and colloid science. 1991. URL https://www.semanticscholar.org/paper/690cc93580f89aa52b76c95cefee6be32ea2a7a8. [Online; accessed 28-March-2019].

[108] S. S. Dukhin, V. N. Shilov, and J. J. Bikerman. Dielectric phenomena and double layer in disperse systems and polyelectrolytes. *Journal of The Electrochemical Society*, 121(4):154C, 1974. ISSN 0013-4651. doi: 10.1149/1.2402374.

[109] G. Schaumburg. Novocontrol introduces high quality low cost interdigitated comb electrodes, 2006.

[110] M. Vakilian and B. Y. Majlis. Study of interdigitated electrode sensor for lab-on-chip applications. In *2014 IEEE International Conference on Semiconductor*

Electronics (ICSE2014), pages 201–204. IEEE, 2014. ISBN 978-1-4799-5760-6. doi: url={10.1109/SMELEC.2014.6920831}.

[111] P. Geng, X. Zhang, W. Meng, Q. Wang, W. Zhang, L. Jin, Z. Feng, and Z. Wu. Self-assembled monolayers-based immunosensor for detection of escherichia coli using electrochemical impedance spectroscopy. *Electrochimica Acta*, 53(14):4663–4668, 2008. ISSN 00134686. doi: 10.1016/j.electacta.2008.01.037.

[112] D. R. Coman. Decreased mutual adhesiveness, a property of cells from squamous cell carcinomas. *Cancer Research*, 1944. URL `https://cancerres.aacrjournals.org/content/4/10/625`.

[113] Micrux Technologies. Thin-film interdigitated electrodes, 2020. URL `https://www.micruxfluidic.com/en/shop/electrochemical-solutions/thin-film-electrochemical-sensors/interdigitated-electrodes-ide/`. [Online; accessed 03-June-2020].

[114] S. Gabriel, R. W. Lau, and C. Gabriel. The dielectric properties of biological tissues: III. parametric models for the dielectric spectrum of tissues. *Physics in Medicine and Biology*, 41(11):2271–2293, nov 1996. doi: 10.1088/0031-9155/41/11/003. URL `https://doi.org/10.1088%2F0031-9155%2F41%2F11%2F003`.

[115] C. Gabriel, S. Gabriel, and E. Corthout. The dielectric properties of biological tissues: I. literature survey. *Physics in Medicine and Biology*, 41(11):2231–2249, nov 1996. doi: 10.1088/0031-9155/41/11/001. URL `https://doi.org/10.1088%2F0031-9155%2F41%2F11%2F001`.

[116] W. D. Hurt. Multiterm debye dispersion relations for permittivity of muscle. *IEEE transactions on bio-medical engineering*, 32(1):60–64, 1985. ISSN 0018-9294. doi: 10.1109/TBME.1985.325629.

[117] S. Gabriel, R. W. Lau, and C. Gabriel. The dielectric properties of biological tissues: Ii. measurements in the frequency range 10 hz to 20 ghz. *Physics in*

medicine and biology, 41(11):2251–2269, 1996. ISSN 0031-9155. doi: 10.1088/0031-9155/41/11/002.

[118] M. Egeblad, A. J. Ewald, H. A. Askautrud, M. L. Truitt, B. E. Welm, E. Bainbridge, G. Peeters, M. F. Krummel, and Z. Werb. Visualizing stromal cell dynamics in different tumor microenvironments by spinning disk confocal microscopy. *Disease models & mechanisms*, 1(2-3):155–67; discussion 165, 2008. doi: 10.1242/dmm.000596.

[119] P. P. Provenzano, K. W. Eliceiri, J. M. Campbell, D. R. Inman, J. G. White, and P. J. Keely. Collagen reorganization at the tumor-stromal interface facilitates local invasion. *BMC medicine*, 4(1):38, 2006. doi: 10.1186/1741-7015-4-38.

[120] e. Y. Lin, J-F. Li, L. Gnatovskiy, Y. Deng, L. Zhu, D. A. Grzesik, H. Qian, X-n. Xue, and J. W. Pollard. Macrophages regulate the angiogenic switch in a mouse model of breast cancer. *Cancer research*, 66(23):11238–11246, 2006. ISSN 0008-5472. doi: 10.1158/0008-5472.CAN-06-1278.

[121] M. Egeblad, E. S. Nakasone, and Z. Werb. Tumors as organs: complex tissues that interface with the entire organism. *Developmental cell*, 18(6):884–901, 2010. doi: 10.1016/j.devcel.2010.05.012.

[122] E. Hirata and E. Sahai. Tumor microenvironment and differential responses to therapy. *Cold Spring Harbor perspectives in medicine*, 7(7), 2017. doi: 10.1101/cshperspect.a026781.

[123] J. Stachura, M. Wachowska, W. W. Kilarski, E. Güç, J. Golab, and A. Muchowicz. The dual role of tumor lymphatic vessels in dissemination of metastases and immune response development. *Oncoimmunology*, 5(7):e1182278, 2016. ISSN 2162-4011. doi: 10.1080/2162402X.2016.1182278.

[124] A. W. Lund and M. A. Swartz. Role of lymphatic vessels in tumor immunity: passive conduits or active participants? *Journal of mammary gland biology and neoplasia*, 15(3):341–352, 2010. doi: 10.1007/s10911-010-9193-x.

[125] T. R. Samatov, V. V. Galatenko, A. Block, M. Yu Shkurnikov, A. G. Tonevitsky, and U. Schumacher. Novel biomarkers in cancer: The whole is greater than the sum of its parts. *Seminars in cancer biology*, 45:50–57, 2017. doi: 10.1016/j. semcancer.2016.09.002.

[126] C-H. Heldin, K. Rubin, K. Pietras, and A. Ostman. High interstitial fluid pressure - an obstacle in cancer therapy. *Nature reviews. Cancer*, 4(10):806–813, 2004. ISSN 1474-175X. doi: 10.1038/nrc1456.

[127] A. I. Minchinton and I. F. Tannock. Drug penetration in solid tumours. *Nature reviews. Cancer*, 6(8):583–592, 2006. ISSN 1474-175X. doi: 10.1038/nrc1893.

[128] D. B. Jackson. Clinical and economic impact of the nonresponder phenomenon– implications for systems based discovery. *Drug discovery today*, 14(7-8):380–385, 2009. doi: 10.1016/j.drudis.2009.01.006.

[129] J-J. Montero-Rodriguez. *Impedance spectroscopy for characterization of biological matter*. Dissertation, Hamburg University of Technology, Hamburg, Germany, August/2018.

[130] R. Pethig and D. B. Kell. The passive electrical properties of biological systems: their significance in physiology, biophysics and biotechnology. *Physics in medicine and biology*, 32(8):933–970, 1987. ISSN 0031-9155. doi: 10.1088/0031-9155/32/8/001.

[131] Yangkyu Park, Hyeon Woo Kim, Joho Yun, Seungwan Seo, Chang-Ju Park, Jeong Zoo Lee, and Jong-Hyun Lee. Microelectrical impedance spectroscopy for the differentiation between normal and cancerous human urothelial cell lines: Real-time electrical impedance measurement at an optimal frequency. *BioMed research international*, 2016:8748023, 2016. doi: 10.1155/2016/8748023.

[132] Fabián Eduardo Giana, Fabián José Bonetto, and Mariela Inés Bellotti. Assay based on electrical impedance spectroscopy to discriminate between normal and cancerous mammalian cells. *Physical review. E*, 97(3-1):032410, 2018. doi: 10. 1103/PhysRevE.97.032410.

191

[133] Ho-Jung Jeong, Kihyun Kim, Hyeon Woo Kim, and Yangkyu Park. Classification between normal and cancerous human urothelial cells by using micro-dimensional electrochemical impedance spectroscopy combined with machine learning. *Sensors (Basel, Switzerland)*, 22(20), 2022. doi: 10.3390/s22207969.

[134] Giseok Kang, Young-Jae Kim, Hong-Sang Moon, Jeong-Woo Lee, Tag-Keun Yoo, Kwangsung Park, and Jong-Hyun Lee. Discrimination between the human prostate normal cell and cancer cell by using a novel electrical impedance spectroscopy controlling the cross-sectional area of a microfluidic channel. *Biomicrofluidics*, 7 (4):44126, 2013. ISSN 1932-1058. doi: 10.1063/1.4818838.

[135] F. Galea, O. Casha, I. Grech, E. Gatt, and J. Micallef. Ultra low frequency low power cmos oscillators for mppt and switch mode power supplies. In *2018 14th Conference on Ph.D. Research in Microelectronics and Electronics (PRIME)*, pages 121–124. IEEE, 7/2/2018 - 7/5/2018. ISBN 978-1-5386-5387-6. doi: 10.1109/PRIME.2018.8430355. URL https://ieeexplore.ieee.org/document/8430355/.

[136] A. K. Mahato. Ultra low frequency cmos ring oscillator design. In *2014 Recent Advances in Engineering and Computational Sciences (RAECS)*, pages 1–5. IEEE, 2014. ISBN 978-1-4799-2291-8. doi: 10.1109/RAECS.2014.6799627.

[137] Changku, H., Bibyk, S., Ismail, M., and Lohiser, B. A very low frequency, micropower, low voltage cmos oscillator for noncardiac pacemakers. *IEEE Transactions on Circuits and Systems I: Fundamental Theory and Applications*, 42(11): 962–966, 1995. doi: 10.1109/81.477208.

[138] Zurich Instruments. Principles of lock-in detection and the state of the art. Technical report, University of Zurich, Department of Informatics, 11 2016. [Online; accessed 09-Agosto-2020].

[139] electronics notes.com. Gilbert cell rf mixer / multiplier, 2021. URL https://www.electronics-notes.com/articles/radio/rf-mixer/gilbert-cell-rf-mixer.php. [Online; accessed 23-December-2021].

[140] S. Winiwarter, M. Ridderström, A.-L. Ungell, T.B. Andersson, and I. Zamora. 5.22 - use of molecular descriptors for absorption, distribution, metabolism, and excretion predictions. In J. B. Taylor and D. J. Triggle, editors, *Comprehensive Medicinal Chemistry II*, pages 531–554. Elsevier, Oxford, 2007. ISBN 978-0-08-045044-5. doi: https://doi.org/10.1016/B0-08-045044-X/00140-1. URL https://www.sciencedirect.com/science/article/pii/B008045044X001401.

[141] National Library of Medicine. Citrate: Compounds summary, 2021. URL https://pubchem.ncbi.nlm.nih.gov/compound/citrate. [Online; accessed 22-June-2021].

[142] J. Ginty. Glucose sensors: What they are & how they work. URL https://agamatrix.com/blog/glucose-sensors/. [Online; accessed 12-September-2021].

[143] K. Rathee, V. Dhull, R. Dhull, and S. Singh. Biosensors based on electrochemical lactate detection: A comprehensive review. *Biochemistry and Biophysics Reports*, 5:35–54, 2016. ISSN 2405-5808. doi: https://doi.org/10.1016/j.bbrep.2015.11.010. URL https://www.sciencedirect.com/science/article/pii/S2405580815001302.

Bisher erschienene Bände der Reihe

Wissenschaftliche Beiträge zur Medizinelektronik

| 10 | Jan Claudio Loitz | Novel Methods in Electrical Stimulation with Surface Electrodes
ISBN 978-3-8325-4885-8   45.00 EUR |
| 11 | Viviane Silva Teixeira | Development of a System for Fast Identifiation and Characterization of Biological Cells
ISBN 978-3-8325-5751-5   54.50 EUR |

This series of publications presents the results of research in the area of integrated circuits for biomedical engineering. In addition to signal acquisition and data analysis techniques, the series covers technological aspects and system solutions.

Bio Impedance Spectroscopy (BIS) consists in the application of a small frequency variable electrical signal to a biological material and measuring its response. This research explores BIS applied to cancer and healthy cells and tissues, with the objective to try to distinguish them and also to explore differences between metastatic and non-metastatic cancers. Important trends were found in the direction of a significant different spectral response between cancerous and healthy tissues, close correlated with the effects of the cancer in the normal tissues. Also, one physical characteristic that can possibly be used to distinguish metastatic from non-metastatic cancer cells was found: the cell surface charge.

Logos Verlag Berlin